

# POLITECNICO DI TORINO

Collegio di Ingegneria Meccanica, Aerospaziale, dell'Autoveicolo e della  
Produzione

**Corso di Laurea Magistrale in Ingegneria Meccanica**

Tesi di Laurea Magistrale

## **Design and modeling of a novel pneumatic passive upper limb exoskeleton based on McKibben artificial muscle**



### **Relatore**

prof. Carlo Ferraresi

### **Correlatori**

prof. Giovanni Gerardo Muscolo

prof. Carlo De Benedictis

prof. Maria Paterna

### **Candidato**

Stefania Magnetti Gisolo

Luglio 2021



# Abstract

The upper extremity is one of the most complex part of human body, consisting of four articulations: the glenohumeral, sternoclavicular, acromioclavicular and scapulothoracic. The glenohumeral joint is commonly referred as shoulder joint. When the upper limb is lifted, the contraction of shoulder complex muscles must balance the torque due to gravity of the arm's segments. Yet, in industrial environment, overhead working tasks could require the user to keep his arms in elevated position for a long time, also holding a load or a tool in hand. Thus, to reduce the effort on shoulder complex muscles, a supportive device is needed, as a wearable equipment interacting with human. Therefore, the aim of this paper is to submit a new passive upper limb exoskeleton for partially compensating the gravitational torque while lifting the arm, working on a McKibben pneumatic artificial muscle (PAM), as passive actuator, that, once pressurized, is able to exert a high force-to-weight ratio, by contraction. At first, a state of art of upper limb exoskeleton devices is presented, by highlighting the main design critical issues. Then, the original design of the proposed exoskeleton is described, by suggesting a possible improvement. This consists of joining a shoulder pad, fixed to the exoskeleton, whose profile is designed to improve the PAM exerted torque characteristic with respect to the gravitational torque, reducing the effort on shoulder muscles. The numerical results test a significant positive effect, yet the design of the shoulder pad is fitted to accomplish the assembly. So, a mounting solution is suggested, working out the CAD model, and the results of FEM analysis are carried out, by choosing the materials in order to make the exoskeleton as light as possible, and estimating the overall weight of the structure. Eventually, the torque due to gravity and the torque generated by the PAM are compared at different values of elevation angle of the upper arm and forearm, to calculate the difference of torques that the shoulder complex muscles should exert to work out of equilibrium, summarizing the performance of the exoskeleton equipped with the shoulder pad in assisting the lifting of the upper limb.



# Acknowledgments

Ringrazio tutti coloro che mi hanno accompagnato in questi anni di studio, amici e figure professionali che hanno contribuito alla mia formazione. Un ringraziamento particolare al relatore e ai correlatori con cui ho avuto il piacere di lavorare. Infine, un ringraziamento speciale è riservato alla mia famiglia, a cui dedico l'elaborato, perché ha reso possibile questo traguardo e per la grande dose di pazienza.



# Contents

1	Introduction .....	1
2	State of art.....	3
2.1	Anatomy of the shoulder complex.....	4
2.2	Design challenges .....	7
2.3	Active exoskeleton systems .....	8
2.3.1	Electric motor driven exoskeletons.....	10
2.3.2	Pneumatic actuator driven exoskeletons.....	17
2.3.3	Hydraulic actuator driven exoskeletons.....	20
2.3.4	Other actuation principles.....	21
2.4	Passive exoskeleton systems.....	22
2.4.1	Passive exoskeletons for assisting upper limb movement.....	22
2.4.2	Passive upper limb exoskeletons for overhead tasks .....	23
2.5	Comparison of upper limb exoskeletons .....	28
3	Original exoskeleton design .....	31
3.1	Standard human body inertia parameters.....	31
3.2	Pneumatic artificial muscles.....	34
3.2.1	FESTO pneumatic artificial muscles modelling.....	36
3.3	Materials and methods .....	39
3.4	Numerical results .....	42
4	Joining the shoulder pad to the exoskeleton design .....	45
4.1	Materials and methods .....	45
4.2	Numerical results .....	47
4.3	Real profile of the shoulder pad.....	49
5	Exoskeleton assembly .....	55
5.1	Materials and methods .....	55
5.1.1	2-DOF Exoskeleton shoulder joint.....	55
5.1.2	Size adjustment systems .....	56
5.1.3	Mounting of the PAM.....	57
5.2	FEM analysis .....	64

5.2.1	SolidWorks simulations .....	65
5.2.2	Altair HyperMesh simulations.....	73
5.3	Exoskeleton weight .....	81
6	Results and discussion.....	83
6.1	Verification of PAM results .....	83
6.2	Verification of shoulder pad contribution.....	85
7	Conclusions and future developments .....	89
	Bibliography .....	91
	Appendix .....	97

# Chapter 1

## Introduction

Exoskeleton technologies have been object of much research through the years. They are meant to be wearable assistive devices for improving body mobility and/or strength, or just balance the weight force of limbs in everyday life, by performing many advantages according to their purpose.

Yet, their development must face different critical issues, to carry out a suitable equipment which needs to be efficient, ergonomic, and lightweight. One of these is the human-robot interaction, besides the implementation of sophisticated control systems, in some cases.

Therefore, exoskeleton devices have been topic of several research articles, meant also to highlighting the benefits of these technologies measured on different subjects. Especially these concern rehabilitation exoskeleton robots meant to assist patients after they have been affected by stroke. Yet, many recent technologies focus on working assistance, so they are meant to help supporting the weight of limbs and loads and amplify human endurance.

Among the implemented technologies, there are different devices which can be classified by the part of the body assisted, that can be the upper limb, the back, the lower limb, or more than one of these at the same time. Thus, since the exoskeleton design submitted in this paper is meant to assist the upper limb, at first a state of art is presented focusing on upper limb exoskeleton devices. This overview includes commercial technologies, but also some exoskeleton designs, developed by researchers and universities, which are later compared to highlight their advantages and drawbacks.



## Chapter 2

### State of art

The exoskeleton technology originally focused on military and rehabilitation applications, as a wearable structure or system designed to enhance the wearer's strength or agility by providing an auxiliary torque or structural support for the body joints, which could reduce the effort on the muscles of the human body [1].

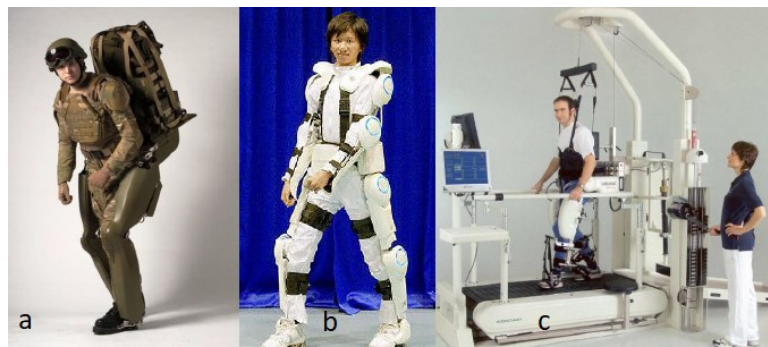


Figure 2.1 Military exoskeleton for power and strength enhancing (DARPA 2000). (b) Exoskeleton for civil applications in mobility assistance. (c) Robotic device for rehabilitation

By amplifying or sensing the physical capabilities of a user, they have been studied since 1960s [2]. For military purposes (Figure 2.1-a) they were thought to assist and protect soldiers or firefighters in harsh or dangerous environment, for example to help carrying heavy loads while running. For medical rehabilitation (Figure 2.1-b-c), exoskeleton devices may be able to support and assist the patient without the presence of the therapist, enabling more frequent treatment and potentially reducing costs. In addition, their development is also due to their capacity to perform repetitive tasks, and because they allow to accurately measure quantitative data to evaluate the patient's condition, analysing the patient's evolution objectively [3].

In 1990s, some exoskeleton robots were proposed to extend the strength of the human body. In the last years, they have been introduced for applications into manufacturing industry, whereby they are designed to enhance user capacity, and so improve the balance between task demands and worker capacity.

Main benefit of exoskeleton is a good merge between human flexibility and robot power enhancing, without the need for robot teaching or programming [4]. In addition, although robots have been widely adopted to perform tasks that require heavy load lifting, they are not as agile, versatile, and intelligent as human workers to solve the problems. Despite a few successful cases on the application of wearable robots to rehabilitation, industrial

exoskeletons have not been widely deployed yet, due to performance limitations such as wearing discomfort due to the heavy weight and insufficient torque transmission [5].

Exoskeleton systems can be classified into three types, as upper extremity (upper limb), lower extremity and full body. In addition, they can be classified by their purposes in in rehabilitation, haptics, assistive device, teleoperations, and power augmentation [6]. This occurs, because, when a robotic exoskeleton is worn by the human, the physical contact between the user and the exoskeleton allows direct transfer of mechanical power and information signals.

In general, exoskeletons employ one or more devices, providing most of the power necessary for performing the task. According to the device, active and passive exoskeletons are classified. Active exoskeleton requires an external power source (such as batteries) in order to supply and control the actuator, that is the device providing the power augmentation, which could be an electric motor, pneumatic or hydraulic actuator. Otherwise, passive exoskeleton cannot actively assist or control movement, but uses mechanical elements (like springs or dampers), which store the energy of the human body motion and release the energy when needed, enhancing the wearer's strength, without adding inertia.

Since the design proposed in this paper is meant to assist the upper limb, in next paragraph some hints are given on the anatomy of the shoulder complex.

## 2.1 Anatomy of the shoulder complex

Upper extremity is one of the most complex part of human body (Figure 2.2 left). It consists of hand, wrist, forearm, elbow, arm, and shoulder complex [7]. The movement of the arm depends on the synchronized interaction of three bones, clavicle, scapula and humerus, and four articulations: the glenohumeral, sternoclavicular, acromioclavicular and scapulothoracic.

The glenohumeral joint is commonly referred as shoulder joint. The sternoclavicular joint is the only joint that connects the shoulder complex to the axial skeleton. The acromioclavicular joint is formed by the lateral end of the clavicle and the acromion of the scapula. The sternoclavicular joint is a compound joint, formed by the parts of clavicle, sternum, and cartilage of the first rib [8].

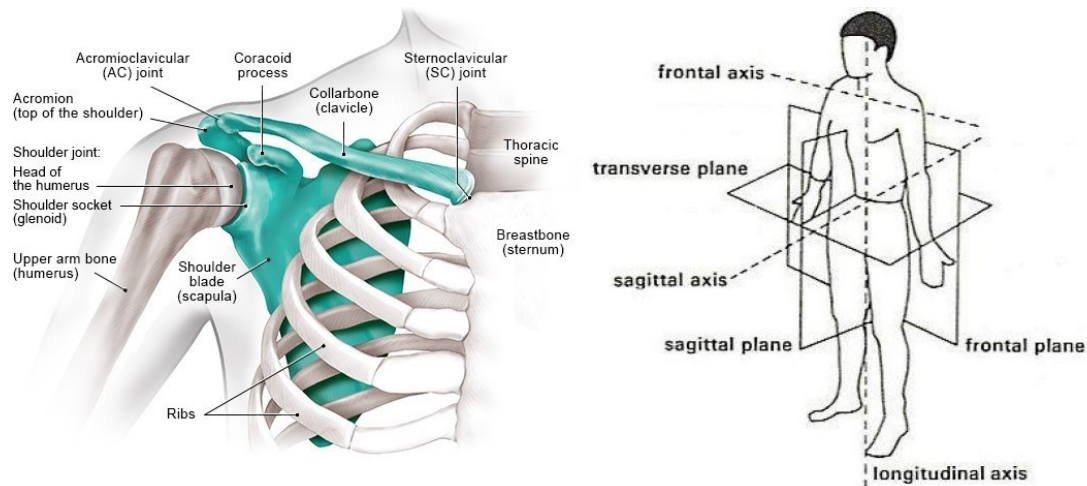


Figure 2.2 Shoulder joint anatomy (left) [63], human body planes and axes (right) [64]

Overall, the arm has nine degrees of freedom (DOF), showed in Figure 2.3, neglecting the adding joints of the fingers. The glenohumeral joint, at the shoulder complex, is a ball-and-socket joint which enables the humerus to rotate about the glenohumeral head in 3 DOF, that are commonly referred to as shoulder flexion/extension (motion in the sagittal plane), abduction/adduction (motion in the frontal plane) and medial/lateral rotation (also regarded as internal/external rotation is the motion in the transversal plane).

The sternoclavicular joint has 2 DOF, commonly known as shoulder elevation/depression and retraction /protraction; these movements induce the translational movement of the glenohumeral joint. Thus, the shoulder has a total of 5 DOF. The elbow complex is capable of 2 DOF, these are elbow flexion/extension and forearm pronation /supination, whereas the wrist joint has 2 DOF, wrist flexion/extension and radial/ulnar deviation. The axes of rotation of both DOF of the wrist pass through the capitate carpal bone. The movement of the shoulder girdle (clavicle and scapula) is more important when raising the arm above the shoulder than the arm motion below the shoulder. As the arm is raised, the ratio of scapulothoracic rotation (rotation of the scapula relative to the torso) to glenohumeral rotation (rotation of humerus relative to the scapula) generally increases. If the movement of the shoulder girdle is restricted, then the arm cannot be raised above a certain posture. Therefore, the translation of the glenohumeral joint is essential to enable the arm to be raised high. If the translational motion is limited by external forces, then the range of motion (ROM) of the shoulder joint is limited and it may cause pain in the joint [9].

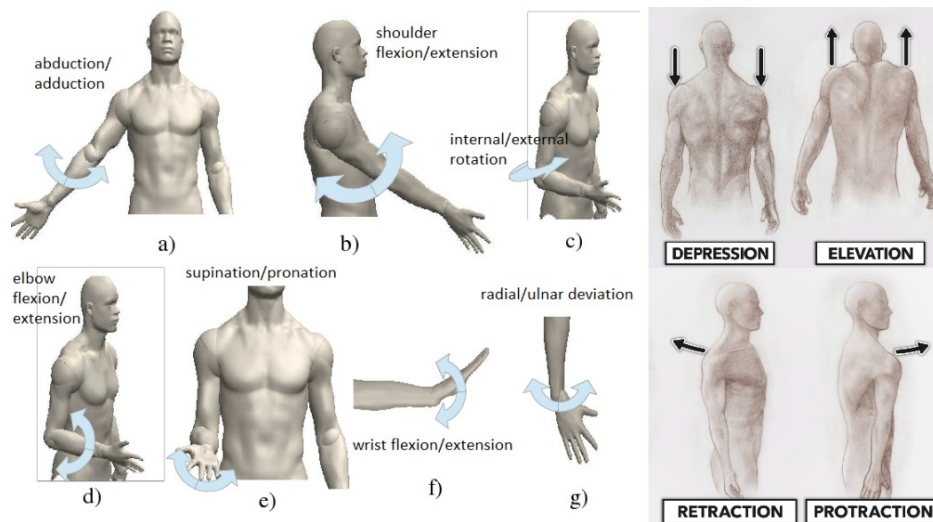


Figure 2.3.9 DOF of the upper limb [65-66]

Although there is variability among various individuals, the following table reports the normal ranges of motion of the shoulder, elbow, and wrist joint, which are the generally accepted values for a normal ROM in each joint as measured in degrees [74].

Table 2.1 Normal range of motions of shoulder, elbow, and wrist joint (degrees) [74]

Shoulder abduction	0 – 90 <sup>1</sup>	From horizontal position
Shoulder adduction	0 – 90	-
Shoulder flexion	0 – 180	From vertical position
Shoulder extension	0 – 50	-
Internal rotation (medial)	0 – 90	With the arm at your side
External rotation (lateral)	0 – 90	-
Elbow flexion	0 – 160	With upper arm horizontal
Elbow extension	145 – 0	Until the arm is vertical at your side
Elbow pronation	0 – 90	
Elbow supination	0 – 90	
Wrist flexion	0 – 90	
Wrist extension	0 – 70	
Wrist radial deviation	0 – 25	
Wrist ulnar deviation	0 – 65	

<sup>1</sup> According to other sources, shoulder's abduction reaches only 60° [75]

## 2.2 Design challenges

The exoskeleton robot should generate natural motions of upper limb with the wearer does not feel any vibration, jerk, or sudden motion change. Small sized high torque actuators with high power-weight ratio are essential to develop such kind of exoskeleton robot, that should not give unbearable weight to the wearer. In this paragraph some critical features of exoskeleton devices are reported, which must be considered in the design.

- Increasing loads and discomfort

While they can reduce efforts on specific body parts, however, exoskeletons can also have unintentional consequences such as increasing loading and/or discomfort on other regions of the wearer's body. Normally, discomfort occurs in areas where the exoskeleton is in contact with the wearer's body. For instance, in a simulation of overhead work, using an upper limb passive exoskeleton reduced loading on the upper arm and shoulder but increased it slightly on the low back. Thus, even if a mechanical advantage was confirmed, eliminating, or minimizing such discomfort is another design goal.

- Centre of rotation of the shoulder complex

Shoulder complex is one of the biomechanically complex area in the human body, in fact, its centre of rotation (CR) changes with its motions. So, design of a proper shoulder mechanism for an upper extremity robotic exoskeleton to change its CR with its motions is a very difficult task to be accomplished. Yet, it is necessary to cancel the ill effects caused by the position difference of the CR of the exoskeleton robot shoulder and that of the human shoulder [10].

- Compatibility

Because upper limb exoskeletons need to operate in parallel with the human upper limb and are attached to the human arm at multiple locations, they are required to adapt to different wearer's arm lengths, thus they need adding prismatic joints.

- Wearability

The structures of the exoskeletons should be flexible with high strength. Those systems should have less weight to eliminate user feeling discomfort or fatigue. Therefore, the materials of the exoskeleton structures should be specially considered so that the exoskeleton system will become a second skin to the wearer.

- Workspace limitation

Wearable exoskeletons are not able to provide a wide range of motion in comparison to the human upper-limb torso. Since the mechanisms supporting shoulder glenohumeral movements tend to reduce the actual upper limb workspace, several studies have tried to approach this limited workspace challenge in their design, by considering shoulder girdle movements accepting complex and heavier mechanism [82]. It is necessary to analyse the mutual ROM for the human arm and exoskeleton to achieve the desired workspace, which can

be done by analysing the kinematic and dynamic model of both systems. Yet, the wide ROM can only be achieved at the cost of a complex and heavier mechanism.

- Misalignment

Furthermore, the misalignment of the arm joint axes with exoskeleton axes, is an important matter, especially of active exoskeleton systems, because it generates parasitic forces that cause discomfort and pain on patient's arm may lead to dislocation and fracture. In order to avoid misalignment, or at least reduce the degrees of misalignment, the means is including redundant DOF into the active exoskeleton structure. This is achieved, by adding passive joints that performs these further DOF, which are free to rotate or translate [11].

- Singularity

Finally, a critical issue is singularity or singular configuration, that can occur in postures where two rotational joint axes align with each other, and that provides the loss of at least 1 degree of freedom. Besides, it needs infinite torque to move the exoskeleton out of a singular configuration. For instance, the rotational axes of the shoulder gimbal joint can align, the shoulder medial/lateral rotation axis aligns with the forearm pronation/supination axis at full elbow extension. This issue can be resolved with two approaches. One is to include possible situations in the control strategy of the exoskeleton. The other approach is to incorporate the possibilities in the design of the exoskeleton by applying mechanical constraints.

In next paragraph, the main active upper arm exoskeletons are described, including the devices employed to solve the design challenges above.

## 2.3 Active exoskeleton systems

The history of the active exoskeleton can be traced back to the 1960s. The US military had developed several exoskeletons to increase and enhance the soldier ability for military purposes. Then, the General Electric Company developed two-armed master–slave manipulator used for handling radioactive equipment, whereby the master is an exoskeleton robot, worn by the operator, while its motion is reproduced by the slave unit [12].

Hardiman (Figure 2.4 left), which was the first whole body robotic exoskeleton system, was actuated by hydraulic actuators and it was supposed to be driven by a human operator from the inside of exoskeleton system.



Figure 2.4 General Electric Hardiman (left), Bleex (middle), Raytheon XOS 2 (right)

The Berkeley Lower Extremity Exoskeleton, or Bleex, was developed under DARPA (Defense Advance Research Projects Agency) funding for operators who must carry heavy loads in dangerous environments, like soldiers and firefighters) [68]. It was meant to be an energetically autonomous exoskeleton to enhance its wearer's strength and resistance, consisting of two motorized lower limbs, a supply unit, and a bag for carrying the load. The drive runs on hydraulic energy, while the control computer runs on electric energy, supplied by a heat engine. Bleex can support a load up to 30 – 60 *kg*. Otherwise, Raytheon XOS 2 is powered by the energy supply through an umbilical cord [69]. The hydraulic drive system is powered by a heat engine, allowing to easily lift 100 kg a hundred times.

Active exoskeletons can be considered real wearable robots. Their advantage is that their ability to support the multiple degrees of freedom of motion, and the sufficient bandwidth of motors. For instance, active gravity-compensation devices are a subset of active systems, which can provide compensation capability in a more controllable way, such as a continuous adjustment of the gravitational force level to be compensated [13]. Moreover, active actuators can provide a variable range of motions, with different torques and speeds.

Yet, they require the implementation of complex control algorithms, therefore they need transducers and sensors for the transmission of command signals and reception of signals from the mechanical joints. When pneumatic or hydraulic actuators are employed, valves are needed to control the supply fluidic pressure and so the actuator exerted force. Control algorithms, sensors and valves make the device more complex and the cost to rise.

Active upper limb exoskeletons can be classified according to:

- the applied segment of the upper-limb (hand exoskeleton robot, forearm exoskeleton robot, upper-arm exoskeleton robot or combined segments exoskeleton robot),
- the numbers of DOF (degrees of freedom),
- the type of the applied actuators (electric motors, pneumatic muscles, hydraulic actuators, shape memory materials), which are usually external or on the user's back,
- the power transmission methods (gear drive, cable drive, linkage mechanism or other),
- the application of the robot (rehabilitation robots, assistive robots, human amplifier, combined use).

Requirements are different, according to their applications. The most important is safety because the actuator interacts actively with the user. Besides assisting the movement, the exoskeleton must allow the motion of the shoulder joint centre of rotation. In addition, as one of the critical issues of upper limb exoskeletons is the weight of actuators, the reduction of inertia is an important purpose. Finally, the singular configurations should not occur in the workspace. In next paragraphs, the exoskeleton designs are classified according to the type of actuators, highlighting their benefits and drawbacks.

### 2.3.1 Electric motor driven exoskeletons

An advantage of electric motors, over pneumatic muscle actuators is their ease to control and sufficient bandwidth, yet they have a poorer power to weight ratio, and because of their power consumption and battery life, they have a reduced load capacity. In addition, they are expensive, large, and heavy and may overheat [14].

Although, while pneumatic and hydraulic systems suffer from high friction and are very difficult to backdrive, electric motors can be much more accurately controlled for position than other types of actuators, and they are easy to program. This is the reason why a majority of the current active exoskeletons use electric motors.

Besides, electrical motors can apply an equal force during the rotation of the joint, while a pneumatic artificial muscle exerts a bigger force at the beginning of its stroke, and a smaller force at the end of the stroke. Most of the existing active exoskeletons employ brushless DC motors due to their better power to weight ratio than others, high torque-to-weight ratio, reduced noise, and reliability.

Electrical motors are usually coupled with a reduction gearing in order to increase their torque and decrease their rotation speed, yet the reduction gearing might be heavier than the motor itself, and certainly it increases the weight of the actuation unit. Then, the efficiency and the weight of gearing systems for a specific reduction ratio varies according to the type of the gearing system. Some exoskeletons use serially coupled motors on the structure to actuate each revolute joint. Yet, placing the actuator at the joints of the user increases both the inertia of the exoskeleton and the size of the motors, besides this inducing misalignment. In addition, the actuator at a joint would have to withstand the load of the actuator of the following joint and so on. A method to resolve these drawbacks, has been the application of cable transmission systems. This approach uses cables to transmit motion and forces, allowing the actuators to be mounted away from the joints at a fixed base, achieving low weight, reducing the size of motors and their cost [15]. Figure 2.5 shows different types of actuation and transmission systems.

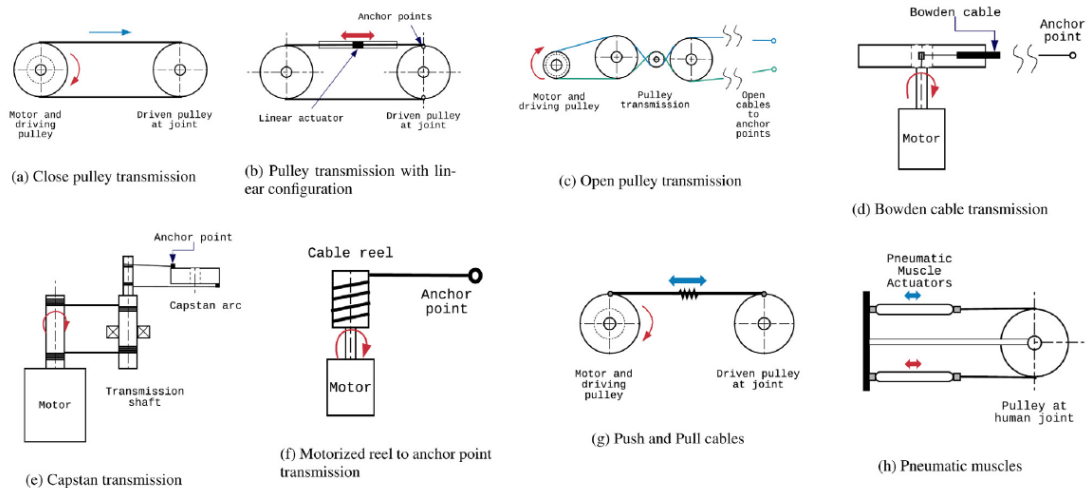


Figure 2.5 Types of actuation and transmission systems [15]

Cable-driven exoskeletons also have other advantages, such as the transmission itself which can allow to implement speed reductions with low friction forces and zero backlash, as long the cables are tensioned.

This is the example of the ARMin, which is an upper-limb exoskeleton with 6 DOF for rehabilitation after stroke [16-17-70]. Developed by the University of Zurich, ARMin supplies four active and two passive degrees of freedom: 3 DOF for the shoulder abduction/adduction, flexion/extension, and internal/external rotation, 1 DOF for the forearm pronation/supination and 2 DOF for the flexion/extension of the elbow and the wrist. In the original design, the actuation unit for the shoulder external/internal rotation consists of a fixed DC motor coupled to an HD (harmonic drive) gear reduction, with an output shaft. The motion transmission is through a toothed belt, tensioned by idle pulleys and connected to a curved rail (Figure 2.6-a). Its third version, ARMin III, introduces a spring and cable mechanism which works as a passive weight compensation system in case of power loss (Figure 2.6-b). Main advantage of all ARMin versions is their capability of allowing a natural motion of the shoulder complex by adding passives DOF. Besides, the original feature is the vertical shoulder rotation, therefore the exoskeleton robot does not inhibit the vertical motion of shoulder complex of the robot user. This motion is not included in any of the other exoskeleton robots.

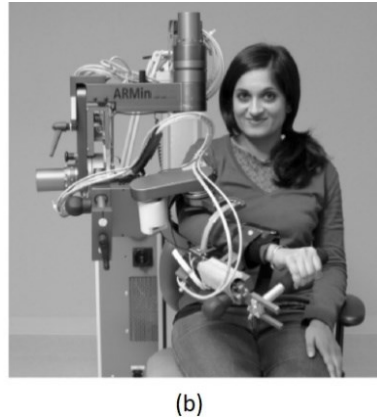
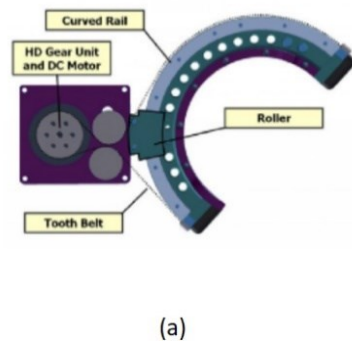


Figure 2.6 (a) Actuation unit for shoulder external/internal rotation in Amin II [16]. (b) Armin III in a healthy user [70]

A similar cable driven upper limb exoskeleton, for rehabilitation, is ABLE, that introduced the concept of Screw Cable System (SCS) [18]. The first stage of the prototype consisted in a rotational motor coupled to a belt and pulley transmission (Figure 2.7-b), a large shaft and two flexible couplings are required to connect the motor with the driving pulley. Then, the second stage transformed the rotational motion into linear by using a ball-screw, guided by a fixed anti-rotation slot, a cable is attached inside the hollow screw and routed through an idle pulley for moving the final pulley joint. It provided 4 DOF: shoulder abduction/adduction, external/internal rotation and flexion/extension movements, and elbow flexion/extension. Nowadays, ABLE is available with 5 DOF, adding pronation/supination of the forearm or also with 7-DOF, including 2 DOF for wrist.

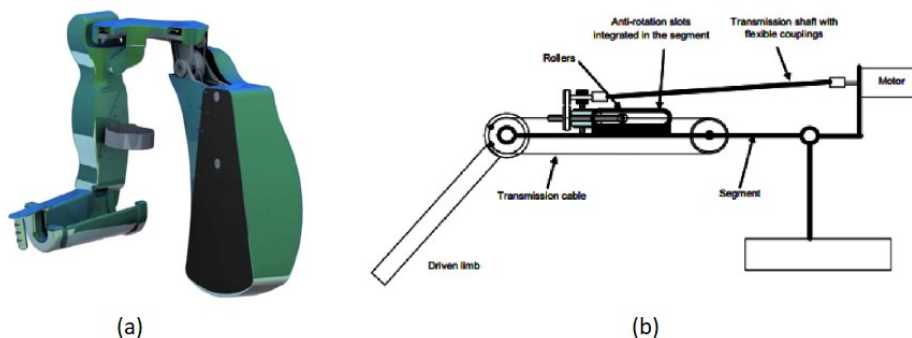


Figure 2.7 (a) Able prototype. (b) Able exoskeleton transmission system [18]

Another example of rehabilitation upper limb exoskeleton is CADEN-7 system that employs DC brushed motors, shown in Figure 2.8-a [19]. It performs 7 DOF: 3 DOF of the shoulder, 3 DOF of the wrist and 1 DOF of the elbow. The system uses three types of configurations for the actuation of each joint movement: 90°; 180°; axial. Both, the 90° and 180° arrangements consist of closed-loop cables with pulleys to transmit the actuation. The pulleys are wrapped

around joint idler pulleys, concentric to the axis of revolution. However, CADEN-7 suffers for not consider the misalignment of each joint of the exoskeleton with the limb joints. Besides, it requires a high number of idle pulleys to maintain the workspace, which increases the bulkiness of the device, and, by using pulleys, it limits the adjustment of its dimensions to different users.

An exoskeleton robot that possesses the same 7 DOF of CADEN-7, is CABXLexo-7 [20]. Its mechanism employs a driving link that rotates over a driving wheel to generate adduction/abduction and it is actuated using open cables capstan transmission system. Around the driving wheel, other pair of wires passes, that reach to a planet wheel, perpendicular to the driving wheel, generating the flexion/extension. On the driving link, CABXLexo-7 uses Bowden cables to actuate the internal/external rotation of the shoulder. By using Bowden cables, it allows the position of the actuator of this joint decreasing its weight, being away from the upper limb.

The CAREX-7 actively drives cables to assist the arm motion [21]. Two cables start from the shoulder cuff and end on the upper-arm cuff. Three cables start from the shoulder cuff, go through the upper arm cuff, and end on the forearm cuff. To control the movement of the upper limb, CAREX-7 uses eight open-ended cables actuated with motorized reels mounted on an external structure. Due to CAREX-7 is designed without links and joints, the systems do not suffer for the issues of misalignment of the axis of rotation, suffered by CADEN-7. Besides, it minimizes the effects of the shoulder girdle. CAREX-7 is shown in Figure 2.8-b.

The EXOSUIT is a rehabilitation active exoskeleton for elbow joint [22]. The actuation unit presents a DC motor input and two Bowden cable outputs. The motor input provides torque to a winch through an intermediate gear reduction (Figure 2.8-c). The use of springs at the end of the transmission allows more compliance in the motion. Due to the different elongations of the cables and the nonlinearity of the flexor cable length, the winch has two sections for each wire. The one with the larger diameter wraps the extensor cable, and the smaller one does the same for the flexor cable. An advantage of EXOSUIT is its light weight, negligible inertia, the soft interface between device and user, while a drawback is the presence of undesired friction for the Bowden cable transmission that affects bandwidth and performance.

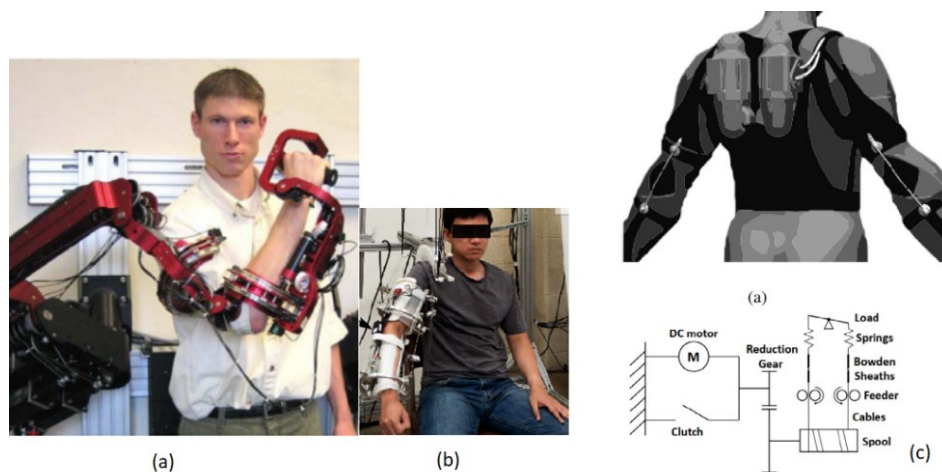


Figure 2.8 (a) CADEN-7 [19]. (b) CAREX-7 [21]. (c) EXOSUIT exoskeleton concept and scheme of actuation system [22].

Sometimes, active exoskeletons also perform passive DOF. This is the example of IntelliArm that provided 7 active DOF, and 2 passive DOF, to compensate for the movements of the shoulder girdle [23]. The movements of abduction/adduction and shoulder flexion/extension are controlled by two motors remotely placed that actuate them through closed-loop cable transmission. Instead, for the vertical shoulder displacement, the mechanism includes a dc motor attached to a linear guide. Although the exoskeleton possesses four motors on the exoskeleton, the three distal motors compensate the additional weight on the arm. Besides, it incorporates a DOF for hand opening/closing, in addition to DOF for the shoulder, elbow and wrist joints.

The ShoulderRO, that does not use electric motors, also possess two passive joints at the coupling point with the arm to allow the movements of the shoulder girdle [24]. This exoskeleton robot takes the shape of a poly-articulated structure actuated by two linear actuators through a Bowden cable transmission and a mechanical inverter device. It is light and small enough to be worn at its proximal end by the patient using a back harness. The structure is composed of a base module, rigidly fixed to the back of the patient, followed by a succession of  $N$  elementary and identical modules, shown in Figure 2.9-a-b. These are composed of two rings and four hinges. serially and perpendicularly placed in twos for giving two rotational DOFs around two perpendiculars axis to each module. It permits a sufficiently large workspace avoiding singularities, but it is just for the shoulder.

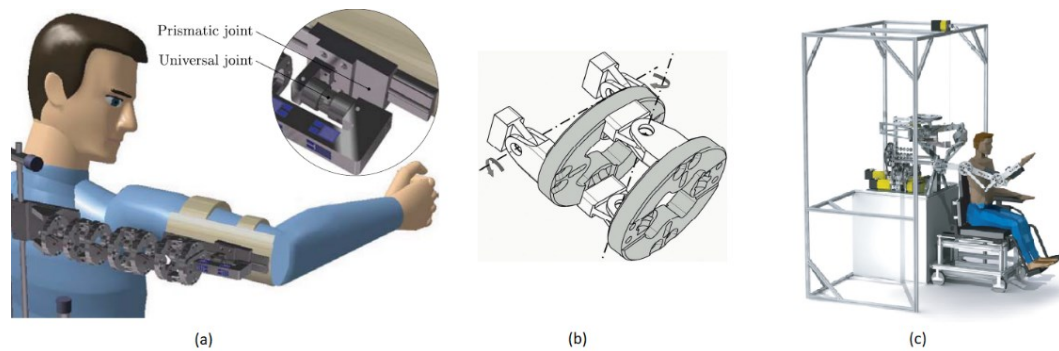


Figure 2.9 (a) ShoulderRO prototype [24]. (b) ShoulderRO elementary modules of the poly-articulated structure [24]. (c) Medarm structure [26]

For SUEFUL-7, the movements of the shoulder complex are transferred by pulleys from motors connected to a steady base except for the internal/external rotation, which occurs due to a spur gear connected directly to a motor [25]. The possibility to be placed on a wheelchair is an advantage of Sueful-7, due to its compactness. Besides, it uses an electromyography (EMG) based control method that determine the required torque of each joint from 16 different EMG signals. Yet, there is a difficulty in the design, because of the spur gears, thus the alignment of the transmission system may difficult its construction. Another advantage is the implementation of a slider mechanism to adjust the misalignments in the shoulder joint. This mechanism is exclusive of the shoulder again.

Then, MEDARM includes 5 DOF to completely emulate the shoulder complex movements, beside 1 DOF of elbow, employing rotatory electrical motors [26]. All the movements are controlled using an open-ended cable system with pulleys, that act on different planes, by using an idle pulley to maintain the tension along the range of movement. Although, the mechanism tends to be heavy and bulky, putting high static torque requirements on the first shoulder girdle joint. In order to make the mechanism work, an external gravity compensation system is employed. MEDARM uses a spherical joint to minimize the effects of singularities within the workspace, that are the main non-linearity considered in the design. The MEDARM structure is reported in Figure 2.9-c.

However, as cables cannot transmit compression forces, most cable transmissions require the utilization of an antagonistic force to control the bidirectional joint movements.

Much research has gone into investigating the complicated relationship between EMG waveforms and joint torque, and this suggests that EMG is a useful measurement for assistive and rehabilitation robotic devices. EMG recordings of the muscles of the upper limb are meant to recognize the intended poses or directions of movements from patients.

An example is EMG-Equipped MAHI Exo-II [80] (see Figure 2.10 left). It is a robot exoskeleton designed for the rehabilitation of elbow, forearm, and wrist, with DC motors that drive capstan driven joints, with the help of the EMG-control system. It also features passive gravity

compensation at the elbow joint. The MAHI Exo-II is equipped with optical encoders at each of the motors, from which it is possible to extract position and velocity of all DOF.

Another example is MyoPro, by Myomo, which is a lightweight electric motor-driven hand and elbow orthosis [80] (see Figure 2.10 right). The powered robotic brace amplifies weak muscle signal to help bend the arm and hand in the desired direction, and so to help move the upper limb. Its goal is to return functionality to the arm and hand to enable the execution of everyday tasks, by using intuitive controls by detecting EMG signals. When the user tries to move the arm, the device works by reading the faint nerve signals (myoelectric signals) from the sensor system on the surface of the skin, then it activates small motors to move the limb as the user intends. Therefore, the user is completely controlling its own hand, wrist, elbow, and arm.



Figure 2.10 MAHI Exo-II rehabilitation exoskeleton [80] (left), MyoPro orthosis [80] (right)

A drawback of rigid body exoskeletons, employing electric motors, is their inability to show natural compliance and to comply with natural human body movements in a flexible way.

To get the required compliance, the electric motor must be controlled. Yet, algorithms for compliant control may prove complex, and if not tested thoroughly, may yield errors that prove hazardous to the patient.

A compliant robotic upper extremity exoskeleton for rehabilitation is CRUX, proposed by Lessard et al. [79]. It is a 3-DOF active compliant exoskeleton, which can conform to the nonlinear musculoskeletal structure, besides, it used a cable-driven mechanism to transmit the power mechanically. These cables were routed on the base layer of the exoskeleton and used to directly supplement the human arm with 6 micro-DC motors mounted on the backplate. The routing path of cables was chosen so that they can supplement the influential muscle group of the human upper limb. Later, the design of CRUX was improved by introducing some extra safety features. A set of inertial measurement units (IMUs) was also used to avoid any harmful configuration achieved by the exoskeleton robot. However, there is no comprehensive study measuring the effectiveness of CRUX for the active assistance and the design needs some additional degrees of freedom to adopt actual human biomechanics.

Instead of having a stiff mechanical design and a compliant control, a better approach could be to use a compliant mechanism, like pneumatic actuators.

### 2.3.2 Pneumatic actuator driven exoskeletons

Two types of pneumatic actuators have been developed till now: pneumatic cylinders and artificial pneumatic muscles (PAMs or PMs). Pneumatic cylinders have formed a simple low-cost actuation source which has been used for many years in mechanical and prosthetic applications, and they are well adapted to simple repetitive tasks requiring only a very limited amount of system control [27].

However, they have not been widely applied in advanced robotics, because of some main problems due to the compressibility of the fluid, such as low accuracy, difficulty of control, and compliance, that means that by varying the load, the position of the piston is significantly affected. Despite they can provide a good control of the force, they cannot offer precision in motion control. Instead, their compactness, high power-weight ratio and safety are good advantages to be exploited in robotic applications.

Nonetheless, the cylindrical shape of the actuators and because the transmission of the force occurs through a piston, make the loading and variable supply pressure to affect the accuracy of position of the system. For this reason, pneumatic muscle actuators have been brought out to overcome these issues, thanks to their elastic material, that forms a seal to limit and control the expansions of the air and control the motion of the actuator. Thus, the idea of a braided pneumatic muscle, the McKibben muscle was developed for prosthetic applications in the 1960s [28-29]. Although, it fell into disuse because of the complexity of control.

Pneumatic artificial muscles are thought to exhibit similar properties as the human muscles. They are composed of an expandable bladder inside of a braided shell. When the bladder is pressurized, it expands in the radial direction against the braided shell, making it to contract.

Nevertheless, PAMs add additional issues to consider when implementing them, such as complexity in the control, and, such as pneumatic cylinders, they are not suitable for motion control. Their principal drawback is that they have a slow response time in force generation, and a low bandwidth which limit their capacity to respond to command signals. Besides, PAMs have a restricted range of motion that depends on the length of the braided shell, and the force exerted during their short stroke is variable. In fact, PAMs can exert a high force at the beginning of the stroke and a smaller one at the end of it. In addition, the exerted force is difficult to control, because of a high nonlinear behaviour. Eventually, they have a variable stiffness, which increases by increasing the pressure, and it decreases by increasing the contraction, tending to a constant value [30-31].

Nevertheless, these actuators have some advantages over motors. The most significant is the high power-to-weight ratio, they are safer to wear, applicable in harsh conditions and environment, and have a lower price. Then, PAMs can exert a high force, need little

maintenance, show flexibility, compactness, and natural compliance, due to air compressibility, so they do not require compliant control algorithms.

An active exoskeleton for rehabilitation, actuated by low-cost pneumatic muscles, is RUPERT [32]. This is a portable upper limb exoskeleton robot, developed by Arizona university, that uses unpaired compliant and safe PAMs to provide movement for 5 DOF of the upper limb (see Figure 2.11-b). Each segment of the device is adjustable to accommodate the variable arm lengths. Yet, the joints can only be actuated in one direction since only one PAM is used for each DOF. It invoked an iterative learning controller to overcome the highly non-linear nature of the PAM actuators and the patient's limb, as well as to adapt to different subjects for performing different reaching tasks (adaptive control). Consequently, this device supports only programmed and repetitive activities, therefore all movements must be defined and programmed. Although being a bit bulky, this exoskeleton robot is very low-weight and compliant, thanks to the pneumatic muscle actuators. As others rehabilitation devices, RUPERT employs EMG (electromyography) control in order to obtain user intention, that is useful for fatigue monitoring, without requiring training.

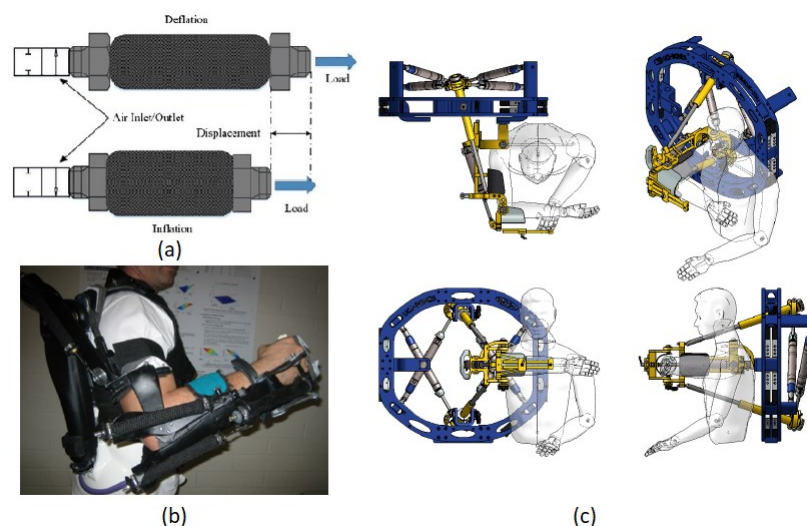


Figure 2.11 (a) A McKibben PAM [71]. (b) Rupert exoskeleton [32]. (c) Views of BONES design [34]

Another system, driven by pneumatic soft actuators, is ASSIST, that is a light weight 1-DOF exoskeleton robot which can be used to assist the wrist flexion/extension motion of elderly [33]. The main advantage of this device is relieving of the restrained feeling when the device is not operated, which is obtained by the plastic interface.

Then, a similar system for rehabilitation is BONES, the Biomimetic Orthosis for the Neurorehabilitation of the Elbow and Shoulder [34] (see Figure 2.11-c). It possesses 4 active DOF by exploiting pneumatic cylinder actuators, together with valves and sensors to provide force control. Four pneumatic actuators are placed behind the main structural frame to control shoulder motion via the sliding rods, and a fifth cylinder is located on the structure to control

elbow flexion/extension. The device fulfils a wide range of motion of the human arm, while achieving low inertia and generating a direct force at the shoulder. A key accomplishment of this design is the ability to generate arm internal/external rotation without any circular bearing element such as a ring. In order to obtain a light-weight robot as well as a good force control, it uses a simple parallel mechanism with mechanically grounded actuators to achieve 3 DOF shoulder movement, including shoulder internal/external rotation. The robot incorporates a serially placed actuator for elbow flexion/extension, by using a pneumatic actuator for this DOF to achieve large force output. The arm is actuated at the elbow by means of two rods that can passively slide. Elastic elements, located in parallel with the first three cylinders, provide weight support for the exoskeleton. In case of emergency or power outage, the exoskeleton returns to the home position, so the subject's arm does not fall. The elements also bias the force operating range of the actuators so that they have a greater, bi-directional range.

Although, in comparison to electric motors, one limit of pneumatic artificial muscles, is that they are single direction-acting elements, thus they can only generate a tension force, through contraction. Therefore, a pair of opposed PMs, as flexor and extensor, is required to drive each DOF to generate bidirectional force and so bidirectional movement, as shown in Figure 2.12-a, where  $\alpha$  is the rotational DOF.

The 7-DOF "Soft Actuated" exoskeleton robot, developed by Tsagarakis and Caldwell for training and rehabilitation purposes, is an example [35]. This active device employs pneumatic muscle actuators especially as an antagonistic pair, generating a bidirectional force, as shown in Figure 2.12. Safety, human 'soft' interaction, low mass, excellent power-weight ratio, thanks to PMs which provide safety and compliance, are amongst the advantages. The motion is achieved producing appropriate antagonistic torques through cables and pulleys driven by the pneumatic actuators. The two opposed acting elements work together in an antagonistic scheme simulating a biceps-triceps. By exploiting the pair, this device takes advantage compared to most of the other systems which use software control methods to regulate their compliance. The PM is constructed as a two-layered cylinder. Besides, the actuators are highly tolerant of mechanical misalignment and the antagonistic action allows compliance control. The pulleys are fastened on the joint shafts and rotate on bearings to minimise friction. The activation of the PM relies on the effective control of the airflow into and from the muscles. This occurs, by monitoring MATRIX valves, that are controlled using a pulse width modulation (PWM).

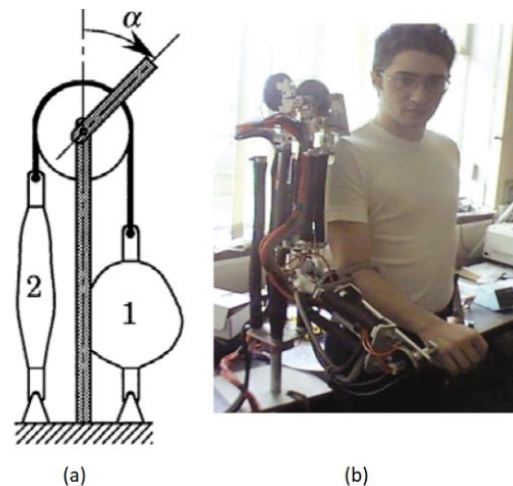


Figure 2.12 (a) Antagonistic pair of PAMs to drive a revolute joint [30]. (b) 7-DOF “Soft Actuated” exoskeleton robot [35]

### 2.3.3 Hydraulic actuator driven exoskeletons

Hydraulic actuators can exert a high constant force, showing a larger torque than other actuators, and a good precision. Despite, they are heavy, require pumps and valves to operate, besides suffering from fluid linkage.

An example of active exoskeleton device, driven by hydraulic power, is NEURARM [36]. It is a 2-DOF planar robotic arm, actuated by Bowden cables and linear hydraulic actuators, that simulates the main functional parameters of the human upper limb. Thus, because of the simplified model, NEURARM is a light robot. Yet, mechanism does not provide the means to deal with the variation of the centre of rotation of the anatomical shoulder joint. The control strategy includes the non-linearities of the actuation and implements a controller to handle the position of the pistons.

Another example is NEUROExos [78], which is a 1-DOF active elbow exoskeleton, as well driven by linear hydraulic actuator. It includes also a 4-DOF adaptive passive compliant mechanism to handle the misalignments of the elbow, employing an antagonistic non-linear elastic action system. The system of actuation is a Bowden cable actuation system with a no linear elastic element, that is based on a linear tension spring coupled with a cam mechanism (see Figure 2.13). NEUROExos links are designed to fit the form of the user’s limb segments and distribute the interaction force between the user and the robot. It has double shelled connections composed of an inner and outer concentric shell. The outer shell provides stiffness and strength to the robot, also optimizing material distribution around the limb to reduce the possibility that the assistive load applies an uncomfortable torque. Instead, the inner shell has two half-shells, both made in ergonomic materials.

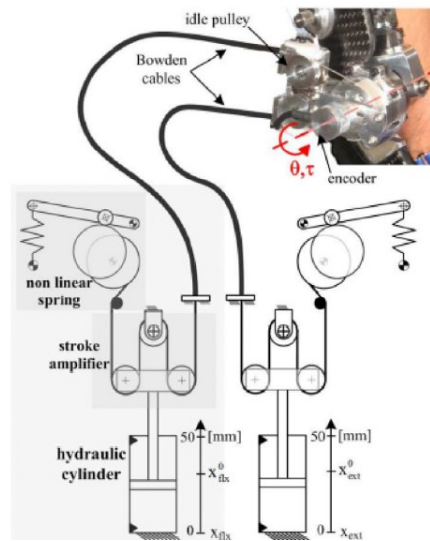


Figure 2.13 NeuroExos double-shell structured links [78]

### 2.3.4 Other actuation principles

A few non-standard actuation methods have also been tried for upper limb exoskeleton systems. For instance, some actuation units use shape memory materials, which are alloys, polymers and composites that can recover their shape after a plastic deformation is induced by phase transformation [83]. A shape memory alloy (SMA) is an alloy that remembers its original shape, so when heated above its transformation temperature, from its deformed shape, it returns to its preformed shape, thanks to the transition between the martensite phase, at low temperature, and the austenite phase at high temperature. The advantage of SMAs is their very high power-to-weight output. Among these alloys there are Ni-Ti (Nitinol is the most used) and Cu-Al-Ti.

An example of exoskeleton system that uses SMA is the Wearable elbow exoskeleton, developed by Copaci et al. for medical rehabilitation [84]. This exoskeleton is actuated by SMA wire-based actuators, that contribute to lightweight and low noise. The SMA material varies its shape due to a change of phase, induced by the Joule effect that produces a higher temperature, at which the phase transformation occurs. Another similar system is the Soft glove conceived by Villoslada et al. [85] for rehabilitation and assistance.

Another type are piezo-electric actuators [86], for controlled micro-manipulation and applications in micro-robotics. Then, in some devices, magneto-strictive materials are employed, for their high force generation potential [87]. Finally, De Rossi et al. [88] have been developing wearable garments using electroactive polymers which allow strain sensing and actuation. These haptic systems are not exoskeletons, but they can be integrated in other equipment for rehabilitation or medical exercises.

## 2.4 Passive exoskeleton systems

Compared to active exoskeleton systems, passive exoskeleton systems are potentially less effective, but they are lighter and simpler because no control is present, providing a high power-to-weight ratio. Passive exoskeletons cannot actively assist movement, so they are limited to generating resistive forces and gravity balancing, for instance, they are used to balance the gravity potential of the human arm [37].

Springs and dampers are often used as “passive actuators”, to provide a resistive force in order to amplify human strength, by storing the energy and release it when needed, and/or transferring the force from one part of the body to another, without adding inertia [5]. In addition, these systems have the advantage that no electrical power is needed, which reduces the weight and volume of the exoskeleton. In this chapter, passive upper limb exoskeletons are classified according to their application.

### 2.4.1 Passive exoskeletons for assisting upper limb movement

Most of the current rehabilitation robots are actively powered and designed to assist arm movements when needed. Providing too much assistance may negatively influence the motor relearning as patients become less actively involved. Furthermore, increasing the therapy intensity can be achieved without active assistance. Then, active actuators may not always be necessary, and passive actuators can still facilitate limb movements, by adding a variable weight support to the device. This idea is meant not only to provide help patients, but also to keep them actively involved [38].

An example of passive exoskeleton, for assistance to disabilities, is WREX (Wilmington Robotic Exoskeleton), that possesses 4DOF [39]. It employs elastic elements that balance the effects of gravity so that the patient can move the arm with minimal effort. WREX is easily mounted to a wheelchair (see Figure 2.14-a). The torques required at the shoulder are, however, nonlinear. The exoskeleton is composed of two links that shadows the upper arm and forearm, arranged in the shape of a parallelogram for the upper arm and a single link for the forearm. Each limb has its own antigravity component as a direct result of the parallelogram structure of the upper-arm linkage. Besides, the WREX is sized for each user and a custom back brace is moulded for each user. Yet, a slight misalignment of the elbow joint occurs.

Another example is the DAMPACE (Figure 2.14-b), that uses hydraulic disk brakes to generate controlled resistive torques for rehabilitation and training. There are additional mechanisms in the exoskeleton to auto-align the exoskeleton joints to the human joints, thus the shoulder joint is fully free to translate in any direction. An overhanging cabling system, connected to a balanced spring mechanism at the base of the Dampace, implements the compensation of the weight of the exoskeleton. Finally, the feedback control is based on the state of the arm [40].

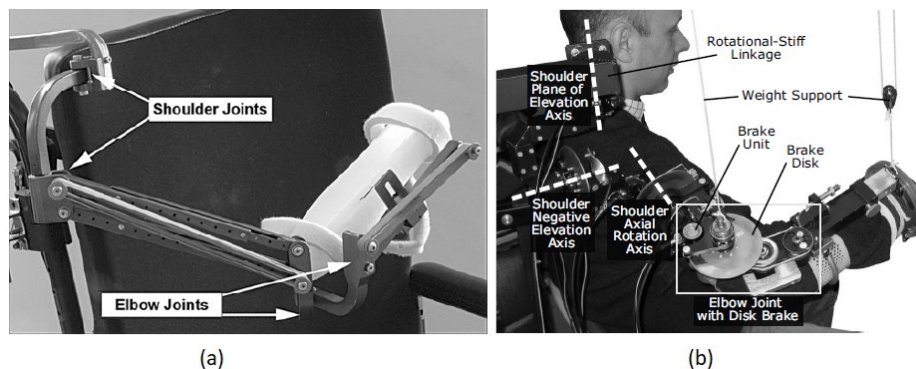


Figure 2.14 (a) Joint configuration of the Wrex [39]. (b) Shoulder and elbow axes of the Dampace [40]

## 2.4.2 Passive upper limb exoskeletons for overhead tasks

Exoskeletons have been developed mainly for medical rehabilitation, medical assistance, and military applications. However, manipulation of heavy goods as seen in industrial applications are rarely addressed, because drawbacks in these applications are the restricted power availability and the weight and volume of the exoskeleton.

Yet, work-related musculoskeletal disorder (WMSD) in the upper extremity is an increasingly concerning issue in modern workplaces, and it is often caused by repeated or long-term physical work, that represent a major health issue and an important cost for companies [41,50]. Even without external load or force exertion, supporting the arms' weight imposes prolonged stress on shoulder muscles.

Although automation has been increasing since years, numerous hard tasks cannot be automatized at all, and human flexibility and cognitive skills are still needed. In order to relieve workers while performing tasks, or keeping them in some uncomfortable position, one solution is to assist them with an exoskeleton.

Exoskeletons can provide physical assistance to its user, by generating torques and structural support. For this reason, they have become appealing for industrial applications, because they fulfil in (at least partially) relieving the wearer from heavy loads, reducing muscular activity during limb movements, reducing the efforts on the limb while performing overhead tasks. In addition, because the system is worn on the body and follows the user's movements, very little, or no, modifications of the workplace occur [5].

Most of these systems are passive, to limit the weight of the device worn by the user, employing spring and damper systems. Moreover, upper arm exoskeletons are required to be passive, without external power sources, because it is difficult to manage regular battery replacement for powered type exoskeletons especially in industrial environments. Recently,

several industrial prototypes providing arm support during overhead tasks have been developed, tested and some are already commercialized, as the following.

A commercial passive exoskeleton, for worker assistance during overhead tasks, is MATE, developed by Comau [42]. The main achievement of its design, weighing 3.5kg, is the reduction of muscular activity up to over 30% during shoulder flexion/extension. Besides, it allows adjustability to different body sizes, pressure distribution, lumbar support, stability, reduced muscular fatigue, improvement of posture and reduced likelihood for diseases, comfort, high breathability, high precision, by following physiological movements without resistance or misalignment. This is achieved through a passive mechanical shoulder chain, that employs a passive spring-based mechanism, within a torque generator box that stores and transforms mechanical energy in order to create an adjustable assistive torque, effectively transferring the loads (see Figure 2.15 left). In addition, the assistance is adjustable, by tuning the assistant torque among 7 levels.

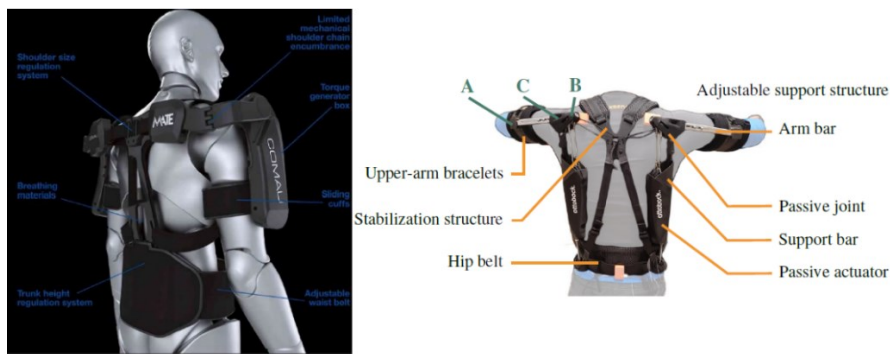


Figure 2.15 Mate exoskeleton by Comau [42] (left). PAEXO structure [43] (right)

Another commercial passive exoskeleton for overhead tasks is PAEXO, developed in to help prevent shoulder injuries and diseases [43]. The results show that using PAEXO reduces shoulder physical strain, without increasing low back strain. It is meant to maintain the user's freedom of movement, transferring a portion of the arm weight from the upper-arm bracelets to the hip belt. Its structure, see Figure 2.15 right, is composed of a support bar and an arm bar that are connected through a hinge joint, that is the passive joint. A passive actuator based on a spring produces the support torque in this joint. The structure is connected to the hip with a belt through a passive ball joint. By adjusting the length of the bars and width of the belt, the whole structure can fit different body sizes.

The Airframe, by Levitate Technologies, was meant to be a passive exoskeleton to assist automotive workers in tasks that involve postures with elevated arms or require repeated arm motion [4]. It had proved to succeed in increasing worker endurance time, while in a posture with raised arms, and work performance, lowering muscle activity by up to 80%. Besides, testers had perceived fatigue to be less when wearing the exoskeleton when than not. Along the arm, mechanical passive elements (springs) are present to partially relieve upper limb

muscles and shoulder joint by transferring the weight of the arms from the shoulders to the core body. The system consists of a metallic frame, cables, pulleys, springs, and aluminium tubing (see Figure 2.16-a). The mechanical elements are ineffective when the arm is in a neutral position, while the support progressively increases when raising the arm, and gradually releases as the arm is lowered.

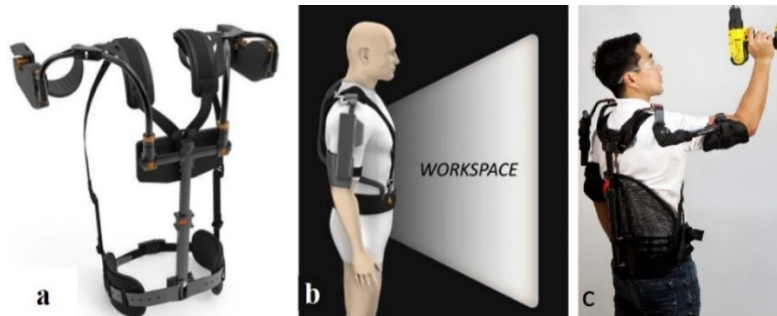


Figure 2.16 (a) Structure of the Airframe exoskeleton by Levitate technology [4]. (b) Workspace of the Airframe [4]. (c) ShoulderX exoskeleton by SuitX [44]

In the ShoulderX, by SuitX, weighing 5.4 kg, the energy store mechanism is a mechanical support structure (leverage), see Figure 2.16-c [44]. It balances the combined weight of the wearer's arm and tools they are holding throughout the body's range of motion, and it can be tuned for different levels of support. Tests have measured that employing the prototype has reduced muscle activation by up to 81%.

Eksovest (from Ekso Bionics), weighing 4.3 kg, also employs a mechanical support structure as energy store mechanism. By wearing the prototype, the level of perceived discomfort for the forearm changed in different work simulations and median muscular activity of shoulder complex was significantly reduced up to 50%. Although working errors increased when using the exoskeleton, the complete time was reduced by 20% while performing overhead work. Yet, shoulder ranges of motion were a bit reduced with the exoskeleton [45]. The evolution of Eksovest is EVO, that manages to lower the bulkiness and weight of the vest.

Hieber, developed by Hyetone [46], provides a high degree of freedom, with a total weight of 1.9 kg, which is lighter than other similar systems (Eksovest, SuitX, MATE). A passive suspension system performs actuation on this passive upper extremity exoskeleton (PULE) and each energy store unit is an actuator driven by a tension spring, see Figure 2.17-a. It generates a torque that gradually increases as the user lifts his arms and decreases when the arms are lowered. In the assessment, physical demands were evaluated using subjective ratings, through EMG signals of selected muscle groups. Tests proved that using the PULE would greatly reduce the physical demands of the muscles of the upper limb [47].

Skelex, weighing 3.4 kg, is another already commercialized passive exoskeleton, that can support biological movement of the shoulder joint, by transferring the weight of the arm, and

possible load in hand, to the lower body, see Figure 2.17-3b. It stores and releases energy in order to compensate the gravity, ensuring comfort of users [48].

EXHAUSS's Stronger is another passive upper limb exoskeleton, weighing 9 kg, meant to assist the user while lifting arms and/or holding objects. It consists of two mechanical arms activated by springs mounted on the support arms, as shown in Figure 2.17-c. The arms are linked to a rigid wearable jacket, with joints, allowing free 3D movements. Applied for shoulders and arms, the assistive torque can be adjusted by prestressing the springs. The energy delivered during arm elevation (shoulder flexion) had to be stored previously through the compression of springs (shoulder extension). In this way, this exoskeleton provides non-linear arm lift assistance over an angular range from  $0^\circ$  to  $135^\circ$  of the shoulder anterior flexion. Results showed that the exoskeleton led to significant reduction of shoulder group muscle activity during load lifting and stacking/unstacking tasks, corresponding on average to 54% and 73% respectively of the EMG activity recorded during the same tasks without the equipment [49].

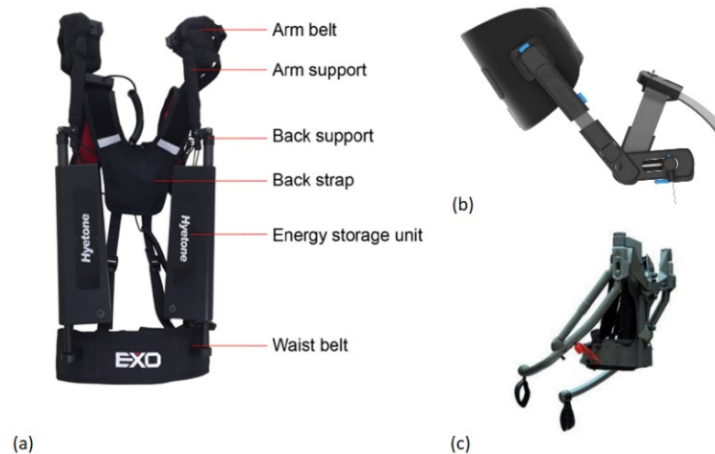


Figure 2.17 (a) Hieber structure by Hyetone [46]. (b) Skelex exoskeleton [48]. (c) Exhauss's Stronger exoskeleton [49]

Hyundai Vest Exoskeleton (H-VEX) is a passive upper exoskeletal vest, developed for assisting overhead tasks in automotive manufacturing centres [51]. It proposes two mechanical elements, see in Figure 2.18: the first is an energy-storage multi-linkage mechanism dissipating spring-loaded energy according to the elevation angle of the wearer's upper arm in order to generate a proper assistive torque, and the second is a poly-centric shoulder joint mechanism on the transverse plane for its proper alignment with the wearer's shoulder joint movement, with the aim to make the exoskeletal shoulder joint well match to shoulder kinematics without large increase in exoskeletal shoulder mass. In fact, another objective of the design, was to keep the overall weight relatively low, reaching about 2.5 kg.



Figure 2.18 Hyundai Vest Exoskeleton (H-VEX) for assisting industrial overhead tasks [51]

Robo-Mate design also employs springs, mounted on support arms, as energy store mechanism. Its equipment weights 3.7 kg per arm [52]. Tests showed that muscle activity was significantly reduced, up to 50%, while lifting a 2 kg load and arms in horizontal position, with respect to performing the same task without the exoskeleton. Besides, perceived effort of the arm was significantly reduced.

Stuttgart Exo-jacket is an exoskeleton proposed for motion assistance in industrial applications by considering the ergonomic aspects [53]. It possesses 9 passive DOF, and 3 active DOF, in fact it was designed to actively support the extension and flexion of the shoulder and elbow joint. However, it was noted that the micro-misalignment caused by the non-coincident centre of rotation between human arm joints and exoskeleton joints is a critical issue, that was minimized by directly installing the drives at joint location. Moreover, a gas spring mechanism, mounted on the back of the user, help to bypass the applied forces on the human elbow and shoulder joints. The jacket also has a passive lower-extremity unit, for helping to ground the applied forces on the upper-limb unit.

Delft upper limb exoskeleton is the design developed by the Universiteit Delft [54], that is able to transmit the angular load between the arm and the direction of gravity to the back, through a link mechanism. It also ensures freedom of the upper limbs. The balance spring is installed on the back of the exoskeleton, shown in Figure 2.19 left, whose elastic potential varies with the angle between the arm and the direction of gravity, in order to achieve the balance of the gravity potential of the human arm; this design have the advantage to allow achieve a zero-work requirement in any position.

The spring is often regarded as the passive energy source in passive exoskeletons. But, because of their low energy density, when the machine needs to support have a heavy load a problem can occur. So, a gas spring can significantly improve the energy density.

This is why a gas spring has been employed for designing the Automatic load-adaptive passive upper limb exoskeleton, developed by Zhu et al [55]. The main purpose of the exoskeleton is to offset the gravitational load due to human upper limb, exploiting the gas spring, that can be regarded as an approximately constant force spring, in order to achieve the transformation between elastic potential energy and gravitational potential energy (see Figure 2.19 right). The

overall structure is implemented in order to keep the relationship, between the gas spring force and the gravity force, directly proportional.

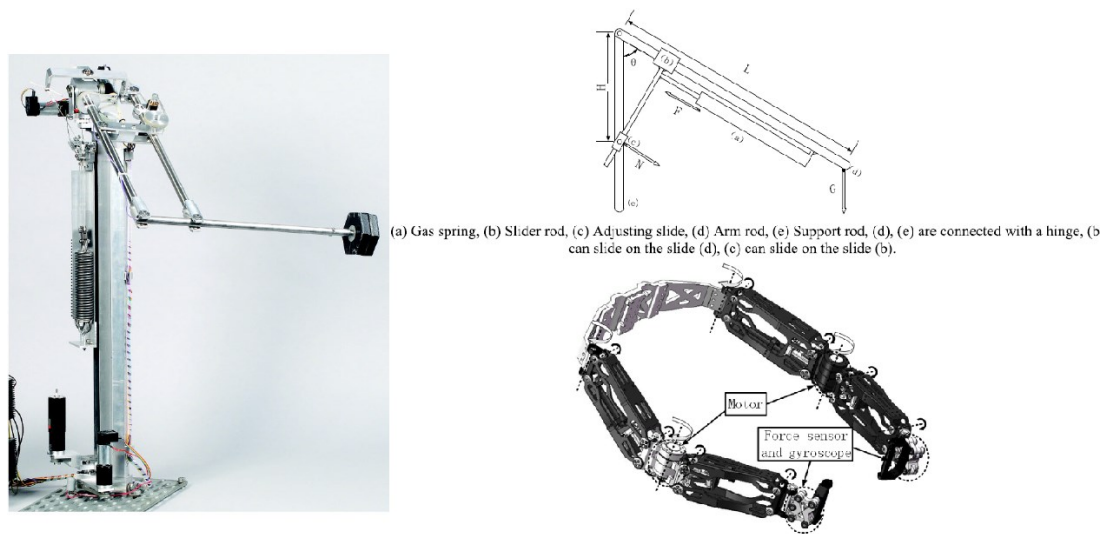


Figure 2.19 Manipulator prototype developed by Universiteit Delft (left) [54]. Upper limb exoskeleton developed by Zhu et al. (right): gas spring mechanism (top), overall structure (down) [55].

The advantage of springs is lightweight, high strength, excellent elastic properties, and their ability to regain their shape after bending, till certain limit. Moreover, springs are appealing because they use stored energy, without adding inertia, to balance the gravitational force of the upper limb and eventual loads, despite counterweights. Yet, sooner or later, they lose their shape and elastic characteristics, and their repair process is complex.

## 2.5 Comparison of upper limb exoskeletons

As seen from former paragraphs, most commercial passive upper limb exoskeletons employ passive spring-based mechanisms to balance the gravitational force, or at least to partially compensate that.

Several tests have been carried out to estimate the effectiveness and consequences of these exoskeletons on the wearer's upper extremity muscles, while performing different static or dynamic tasks [4,43,49,51]. By using different benchmarks, these tests have proved an actual muscle activity reduction of at least almost all the muscles involved, a peak fatigue reduction, and work performance increase.

HIEIBER exerts a torque that gradually increases as the user lifts his arm and decreases when the arm is lowered. The same can be observed with AIRFRAME (by Levitate technology). The energy delivered during shoulder flexion had to be stored previously via the compression of springs.

Otherwise, springs lose shape and stability as time goes on, therefore, for the passive exoskeleton design submitted in this paper, pneumatic artificial muscles are suggested, also because of their lightness and natural compliance.

Other pneumatic upper limb exoskeletons have been designed, such as BONES, that provides a shoulder flexion range of motion of  $100^\circ$ , and weight support through elastic elements, or RUPERT which exploits PAMs as actuators, performing a natural compliance control, and more flexible movements than electric motors. However, these last two require pneumatic valves and force sensors that raise the complexity and price of the device, allowing only programmed activities.

Despite being an active exoskeleton as well, the 7-DOF "Soft actuated" exoskeleton design can be observed, as it shows a shoulder flexion/extension angles up to  $110/25^\circ$  of the training arm, thanks to the antagonistic pneumatic pair, and an achievable output torque of  $30 Nm$ , considering a  $110 Nm$  human strength. In this design, two muscles are along the upper arm and forearm, and the choice of their active length and diameter depends on range of motion of the joint and the torques required.

Although, for working assistance applications in industrial environment, a passive exoskeleton is preferred because no force or position control is needed. In fact, since this design is meant to aid the user on overhead tasks with elevated arms, it needs to be simple, lightweight, and natural compliant, letting the user's movement, without limiting the degrees of freedom of the shoulder complex.

For this reason, pneumatic artificial muscles are suggested in place of springs, also because of their spring-damper-like behaviour, as shown later in this paper.



## Chapter 3

# Original exoskeleton design

During industrial overhead tasks, the contraction of the human shoulder complex muscles should balance the torque generated by the weight of arm's segments. Yet, if the user is required to keep his arms lifted for a long time, also carrying an eventual load or a tool in hand, a compensating device is needed, in order to reduce the effort on shoulder muscles and hold the arms in that position.

The torque (or moment) due to gravity can be calculated from the inertial body parameters, as shown in next paragraph. This torque assumes the maximum value when the elevation angle  $\vartheta_1$  of the upper arm (that consists mainly in shoulder flexion), with respect to vertical position, is  $90^\circ$  and the forearm elevation angle (elbow flexion)  $\vartheta_2$  is  $0^\circ$ .

Since the upper limb exoskeleton is meant to assist the user during overhead tasks, the range of elevation angle of interest is assumed to be from  $\vartheta_1 = 90^\circ$  (when the upper arm is horizontal) to  $120^\circ$ -  $135^\circ$ . In these applications the shoulder internal/external rotation is assumed to be null, as the shoulder abduction/adduction rotation. To accomplish the compensation of the gravitational torque, pneumatic artificial muscles are suggested for their ability to exert a high force by contraction. Thus, their characteristics and modelling are discussed in the following paragraph.

### 3.1 Standard human body inertia parameters

In order to evaluate the contribute of the exoskeleton in compensating the gravity force of the upper limb, a standard of body segment inertia parameters (BSIPs) must be defined.

Several studies have been carried out for estimating human inertial characteristics, which mainly consists in mass, position of the centre of mass, length of body segments, radii of gyration and moment of inertia.

In this paper, the Zatsiorsky et al.'s body segment inertia parameters, adjusted by de Leva, have been chosen, to estimate the characteristics of the upper limb [73]. Through a gamma-ray scanner, Zatsiorsky et al. defined the BSIPs of 100 male and 15 female Caucasian subjects (mean ages: 24 and 19 years, respectively). Though, for estimating the inertial properties of healthy young adults, other biomechanical analyses' data have often been preferred to their results, probably because Zatsiorsky's group used bony landmarks as reference points for locating segment centres of mass (CMs) and defining segment lengths. Some of these points are rather distant from the centres of the neighbouring joints. Consequently, when a subject bends his joints the distances of these reference points from the respective proximal or distal

segment CMs significantly decrease. These and other related changes, which make it impossible to accurately locate segment CMs, can be minimized only by using joint centres as reference points.

For this reason, the purpose of de Leva's research was to adjust the mean relative CM positions and radii of gyration reported by Zatsiorsky's group, to reference them mainly to the positions of joint centres rather than bony landmarks. In some cases, the original landmarks were either considered adequate, or substituted with other commonly used bony landmarks.

Figure 3.1 reports the longitudinal length, the mass (relative to body weight), longitudinal CM position (relative to the respective segment lengths, with respect to proximal joint or other endpoints) of the different segments, which are the adjusted parameters for male subjects whose mean stature is 1.741m and mean weight equal to 73.0 kg, and for females subjects whose mean stature is 173.5m and mean weight 61.9 kg.

Segment	Endpoints		Longitudinal length (mm)		Mass* (%)		Longitudinal CM position (%)		Sagittal r (%)		Transverse r (%)		Longitudinal r (%)	
	Origin	Other	F	M	F§	M¶	F	M	F	M	F	M	F	M
Head	VERT†	MIDG†	200.2	203.3	6.68	6.94	58.94	59.76	33.0	36.2	35.9	37.6	31.8	31.2
Trunk	SUPR†	MIDH‡	529.3	531.9	42.57	43.46	41.51	44.86	35.7	37.2	33.9	34.7	17.1	19.1
UPT	SUPR†	XYPH†	142.5	170.7	15.45	15.96	20.77	29.99	74.6	71.6	50.2	45.4	71.8	65.9
MPT*	XYPH†	OMPH†	205.3	215.5	14.65	16.33	45.12	45.02	43.3	48.2	35.4	38.3	41.5	46.8
LPT	OMPH†	MIDH‡	181.5	145.7	12.47	11.17	49.20	61.15	43.3	61.5	40.2	55.1	44.4	58.7
Upper arm	SJC‡	EJC‡	275.1	281.7	2.55	2.71	57.54	57.72	27.8	28.5	26.0	26.9	14.8	15.8
Forearm	EJC‡	WJC‡	264.3	268.9	1.38	1.62	45.59	45.74	26.1	27.6	25.7	26.5	9.4	12.1
Hand	WJC‡	MET3†	78.0	86.2	0.56	0.61	74.74	79.00	53.1	62.8	45.4	51.3	33.5	40.1
Thigh	HJC‡	KJC‡	368.5	422.2	14.78	14.16	36.12	40.95	36.9	32.9	36.4	32.9	16.2	14.9
Shank	KJC‡	LMAL†	432.3	434.0	4.81	4.33	44.16	44.59	27.1	25.5	26.7	24.9	9.3	10.3
Foot*	HEEL†	TTIP†	228.3	258.1	1.29	1.37	40.14	44.15	29.9	25.7	27.9	24.5	13.9	12.4
Using alternative endpoints:														
Head*	VERT†	CERV†	243.7	242.9	6.68	6.94	48.41	50.02	27.1	30.3	29.5	31.5	26.1	26.1
Trunk	CERV†	MIDH‡	614.8	603.3	42.57	43.46	49.64	51.38	30.7	32.8	29.2	30.6	14.7	16.9
Trunk	MIDS‡	MIDH‡	497.9	515.5	42.57	43.46	37.82	43.10	37.9	38.4	36.1	35.8	18.2	19.7
UPT*	CERV†	XYPH†	228.0	242.1	15.45	15.96	50.50	50.66	46.6	50.5	31.4	32.0	44.9	46.5
Forearm	EJC‡	STYL†	262.4	266.9	1.38	1.62	45.92	46.08	26.3	27.8	25.9	26.7	9.5	12.2
Hand	WJC‡	DAC3‡	170.1	187.9	0.56	0.61	34.27	36.24	24.4	28.8	20.8	23.5	15.4	18.4
Hand*	STYL†	DAC3‡	172.0	189.9	0.56	0.61	35.02	36.91	24.1	28.5	20.6	23.3	15.2	18.2
Hand	STYL†	MET3†	79.9	88.2	0.56	0.61	75.34	79.48	51.9	61.4	44.3	50.2	32.7	39.2
Shank	KJC‡	AJC‡	438.6	440.3	4.81	4.33	43.52	43.95	26.7	25.1	26.3	24.6	9.2	10.2
Shank	KJC‡	SPHY†	426.0	427.7	4.81	4.33	44.81	45.24	27.5	25.8	27.1	25.3	9.4	10.5

Figure 3.1 Zatsiorsky-Seluyanov-de Leva adjusted parameters for males (mean weight 73.0 kg, mean stature 1.741 m) and females (mean weight 61.0 kg, and mean stature 173.5 m) [73].

In this paper, the average male subjects' BSIPs have been referred to estimate the upper limb's characteristics, reported in Table 3.1. They consist of the mass and length of the segments, the position of the centre of mass with respect to the segments' proximal joint, or with respect to the shoulder joint (SJ), while the arm is supposed to be totally extended, thus the upper arm elevation angle  $\vartheta_1$ , that consists mainly in shoulder flexion, is  $90^\circ$ , and the forearm elevation angle  $\vartheta_2$  (elbow flexion) and the wrist flexion angles are  $0^\circ$ .

Table 3.1 Average male subjects' BSIPs with totally extended arm.

	Mass [kg]	Length [m]	CM position wrt proximal joint [m]	CM position wrt SJ [m]
Upper arm	1.9783	0.2817	0.1626	0.1626
Forearm	1.1826	0.2689	0.1230	0.4047
Hand	0.4453	0.0862	0.0681	0.6187

Starting from these calculated data, the position of the centre of gravity ( $l_g$ ) of the overall upper limb, with respect to the shoulder joint, without any load in hand, has been evaluated as:

$$l_g = 0.2983 \text{ m} \quad (3.1)$$

Therefore, the torque due to gravity of the arm is calculated, from equation (3.2) by rotating the arm with an elevation angle from  $\vartheta_1 = 90^\circ$  to  $120^\circ$ , supposing the forearm elevation angle  $\vartheta_2 = 0^\circ$ . The torque due to gravity assumes the maximum value at  $\vartheta_1 = 90^\circ$ , when the upper arm and forearm are horizontal.

$$M_{dtg} = m_{arm} \cdot g \cdot l_g \cdot \sin(\vartheta_1) \quad (3.2)$$

Figure 3.2 reports the moment due to gravity with respect to  $\vartheta_1$  and  $\vartheta_2$ .

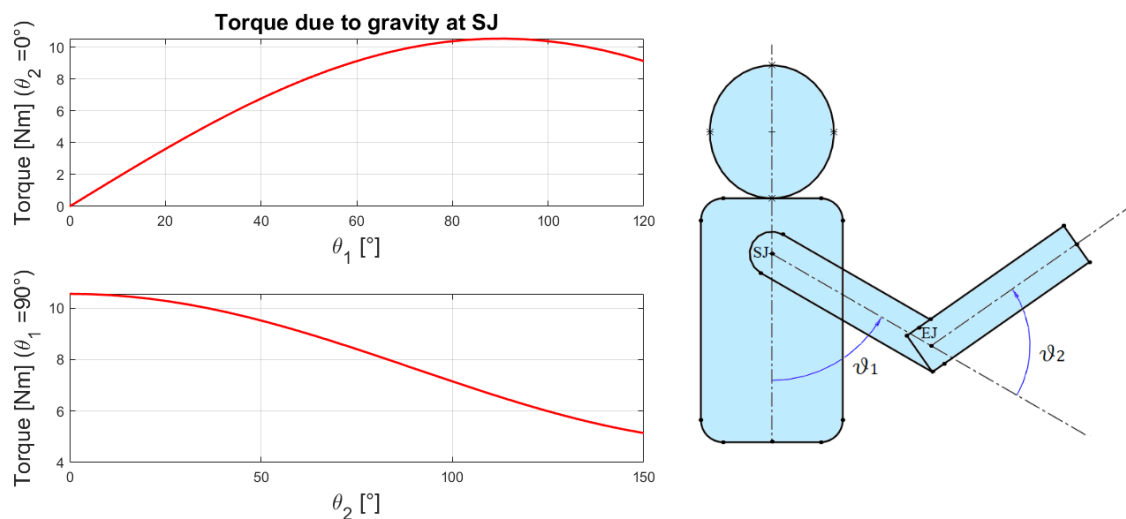


Figure 3.2 Moment due to gravity with respect to upper arm elevation angle  $\vartheta_1$ , obtained by rotating the upper arm around the shoulder joint, from  $\vartheta_1 = 90^\circ$  to  $120^\circ$  whilst forearm elevation angle  $\vartheta_2 = 0^\circ$  (top). Moment due to gravity with respect to forearm elevation angle  $\vartheta_2$ , obtained by rotating the forearm around the elbow joint, from  $\vartheta_2 = 0^\circ$  to  $150^\circ$ , whilst upper arm elevation angle  $\vartheta_1 = 90^\circ$  (down).

## 3.2 Pneumatic artificial muscles

As explained in the state of art, a particular kind of pneumatic actuators, less common than pneumatic cylinders, are flexible pneumatic actuators, which exploit the deformability of an elastomeric wall. Among these, there are pneumatic artificial muscles (PAMs or PMs). They are made of a thin-walled membrane, that delimits a chamber, in which the pressurized fluid acts. The chamber is subject to constraints that make it dilate either radially or axially. By pressurizing it, the PAM behave like a “pneumatic” spring when an external force is applied, exhibiting a variable stiffness during its stroke.

These devices are cheap, light, capable of great force-to-weight ratio, and power-to-weight ratio. Besides, they can operate in hostile environments, with strong temperature gradients, because they are not sensitive to high temperatures, thermal gradient, vibrations, dust, dirt, or electromagnetic disturbances. Finally, they do not need a precise alignment during the installation, thanks to the flexibility of the muscle.

The drawback of this kind of soft actuators is that they can apply a large output force, but for a restricted stroke with respect to its nominal length. There are different types of PAMs, as reported in Figure 3.3.

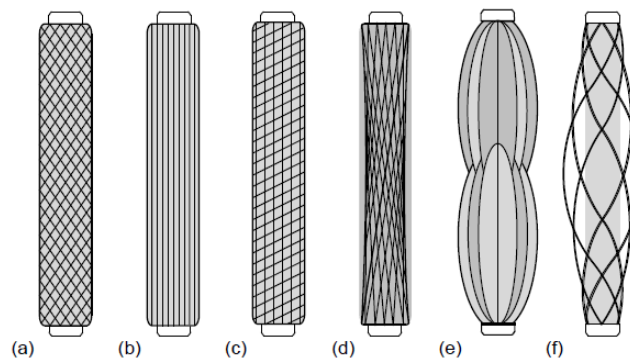


Figure 3.3 Types of PAMs: (a) McKibben muscle, (b) pleated muscle, (c) Yarlott netted muscle, (d) Painter hyperboloid muscle, (e) ROMAC muscle, (f) Kukolj muscle [61]

The most widespread PAM is the McKibben muscle, invented by an American physicist [56]. McKibben muscle is made of a braided outer mesh that encloses and constraints the rubber inside chamber, as shown in Figure 3.4 left. Both the chamber and the outer mesh are sealed and fixed to rigid terminal fittings, or heads, that allow the connection and air supply.

By pressurizing the inside chamber, the dilation of the chamber itself occurs, that is constrained by the inextensible fibres of the outer mesh around it. The fibres, anchored to the heads, get them closer, under the action of the pressurized fluid, making the chamber to

contract in axial direction and expand in radial direction. Thus, by pressurizing the inside chamber, the contraction of the PAM occurs, and a traction force is generated.

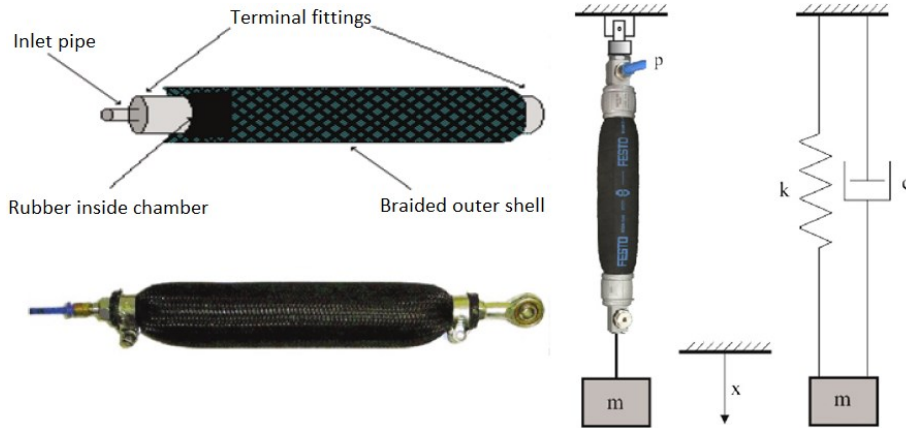


Figure 3.4 McKibben PAM design (left) [35], PAM modelled as a 1-DOF oscillatory system following modified Hill's model (right) [72]

The static characteristic of McKibben PAM represents the relationship between the pneumatic muscle exerted force  $F_{mu}$  and the muscle percentage contraction  $\kappa$ , occurring at a constant supply relative pressure  $p$ . This relationship has been the topic of several researchers, with the aim to bring out a good theoretical approach for the equation of force produced by PAMs [57-58-59-60].

Some of them have found out different mathematical models, in order to make the theoretical results to fit the experimental ones, and therefore to describe the real behaviour of PAMs, using the measured data.

The modified Hill's muscle model uses an engineering approach to muscle modelling, it is one of the oldest phenomenological models, that consists of a variable damper and a variable spring connected in parallel [61], (see Figure 3.4 right). This approach derives from the original viscoelastic two-element model proposed by Hill [67]. By using this muscle model, several approximations of the static characteristics have been worked out, including equations that relate the output force to geometric parameters of the pneumatic muscle, such as its initial radius and initial angle of the fibers. Yet, other approximations use a numerical function.

For instance, the muscle force  $F_{mu}$  dependence can be approximated with a good precision using an exponential function, from [62], with six different unknown parameters,  $a_1, a_2, a_3, a_4, a_5, a_6$ , as follows:

$$F_{mu}(\kappa, p) = (a_1 + a_2 \cdot p) \cdot e^{a_3 \kappa} + a_4 \cdot \kappa \cdot p + a_5 \cdot p + a_6 \quad (3.3)$$

In order to calculate the muscle force, dependant on the percentage contraction  $\kappa$  and the supply pressure  $p$ , this approximation function has been applied to find out the static characteristics of Festo PAMs (Festo, Germany), employed or tried in this exoskeleton.

### 3.2.1 FESTO pneumatic artificial muscles modelling

- Festo DMSP-20-200N

At first, the FESTO DMSP-20-200N pneumatic muscle has been tried. To find out the numerical coefficients of equation (3.3), Matlab Curve Fitting Toolbox (The MathWorks, USA) has been used, starting from the experimental data of the commercial PAM available in Festo catalogue [77]. This PAM can exert a theoretical output force at maximum operating pressure equal to  $1500\text{ N}$ , within an operating range of contraction from 0% to 25% of its nominal length. The nominal length is the length of the PAM in the non-pressurized load-free state, and it can vary from  $60\text{ mm}$  to  $9000\text{ mm}$ , while the range of operating pressure is  $0 - 6\text{ bar}$ . These curves describe the output force, dependant on the contraction (%) of the PAM's nominal length, chosen as  $210\text{ mm}$ , at different air supply relative pressure ( $\text{bar}$ ). Table 3.2 reports the estimated coefficients. The goodness of fit is high, expressed by  $R_{square} = 0.999$ .

Table 3.2 Coefficients from eq. (3.3) for Festo DMSP-20-200N static characteristics using modified Hill's model.

	<i>coefficient</i>	<i>95% confidence bounds</i>
$a_1$	0.0524	(0.02523, 0.07958)
$a_2$	257.6	(241.7, 273.6)
$a_3$	-0.3758	(-0.3887, -0.3628)
$a_4$	-0.08369	(-0.08546, -0.08191)
$a_5$	2.583	(2.545, 2.622)
$a_6$	-242.6	(259.1, -226.2)

By using these coefficients, the curves showed in Figure 3.5 have been carried out, while Figure 3.6 shows the results of curve fitting from the experimental data in Festo catalogue, represented by the dark blue points.

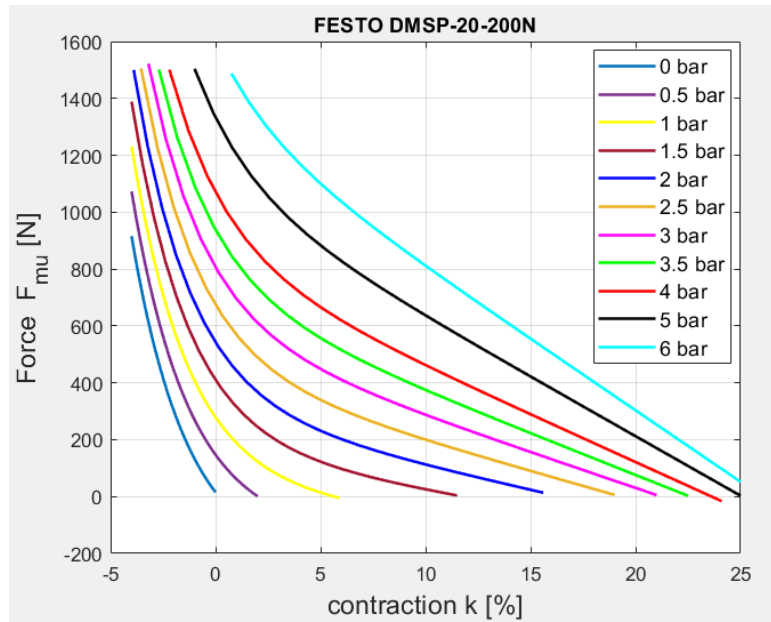


Figure 3.5 Static characteristics of Festo DMSP-20-200N PAM of output force  $F_{\mu}$  [N] dependant on contraction of the nominal length  $\kappa$  [%] and supply relative pressure inside  $p$  [bar].

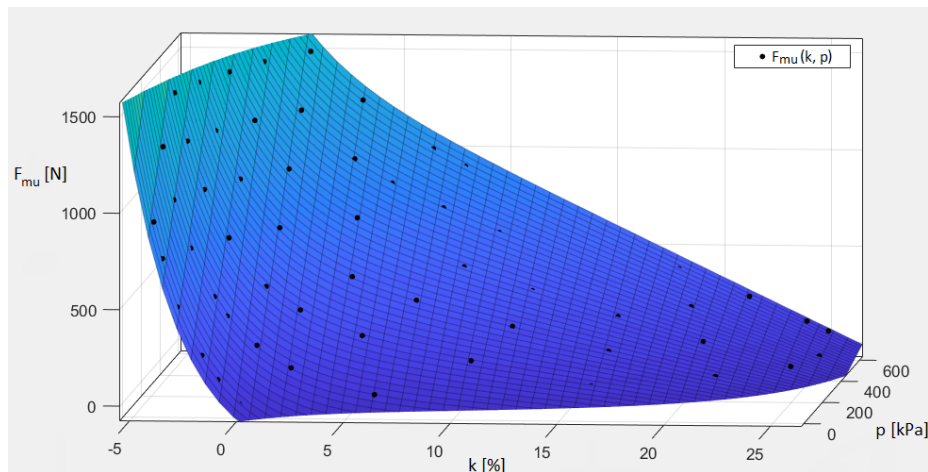


Figure 3.6 Force  $F_{\mu}$  [N]-contraction  $\kappa$  [%]-pressure  $p$  [kPa] relations approximated by equation (3.3).

- Festo DMSP-10-100N

Festo DMSP-10-100N can exert a lifting output force from 0 N to 630 N at the maximum operating pressure, whose range is 0 – 8 bar, and can contract up to 25% of its nominal length, which can vary from 40 mm to 9000 mm. The nominal length has been chosen again as 210 mm. Table 3.3 reports the estimated coefficients. The goodness of fit is high, expressed by  $R_{square} = 0.9988$ . By using these coefficients, the curves of output force displayed in Figure 3.7 are generated at different pressures, with respect to the percentage contraction.

Table 3.3 Coefficients from eq. (3.3) for Festo DMSP-10-100N static characteristics using modified Hill’s model.

	<i>coefficient</i>	<i>95% confidence bounds</i>
$a_1$	0.01534	(0.005408, 0.02526)
$a_2$	130.8	(123.3, 138.2)
$a_3$	-0.3972	(-0.4116, -0.3827)
$a_4$	-0.02605	(-0.02669, -0.02541)
$a_5$	0.7911	(0.7775, 0.8047)
$a_6$	-127.1	(-134.6, -119.6)

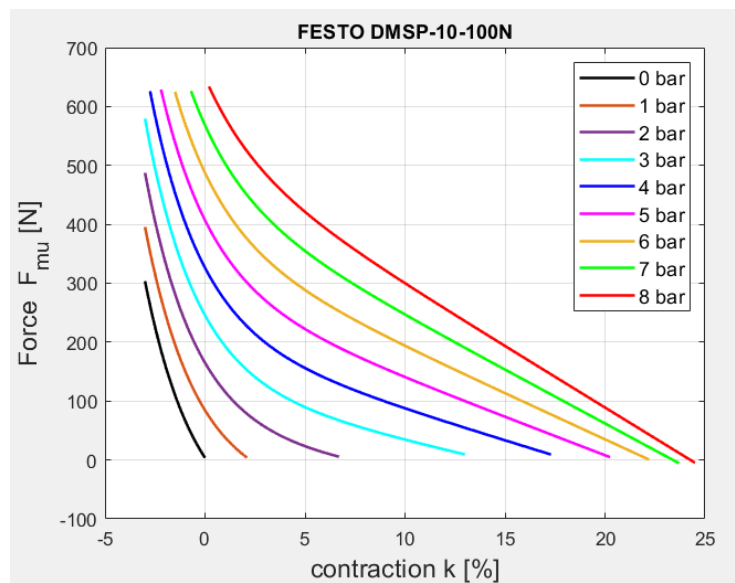


Figure 3.7 Static characteristics of Festo DMSP-10-100N PAM of output force [N] dependant on contraction of the nominal length [%] and supply relative pressure inside [bar].

- Festo DMSP-40-400N

Finally, the Festo DMSP-40-400N has been tried, which can exert a lifting output force from 0 N to 6000 N at the maximum operating pressure, whose range is 0 – 6 bar, and can contract up to 25% of its nominal length, which can vary from 120 mm to 9000 mm. The nominal length has been chosen again as 210 mm. Table 3.4 reports the estimated coefficients. The goodness of fit is high, expressed by  $R_{square} = 0.9984$ .

By using these coefficients, the curves of output force, displayed in Figure 3.8, are generated at different pressures, with respect to the percentage contraction.

Table 3.4 Coefficients from eq. (3.3) for Festo DMSP-40-400N static characteristics using modified Hill's model.

	<i>coefficient</i>	<i>95% confidence bounds</i>
$a_1$	0.01534	(0.005408, 0.02526)
$a_2$	130.8	(123.3, 138.2)
$a_3$	-0.3972	(-0.4116, -0.3827)
$a_4$	-0.02605	(-0.02669, -0.02541)
$a_5$	0.7911	(0.7775, 0.8047)
$a_6$	-127.1	(-134.6, -119.6)

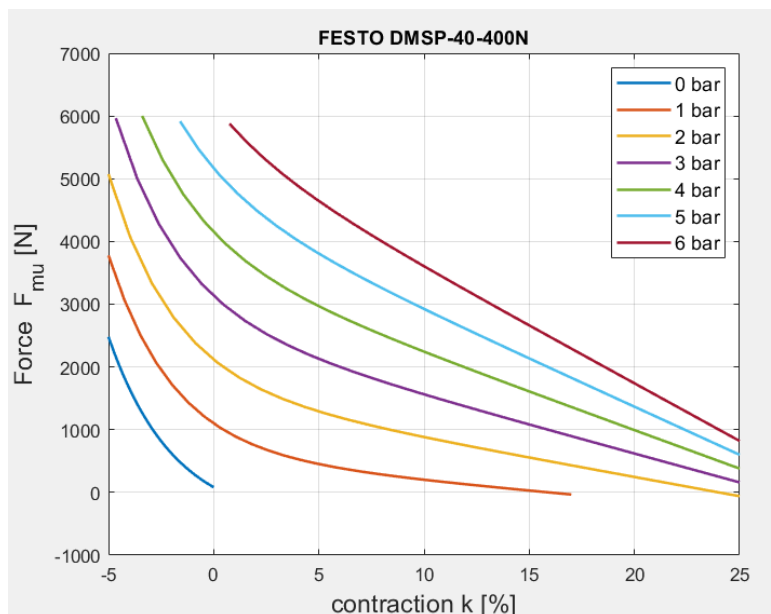


Figure 3.8 Static characteristics of Festo DMSP-40-400N PAM of output force [N] dependant on contraction of the nominal length [%] and supply relative pressure inside [bar].

### 3.3 Materials and methods

The original design consists in a cable and pulley transmission, driven by the pneumatic artificial muscle [76]. The PAM is positioned on the user's back, fixed to the rear part of the structure by its lower end, while its upper end is free to move and is connected to the cable. Through a system of pulleys, the cable is hooked to the arm bracelet, whose position with respect to the shoulder joint is fixed.

By pressurizing the artificial muscle, a traction force is produced and transmitted to the cable, though the pulley transmission. Thus, the cable, that is supposed to be inextensible, transmits the tension force to the arm bracelet, located on the upper arm. Therefore, the pneumatic artificial muscle acts on the arm via the cable and pulley transmission. Alternatively, the fixed pulley could be replaced by a fixed passing point for the cable.

To check the performance of the exoskeleton, the heaviest working condition has been considered, by varying only the elevation angle of the upper arm  $\vartheta_1$ , and keeping the elevation angle of the forearm  $\vartheta_2$  equal to zero. The transmission system can be simplified, in order to clear the relations between the elevation angle of the upper arm and its lever arm with respect to the ideal shoulder joint (SJ). In reference to Figure 3.9, the geometric parameters  $a$ ,  $\alpha$ ,  $\beta$  and  $c_0$  are constant, so the constant segment  $c$  is calculated:

$$c = c_0 / \cos(\beta) \quad (3.4)$$

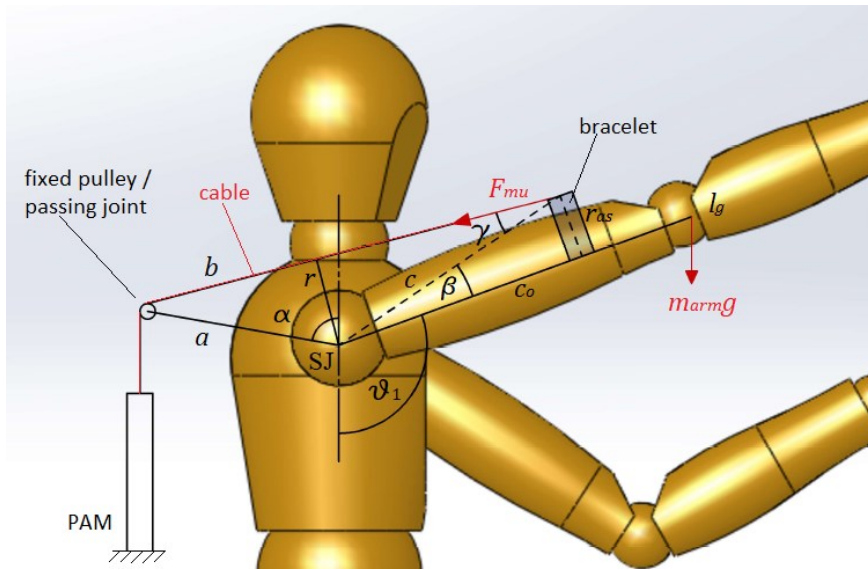


Figure 3.9 Simplified scheme of the original design:  $\vartheta_1$  is the elevation angle of the upper arm,  $l_g$  is the position of the centre of gravity of the arm with respect to the SJ,  $a$  is the length of the bar supporting the last fixed pulley (or fixed passing joint),  $\alpha$  is its angle with respect to the vertical axis,  $c_0$  is the distance between the bracelet and the SJ,  $r$  is the lever arm of the PAM force  $F_{mu}$  with respect to the SJ,  $b$  is the distance of the attachment point of the cable on the bracelet with respect to the fixed pulley.

By neglecting the radius of the pulley, or assuming to employ a fixed passing point for the cable instead,  $b$ , the distance of the attachment point of the cable on the bracelet with respect to the fixed pulley, is calculated as a function of the only elevation angle  $\vartheta_1$ :

$$b = \sqrt{a^2 + c^2 + 2ac \cdot \cos(\vartheta_1 + \beta - \alpha)} \quad (3.5)$$

Then, the angle  $\gamma$  is calculated from (3.6).

$$\gamma = \cos^{-1}\left(\frac{b^2 + c^2 - a^2}{2bc}\right) \quad (3.6)$$

By calculating the semi-perimeter,  $S$ , and the area of the triangle ( $a, b, c$ ),  $A$  from equation (3.7), the lever arm of the tension force  $r$  is evaluated as a function of  $\vartheta_1$  from equation (3.8):

$$A = \sqrt{S \cdot (S - a) \cdot (S - b) \cdot (S - c)} \quad (3.7)$$

$$r = 2A/b \quad (3.8)$$

At first, the air relative pressure inside the PAM inner chamber is null and the exoskeleton can be worn. When the arm is in its initial position at  $\vartheta_1 = 90^\circ$ ,  $\kappa_1$ , the initial percentage contraction of the PAM's nominal length is chosen. Thus, the initial length  $L_1$  is calculated as follows, by choosing the PAM's nominal length  $l_0 = 0.21m$  and initial contraction  $\kappa_1 = 5\%$ :

$$L_1 = l_0 \cdot \left(1 - \frac{\kappa_1}{100}\right) = 0.1995 \text{ m} \quad (3.9)$$

The PAM is pressurized at the desired supply pressure value, so contracts lifting the arm until the torque generated by the pneumatic muscle achieve the static equilibrium with the moment due to gravity of the arm  $M_{dtg}$ . For each elevation angle  $\vartheta_1$ , the shortening  $\Delta b$  of the wire, that is considered non-extendible, is equal to the contraction of the pneumatic muscle, thus the length of the PAM can be calculated for each  $\vartheta_1$  from equation (3.11):

$$\Delta b(\vartheta_1) = b(90^\circ) - b(\vartheta_1) \quad (3.10)$$

$$L(\vartheta_1) = l_0 - \Delta b(\vartheta_1) \quad (3.11)$$

Finally, from the actual length  $L(\vartheta_1)$ , the contraction of the PAM is calculated:

$$\kappa(\vartheta_1) = 100 \left(1 - \frac{L(\vartheta_1)}{l_0}\right) \quad (3.12)$$

According to the selected supply pressure, the PAM tension force,  $F_{mu}$ , is evaluated from equation (3.3). Then the torque exerted by the PAM with respect to the shoulder joint is:

$$M_{mu} = r \cdot F_{mu} \quad (3.13)$$

### 3.4 Numerical results

For a good compromise between the exerted force and inlet supply pressure, the Festo DMSP-20-200N pneumatic artificial muscle has been chosen as actuator. By pressurizing the PAM at  $p = 3 \text{ bar}$ , the effect of the geometric parameters  $a$  and  $\alpha$  has been appreciated, by assuming  $\beta = 14^\circ$  and  $c_0 = 0.20 \text{ m}$ , and initial contraction of the PAM as  $\kappa_1 = 5\%$ . In Figure 3.10, the length of the bar supporting the fixed pulley (or fixed passing point) is chosen equal to  $a = 0.15 \text{ m}$ , while the angle  $\alpha$  assumes different values:

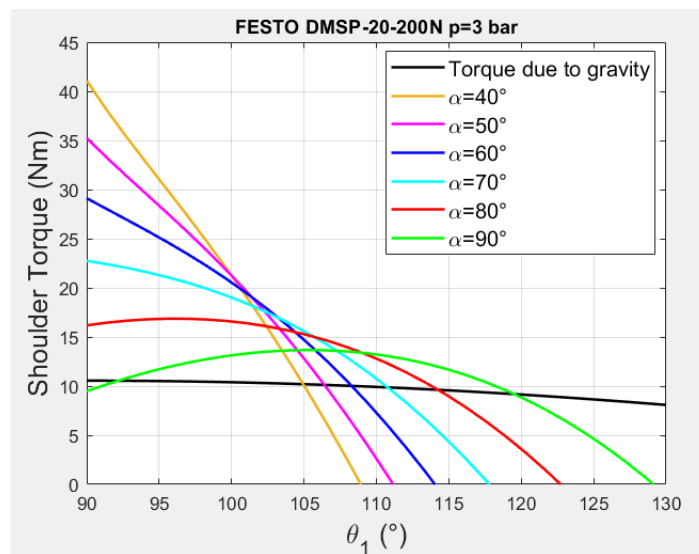


Figure 3.10 Torque due to gravity of the arm and torques exerted by the PAM, with supply pressure  $p = 3 \text{ bar}$ ,  $\kappa_1 = 5\%$ ,  $a = 0.15 \text{ m}$ ,  $\beta = 14^\circ$  and  $c_0 = 0.20 \text{ m}$ , by varying the angle of the bar supporting the fixed pulley  $\alpha$ .

Figure 3.10 shows that the angle  $\alpha$  has a rather big effect on varying the torque exerted by the PAM. In particular, the higher  $\alpha$  the lower is the initial torque value at  $\vartheta_1 = 90^\circ$ , thus the higher is the elevation angle at which the equilibrium of torques occurs.

At the same other parameters, by keeping the angle  $\alpha$  constant and varying the length of the bar  $a$ , Figure 3.11 is produced. The figure shows that the parameter  $a$  has a poorer effect than the angle  $\alpha$  in varying the torques, and, by increasing  $a$ , the initial value of torque gets higher, hence the equilibrium of torques occurs at lower values of elevation angle  $\vartheta_1$ .

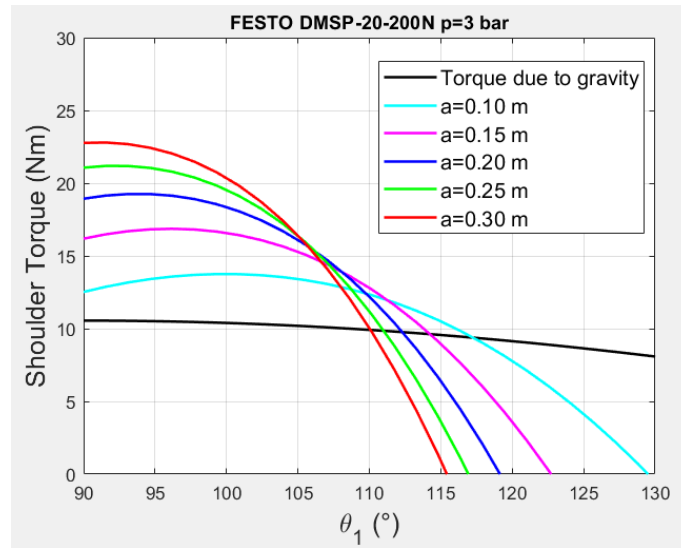


Figure 3.11 Torque due to gravity of the arm and torques exerted by the PAM, with supply pressure  $p = 3 \text{ bar}$ ,  $\kappa_1 = 5\%$ ,  $\alpha = 80^\circ$ ,  $\beta = 14^\circ$  and  $c_0 = 0.20 \text{ m}$ , by varying the length of the bar supporting the fixed pulley  $a$ .

By choosing the geometric parameters  $a = 0.15 \text{ m}$ ,  $\alpha = 80^\circ$ ,  $\beta = 14^\circ$ ,  $c_0 = 0.20 \text{ m}$ , and assuming the initial contraction of the pneumatic muscle  $\kappa_1 = 5\%$ , the nominal supply pressure in the inner chamber has been varied from  $p = 2 \text{ bar}$  to  $4 \text{ bar}$ , and the curves in Figure 3.12 have been generated, by hypothesizing a working range of  $\vartheta_1$  from  $90^\circ$  to  $135^\circ$  for overhead working tasks. To move the arm below  $90^\circ$ , the shoulder complex muscles should apply a great effort, so a reduction of the supply pressure could be realized to reach the resting position.

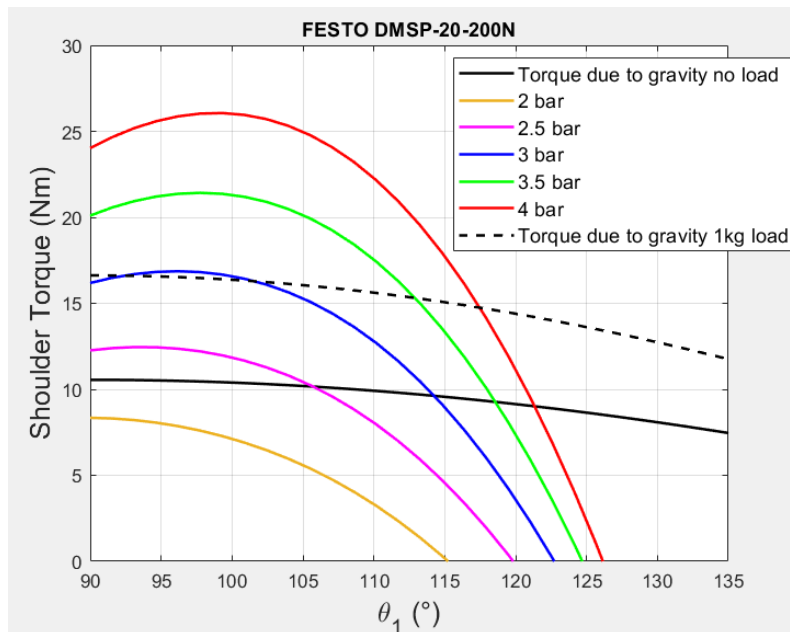


Figure 3.12 Torque due to gravity, in unloaded and loaded condition, and torques exerted by the PAM, with respect to the elevation angle, at different supply pressures by selecting the initial contraction  $\kappa_1 = 5\%$ .

Figure 3.12 shows that, by increasing the supply pressure, the compensation capacity of the exoskeleton raises, and the elevation angle, at which the equilibrium between the torques occurs, gets higher, allowing the arms to reach a higher position.

Then, the figure compares the unloaded and loaded condition. In the loaded condition, the user is supposed to hold a load of 1 kg in hand, representing a working situation in which he is holding a tool while his arms are lifted. By adding the load at the same pressure, the elevation angle of the equilibrium points decreases, lifting the arms lower.

Yet, curves of the torques exerted by the pneumatic muscle do not have a suitable trend, because of their slope, that is much larger than the one of the torques due to gravity. This characteristic causes that, when the arm is lifted at the equilibrium point, the shoulder complex muscles must apply a high effort for moving the arm from that point and reach a different position. This effort is equal to the difference between the torque exerted by the PAM and the torque due to gravity at the same value of elevation angle. To make this effort to reduce, the trend and the slope of the torques exerted by the PAM must be as similar as possible to the ones of the torque due to gravity. Besides, the range of elevation angle in which the compensation is provided is limited, due to the steep slope.

By applying the same equations, and assuming the initial contraction  $\kappa_1 = 3.5\%$  of the PAM at  $\vartheta_1 = 90^\circ$ , the curves shown in Figure 3.13 are generated, within a range from  $\vartheta_1 = 90^\circ$  to  $120^\circ$ .

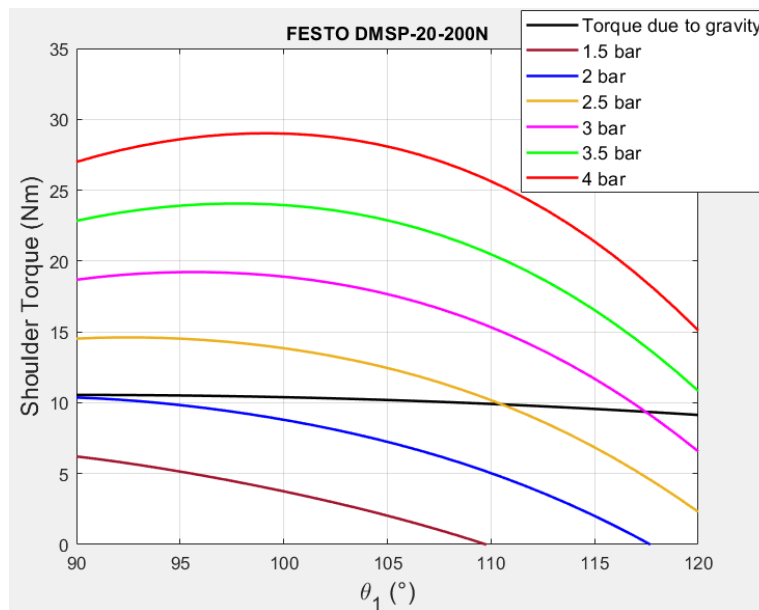


Figure 3.13 Torque due to gravity, in unloaded and loaded condition, and torques exerted by the PAM, with respect to the elevation angle, at different supply pressures by selecting the initial contraction  $\kappa_1 = 3.5\%$ .

## Chapter 4

# Joining the shoulder pad to the exoskeleton design

Instead of the pulley transmission, with the bar long  $a$ , the idea of a cam profile is proposed. The proposed device consists of a rigid shoulder pad, centred in the ideal shoulder joint, and fixed to the frame of the exoskeleton. This profile has a growing radius, meant for:

- making the lever arm of the tension force of the PAM to grow as the elevation angle of the arm rises, resulting in a better compensation torque  $M_{mu}$ ;
- extending as much as possible the range of elevation angle in which the compensation is accomplished, better distributing the power provided by the pneumatic artificial muscle over the range;
- to design a device in order to make the curves of the torques exerted by the PAM to have a similar trend as the curve of the torque due to gravity. Thus, the initial values of  $M_{mu}$  must be lower, and closer to the moment due to gravity, in order to make the equilibrium of torques to occur at higher positions. In fact, if the torque exerted by the PAM, at low elevation angles, is much higher than the moment due to gravity, a large part of the power of the PAM is already consumed, and since PAMs have a short stroke, it causes that the elevation angles of the equilibrium point are relatively low;
- to reduce the effort required to the wearer to balance the PAM generated force and move the upper limb from the equilibrium position.

## 4.1 Materials and methods

The shoulder pad is meant to replace the fixed pulley (or fixed passing joint), so the wire, whose end is attached to the bracelet supporting the upper arm, flows without crawling on the shoulder pad, and it is attached to the PAM, by its other end. The transmission is simplified in next figure.

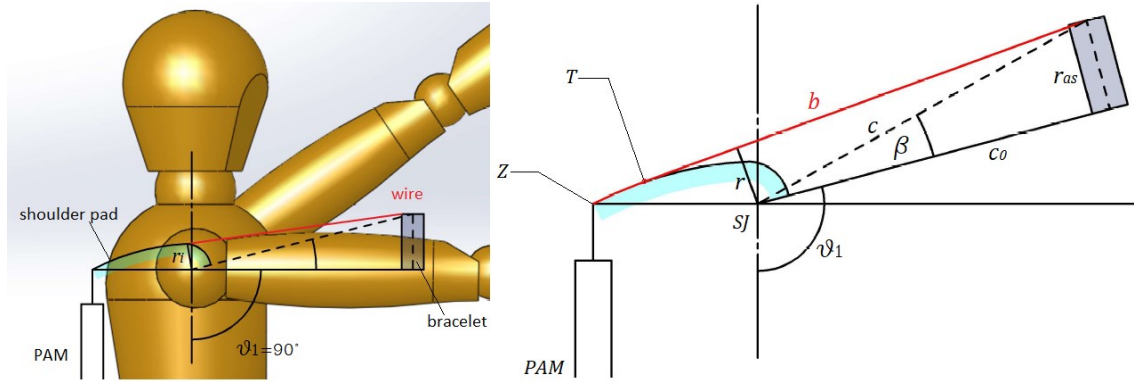


Figure 4.1 Simplified scheme of the novel design by joining the shoulder pad:  $\vartheta_1$  is the elevation angle of the upper arm,  $c_0$  is the distance between the bracelet and the shoulder joint (SJ),  $r$  is the lever arm of the tension force  $F_{mu}$  with respect to the SJ,  $b$  is the distance of the attachment point of the wire on the bracelet with respect to the final contact point on the shoulder pad ( $Z$ ),  $T$  is the tangency point of the wire on the shoulder pad.

To design the shoulder pad, a graphical method has been implemented. First, by selecting the nominal supply pressure,  $p = 3 \text{ bar}$ , and the initial contraction of the PAM  $\kappa_1 = 5\%$  (as for Figure 3.12 with the fixed pulley transmission), the initial lever arm  $r_i$ , at  $\vartheta_1 = 90^\circ$ , has been calculated, to make the torque exerted by the PAM to balance the torque due to gravity at  $\vartheta_1 = 90^\circ$ :

$$r_i = m_{arm} \cdot g \cdot \frac{l_g}{F(\kappa_1, p)} = 23.50 \text{ mm} \quad (4.1)$$

The initial lever arm,  $r_i$ , is equal to the initial cam radius. As the elevation angle gets higher, the wire keeps itself tangent to the cam profile (in Figure 4.1 right  $T$  is the tangency point of the wire on the shoulder pad).

Yet, the lever arm of the tension force does not match the cam radius anymore, when  $\vartheta_1$  is not equal to  $90^\circ$ . For this reason, by considering that the wire must pass through the fixed final point of the profile ( $Z$  in Figure 4.1 right), the lever arm  $r$  and  $b$ , the distance between the attachment point of the wire on the bracelet and the point  $Z$  on the shoulder pad, must be determined graphically from the CAD design, by ensuring the tangency condition of the wire on the cam profile, and from that the actual length of the PAM.

After determining the initial radius of the cam, the lever arm of the tension force at  $\vartheta_1 = 135^\circ$ ,  $r_f$  has been chosen, by iteration, in order to keep the final output torque as high as possible. Then, it has been used to calculate the distance  $b$  graphically. By applying the equations (3.10), (3.11), (3.12), (3.3) and (3.13), the corresponding value of tension force  $F_{mu}$  has been evaluated at  $p = 3 \text{ bar}$  and the torque exerted by the exoskeleton,  $M_{mu}$ . The choice of  $r_f$  requires several iterations to keep the value of  $M_{mu}$  as close as possible to the torque due to gravity at  $\vartheta_1 = 135^\circ$ . Once having found the optimal value of  $r_f$ , the same method has been applied for the intermediate configurations at  $\vartheta_1 = 105^\circ$  and  $120^\circ$ .

Thus, from the graphic discrete results, a 4-degree-polynomial function has been applied to approximate the discrete profile of the shoulder pad, carrying out a continuous profile. This latter allows to approximate the lever arm  $r$ ,  $b$ ,  $L$  (see Figure 4.2 and Figure 4.3) and so to calculate  $k$ ,  $F_{mu}$  and the torque  $M_{mu}$  for each elevation angle from  $\vartheta_1 = 90^\circ$  to  $135^\circ$ .

## 4.2 Numerical results

Figure 4.2 and Figure 4.3 shows the approximation of the cam profile with the 4-degree-polynomial function, and the approximation of  $r$ , the lever arm of the tension force,  $b$ , the distance of the attachment point of the wire on the bracelet with respect to  $Z$  (the final point on the shoulder pad), and  $L$ , the actual length of the pneumatic artificial muscle.

Then, Figure 4.4 shows the profile of the shoulder pad graphically obtained from  $r_i = 23.50 \text{ mm}$ ,  $r_f = 40.38 \text{ mm}$  and the intermediate positions.

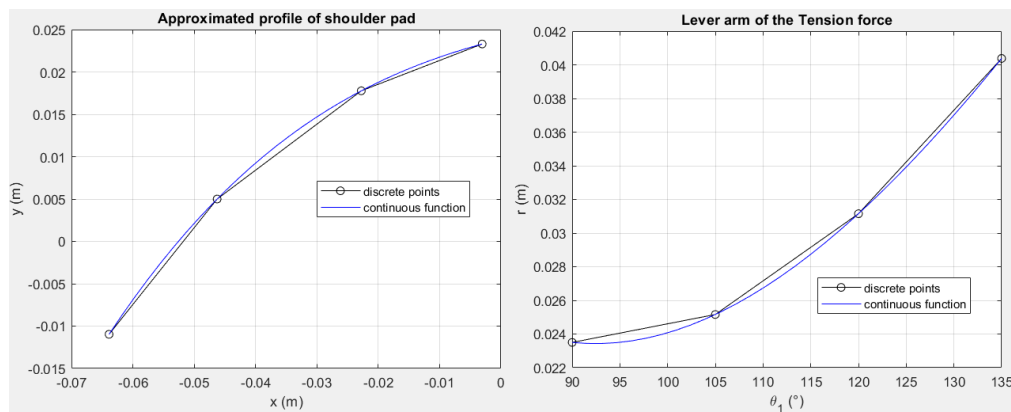


Figure 4.2 Approximation of the cam profile with the 4-degree-polynomial function (left). Approximation of  $r$ , the lever arm of the tension force, function of the elevation angle (right).

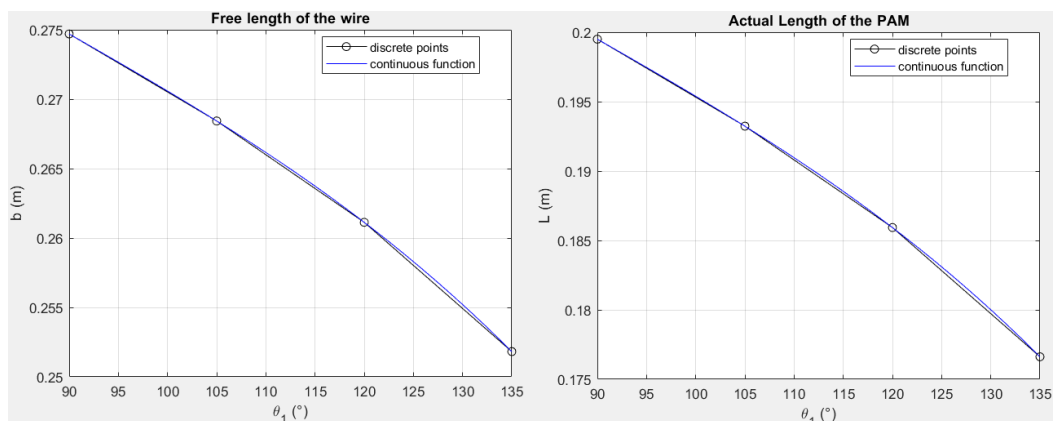


Figure 4.3 Approximation of  $b$ , distance of the attachment point of the wire on the bracelet with respect to  $Z$ , final point on the shoulder pad profile, function of the elevation angle (left). Approximation of the actual length of the pneumatic muscle, function of the elevation angle (right).

The same profile is employed at different supply pressure in the pneumatic muscle, always assuming an initial contraction of the PAM of  $\kappa_1 = 5\%$ . By selecting different supply pressures, Figure 4.5 is produced. It shows that the curve of torque, exerted by the PAM at  $p = 3 \text{ bar}$ , follows the one of the torque due to gravity with a rather similar trend, as the curves at other pressures. Besides, the useful range of elevation angle is extended with respect to the one obtained with the original design. According to the supply pressure, different tasks can be performed with the exoskeleton. In fact, if only the upper limb is to be kept in elevated position, the PAM should be pressurized at 3 or 3.5 bar, while, if also a 1kg load is to be kept in hand, the PAM is better to be pressurized at 4 bar.

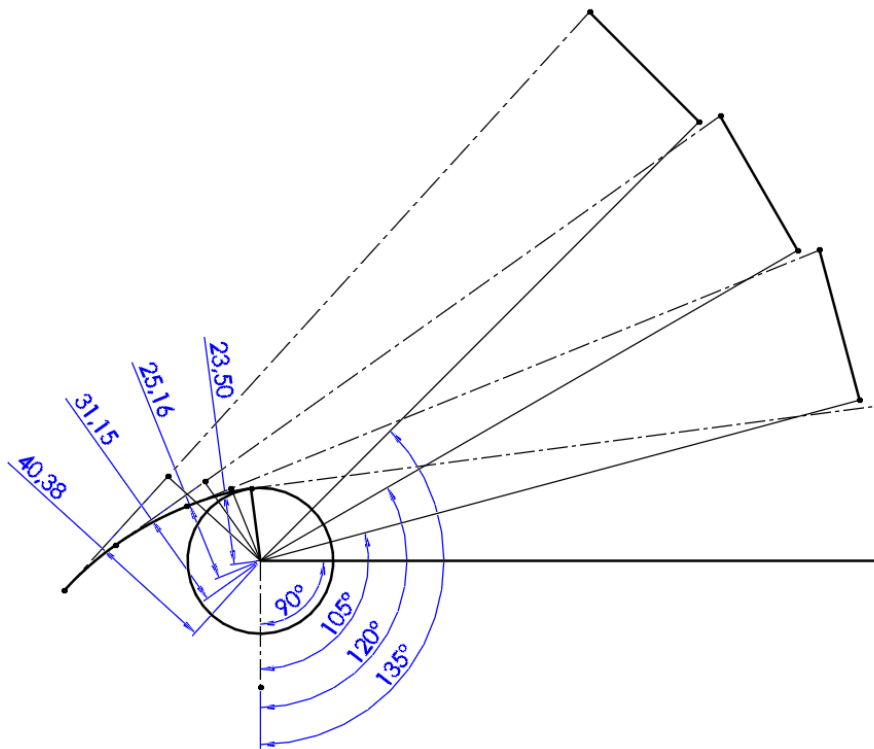


Figure 4.4 Profile of the shoulder pad from graphical approach from intermediate configurations with  $r_i = 23.50 \text{ mm}$  and  $\kappa_1 = 5\%$  at  $\vartheta_1 = 90^\circ$  and  $r_f = 40.38 \text{ mm}$  at  $\vartheta_1 = 135^\circ$ . The lever arms ( $\text{mm}$ ) are in blue, as the corresponding elevation angles, the point-dotted line represents the wire in different positions.

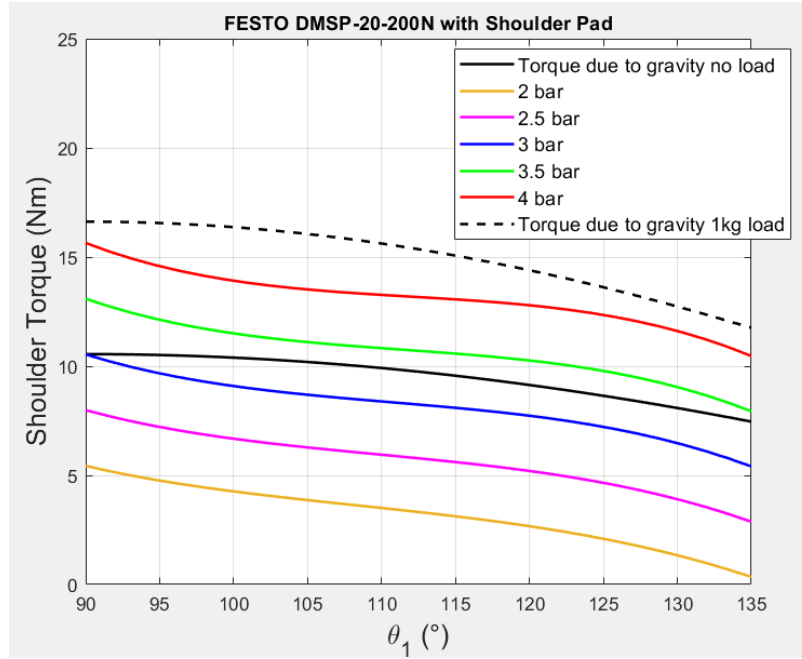


Figure 4.5 Torque due to gravity, in unloaded and loaded condition, and torques exerted by the PAM at different supply pressures, by employing the shoulder pad, whose profile is obtained in Figure 4.4.

### 4.3 Real profile of the shoulder pad

The shoulder pad must be fixed to the frame of the exoskeleton, while the wire flows along it, as the elevation angle rises. Then, it must be centred in the shoulder joint of the exoskeleton, that must match the ideal shoulder complex joint, in order to prevent misalignment between the axes of the exoskeleton and the ones of the user’s human body. Therefore, the shoulder pad must be designed to be fixed on the user’s shoulder.

From [73], Zatsiorsky-Seluyanov-de Leva adjusted body segment inertia parameters suggest the mean longitudinal distance of the acromion point with respect to the shoulder joint is:

$$r_{acromion} = 34.5 \text{ mm} \quad (4.2)$$

Whereas the acromion is the bone that forms the peak of the human shoulder complex. Thus, the initial radius of the shoulder pad at  $\vartheta_1 = 90^\circ$  must be bigger than this value. So, the same graphic and iterative approach, as the former paragraph, has been employed.

This time, the initial contraction of the nominal length is chosen as  $\kappa_1 = 3.5\%$  (as for Figure 3.13 with the fixed pulley transmission). Then, the initial radius of the profile, that is the lever arm at  $\vartheta_1 = 90^\circ$ , has been chosen as:

$$r_i = 37 \text{ mm} \quad (4.3)$$

Which is similar to the lever arm calculated from the static equilibrium with the torque due to gravity at  $\vartheta_1 = 90^\circ$ , by selecting the supply pressure  $p = 2 \text{ bar}$ ,  $r = 36.7 \text{ mm}$ .

At first, the lever arm at  $\vartheta_1 = 120^\circ$  has been chosen equal to  $r_f = 46 \text{ mm}$ . By setting the values of lever arm also in the intermediate positions  $\vartheta_1 = 100^\circ$  and  $110^\circ$ , the graphic method has been applied again, by ensuring the tangency of the wire on the cam profile. Thus, the 4-degree-polynomial function has been used for approximating the discrete profile of the shoulder pad. Because of the graphic approach and by imposing the tangency condition of the cable for every position, the final lever arm, at  $120^\circ$ , results  $r_f = 45.93 \text{ mm}$ .

Figure 4.6 shows the approximations of the profile of the shoulder pad (left) and the lever arm  $r$  for each elevation angle from  $\vartheta_1 = 90^\circ$  to  $120^\circ$  (right). Instead, Figure 4.7 shows the approximation of  $b$ , the distance of the attachment point of the wire on the bracelet with respect to the  $Z$  point on the shoulder pad, and the actual length of the PAM, function of the elevation angle.

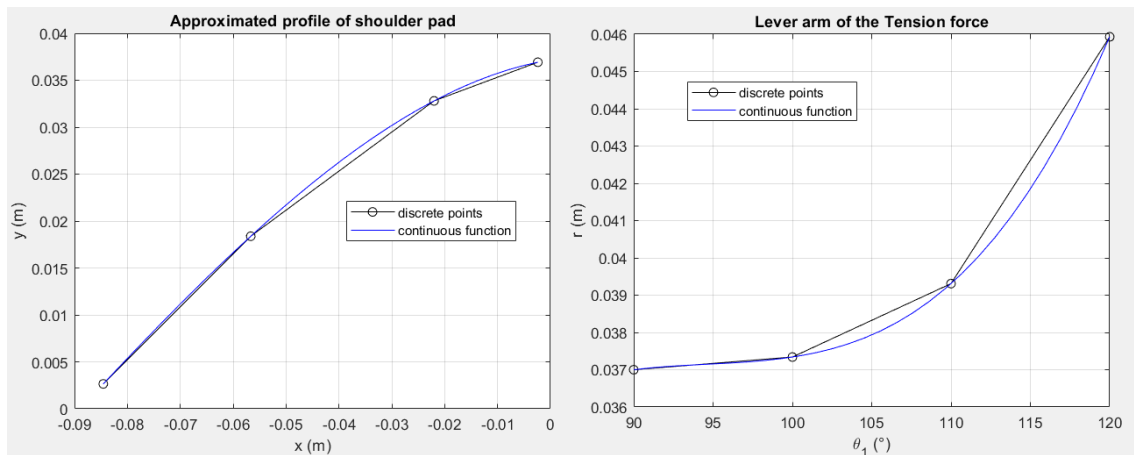


Figure 4.6 Approximation of the cam profile with the 4-degree-polynomial function (left). Approximation of  $r$ , the lever arm of the tension force, function of the elevation angle (right).

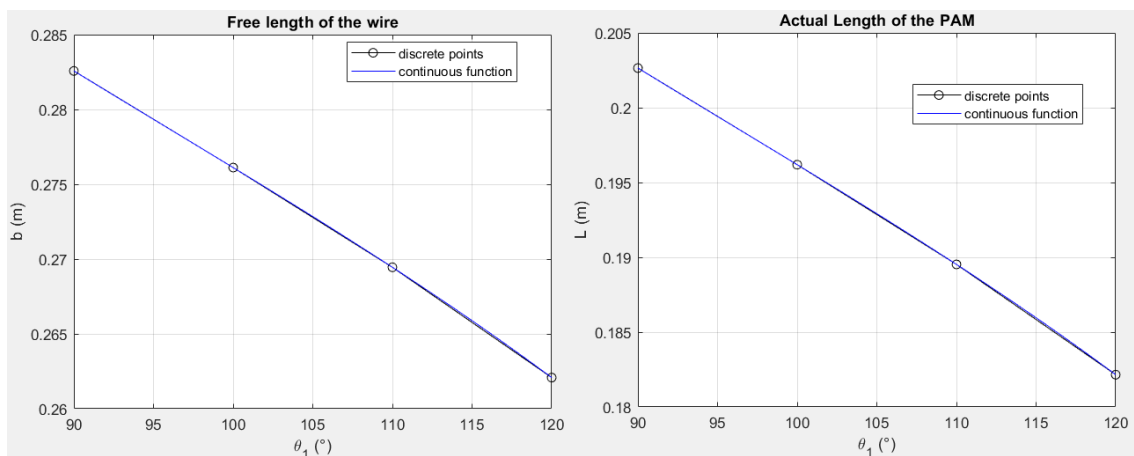


Figure 4.7 Approximation of  $b$ , the distance of the attachment point of the wire on the bracelet with respect to  $Z$ , the final point on the shoulder pad profile, function of the elevation angle (left). Approximation of the actual length of the pneumatic muscle, function of the elevation angle (right).

Figure 4.8 shows the approximated profile of the shoulder pad, highlighting the lever arms in the intermediate positions, with the relative elevation angles. Figure 4.9 shows the curves of torque produced by the PAM at different supply pressures, by employing the shoulder pad. According to the task to be performed by the user, the PAM should be pressurized at appropriate nominal pressure.

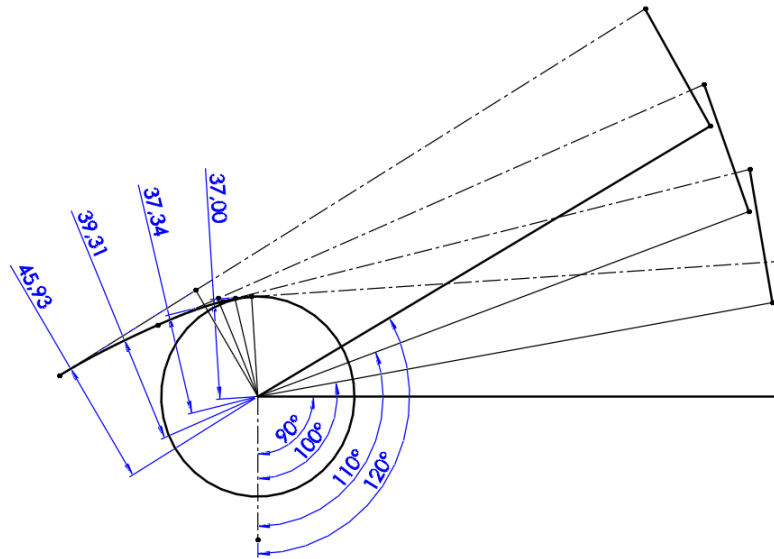


Figure 4.8 Profile of the shoulder pad for Festo DMSP-20-200N, from graphical approach from intermediate configurations with  $r_i = 37.00 \text{ mm}$  and  $\kappa_1 = 3.5\%$  at  $\vartheta_1 = 90^\circ$  and  $r_f = 45.93 \text{ mm}$  at  $\vartheta_1 = 120^\circ$ . The lever arms are in blue, as the corresponding elevation angles, the point-dotted line represents the wire in different positions.

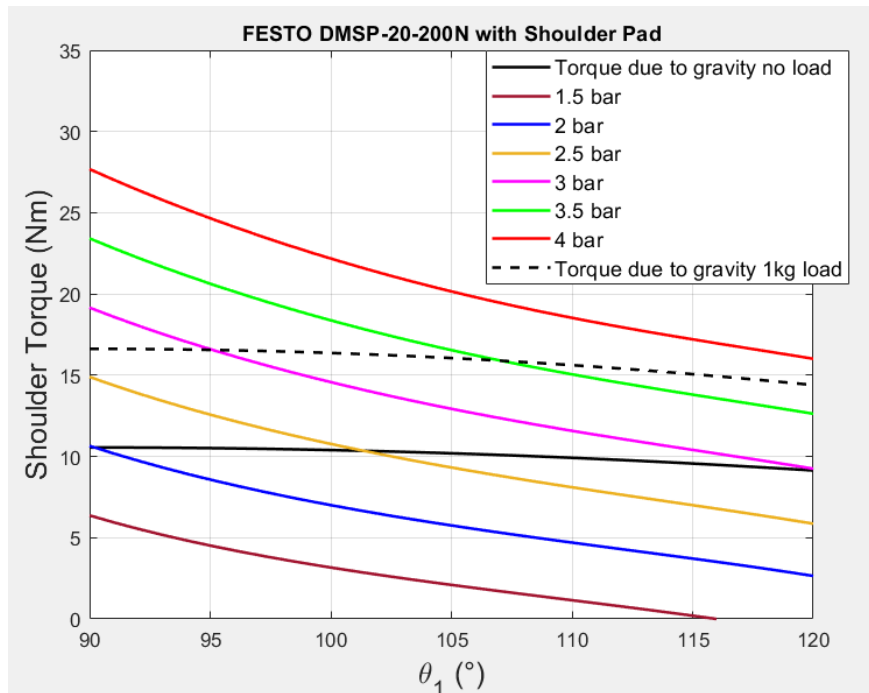


Figure 4.9 Torque due to gravity, in unloaded and loaded condition with 1kg in hand, and torques exerted by the PAM at different supply pressures, by employing the shoulder pad, whose profile is obtained in Figure 4.8.

The same graphic method has been applied by using the Festo DMSP-10-100N, with initial radius  $r_i = 37 \text{ mm}$  assuming the initial contraction  $k_i = 1\%$  of the nominal length  $0.21 \text{ m}$ .

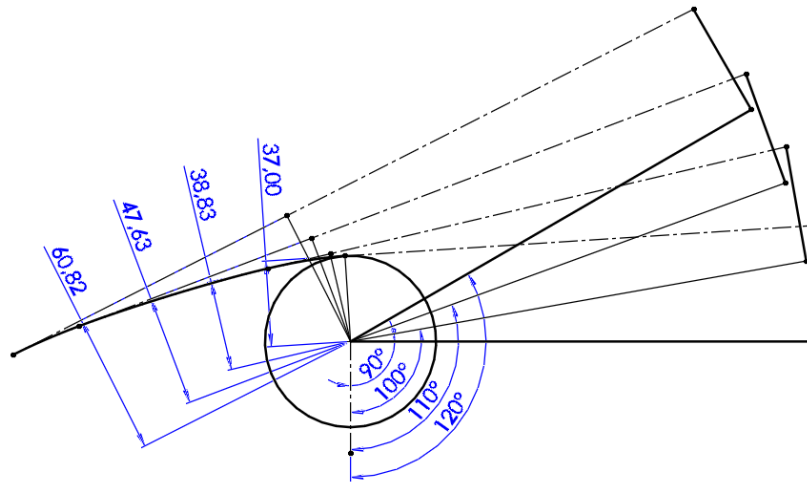


Figure 4.10 Profile of the shoulder pad for Festo DMSP-10-100N, from graphical approach from intermediate configurations with  $r_i = 37.00 \text{ mm}$  and  $\kappa_1 = 1\%$  at  $\vartheta_1 = 90^\circ$  and  $r_f = 60.82 \text{ mm}$  at  $\vartheta_1 = 120^\circ$ . The lever arms are in blue, as the corresponding elevation angles, the point-dotted line represents the wire in different positions.

From this profile, the following figure is obtained, which compares the torque due to gravity with the torque exerted by the Festo DMSP-10-100N at different supply pressures, assuming the initial contraction of the PAM  $\kappa_1 = 1\%$ .

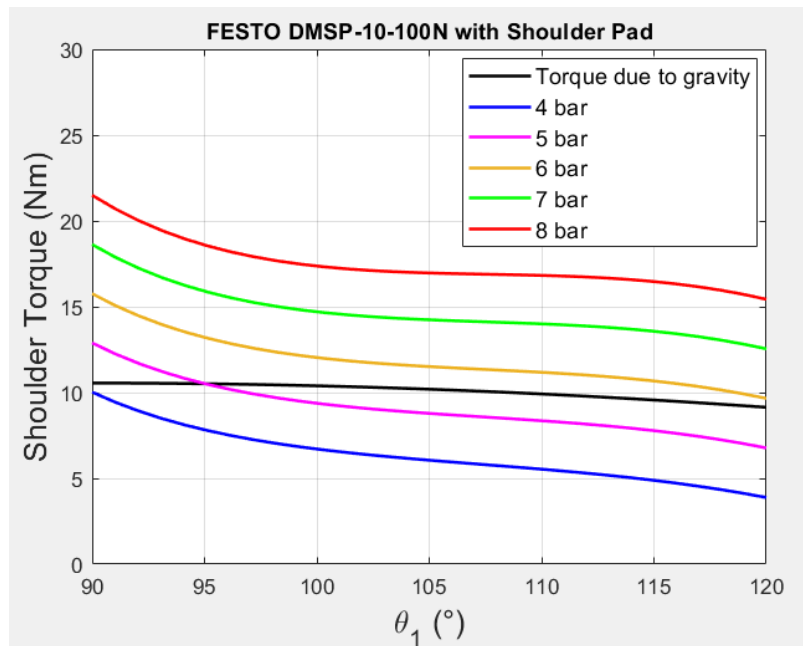


Figure 4.11 Torque due to gravity, in unloaded and loaded condition, and torques exerted by the PAM at different supply pressures, by employing the shoulder pad, whose profile is obtained in Figure 4.10.

Despite the curves of exerted torques, obtained from Festo DMSP-10-100N and the shoulder pad profile in Figure 4.10, have a better trend than the ones generated in Figure 4.9 with the Festo DMSP-20-200N, in following the torque due to gravity, a higher supply inlet pressure must be applied to accomplish a good compensation, of about 4 *bar*. For this reason, to have a good compromise the Festo DMSP-20-200N had been chosen as actuator.



## Chapter 5

# Exoskeleton assembly

## 5.1 Materials and methods

The exoskeleton is meant to join a commercial harness, the TITAN safety harness by Honeywell, on which the structure is mounted. To the hip belt a vertical telescopic rod is connected by a hinge in the rear. Then, the telescopic rod is welded to a horizontal beam at shoulder height, on which the exoskeleton 2-DOF shoulder joint is mounted. The latter is linked to a strut that, running along the arm, bears the upper arm bracelet.

### 5.1.1 2-DOF Exoskeleton shoulder joint

The aim of the exoskeleton is to assist the user's upper limb movements while performing overhead job, trying not to reduce the DOF of the limb.

Mainly the equipment must replicate the flexion/extension and abduction/adduction of the shoulder complex. Thus, a 2-DOF exoskeleton shoulder joint is needed, which must be aligned with respect to the human body shoulder joint as much as possible. To carry out the 2-DOF shoulder joint, the universal joint is suggested, which consists in two arches, and two bushings. Two commercial SKF sintered bronze bushings have been chosen for this purpose. The two arches must be produced and mounted in order to make the 2 rotational axes (flexion/extension and abduction/adduction) align with the shoulder complex DOF axes. Therefore, the point in which the 2 exoskeleton axes encounter is the hypothetical centre of the human shoulder joint (SJ point), as shown in Figure 5.1. The first arch of the universal joint is fixed to the frame, while the second one is movable and it can rotate with respect to the first one, by means of the bushing. The relative motion, of the second arch with respect to the first one, performs the shoulder abduction/adduction DOF. Then, a strut is mounted into the movable arch, by means of the second bushing, and the rotation of the strut performs the flexion/extension DOF. The strut, at its extremity, carries a bracelet where the limb slips.

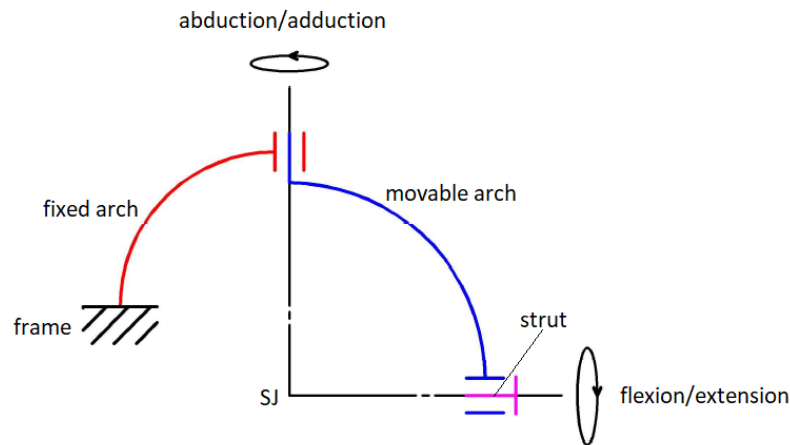


Figure 5.1 Diagram of the universal joint on the frontal plane of human body: flexion/extension and abduction/adduction axes meet in the SJ point, which is the hypothetical centre of the shoulder complex; the fixed arch is connected to the frame, that represents the horizontal beam; the movable arch rotates with respect to the fixed arch, by means of the first bushing; the strut rotates with respect to the fixed arch by means of a second bushing.

The pneumatic artificial muscle lifts the bracelet and the upper limb through the wire, then the strut rotates with respect to the movable arch around the shoulder flexion/extension axis (which is the main contribute of the elevation angle of the upper arm). In addition, the wearer is free to move the upper arm in abduction/adduction, thanks to the rotation of the movable arch with respect to the fixed one.

Then, on the wearer's shoulder complex, the shoulder pad must be mounted to improve the curve of torque exerted by the pneumatic muscle with respect to the shoulder joint. As the upper arm lifts in elevation (which mainly consists of flexion), the shoulder pad must be fixed to the frame and the wire runs along its grooved profile. Yet, as the wearer moves the upper limb in abduction/adduction, the shoulder pad should follow the wire anyway, so that the wire keeps aligned with the grooved profile, and therefore limit friction on the profile. Thus, to get the shoulder pad fixed to the frame while the upper arm moves in flexion/extension, and movable while the limb moves in abduction/adduction, the shoulder pad should be rigidly connected to the movable arch of the universal joint. The connection is meant to be by welding, in order to avoid bolts and nuts.

### 5.1.2 Size adjustment systems

In addition, there are some linear guides to adjust the position of the universal joint with the shoulder pad in vertical and horizontal direction, and the position of the bracelet on the upper arm, according to the user's sizes:

- For the horizontal adjustment of the position of the fixed arch of the universal joint on the frame, a spring plunger (Misumi PXA) is suggested. The main body of the spring plunger is screwed and fixed to the horizontal beam (the frame), while its pin fits into the fixed arch of the universal joint. Thus, to adjust the position of the shoulder pad, the handle is pulled back, resulting in a compression of the inner spring, disengaging the pin from the fixed arch.
- To adapt the position of the shoulder pad in vertical direction, a telescopic rod is suggested, by employing a commercial pawl spring, for nautical items, to stop the movable element into the fixed one.
- A telescopic linear guide could be employed for adjusting the position of the bracelet on the strut. In the proposed design, the fixed element of the guide is part of the strut by welding, while the movable element is connected to the bracelet through two bolts and nuts. The movable element can slide along the strut, then, it is blocked on the strut with another bolt and nut.

### 5.1.3 Mounting of the PAM

The Festo DMSP-20-200N-RMCM fluidic muscle has been chosen as actuator, with a pneumatic radial connection (RM) at its fixed extremity, and with male thread at its free end (CM). At the RM end push-in fitting (QS-G1/4-8 by Festo) is mounted for injecting air inside the PAM.

A mounting solution is suggested so that the fixed extremity of the PAM is screwed to the horizontal beam of the exoskeleton in the upper back, while the free end is located in the lower back. To reverse the direction of the cable, from the shoulder pad to the PAM, it is proposed to use a sheath held by two commercial sheath clips. In this way, the wire, after running along the profile of the shoulder pad, enters the sheath, and, making a U-turn, is then connected to the free end of the PAM. The adhesive sheath clips are meant to be stuck on the hip belt.

For the connection of the wire to the PAM, a rod eye SGS-M10x1.25 (from Festo data sheet, Festo, Germany), screwed to the threaded free end of PAM, and a cable clamp are suggested, so that the wire coming out from the sheath enters the cable clamp, making an eyelet that hooks onto the rod eye. Figure 5.2 shows the CAD model of the human body of mean sizes wearing half the exoskeleton assisting the right arm. The bracelet is proposed to be produced ad hoc, so that the wire can hook it through a hole.

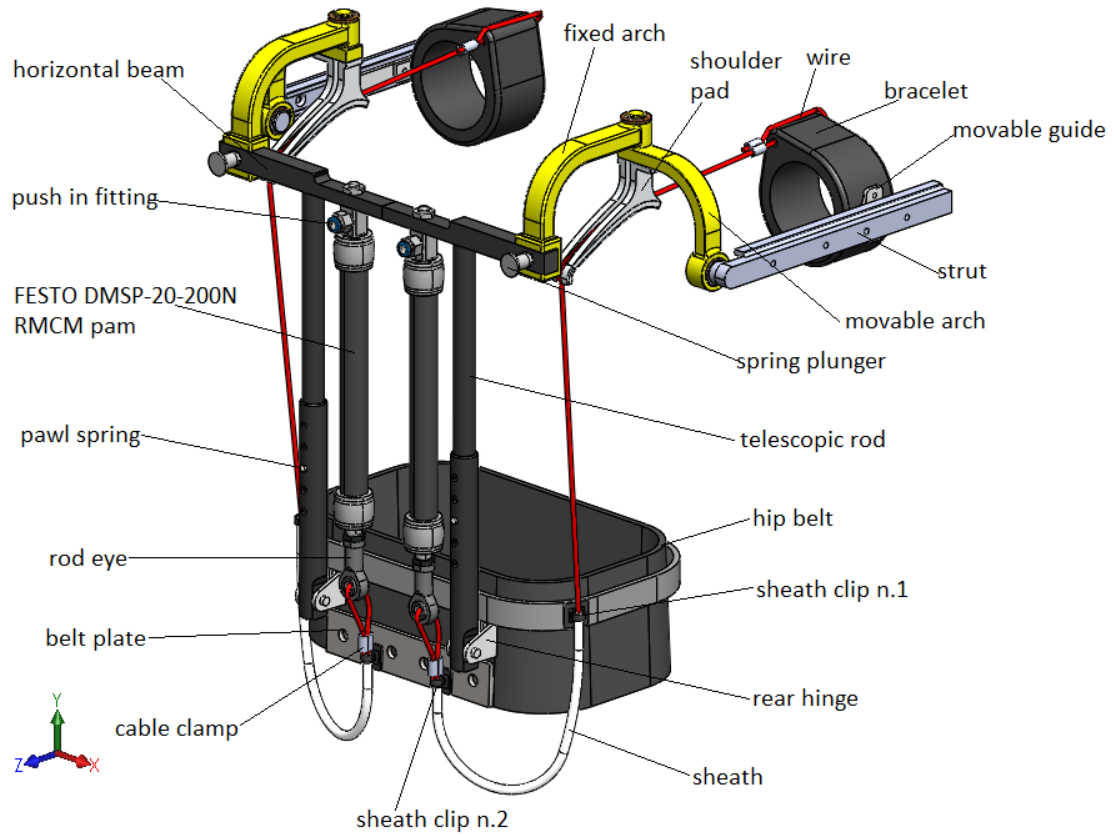


Figure 5.2 CAD model of the overall exoskeleton, without the safety harness, at elevation angle of the upper limb  $90^\circ$  with respect to vertical direction, with the fixed end of the PAM at the top and the free end at the bottom; the wire (in red), after scrolling along the shoulder pad groove and coming out from the sheath, passes into a cable clamp, hooking the rod eye.

Next figures show the entire exoskeleton design, assisting the two upper limbs, worn by the human body.

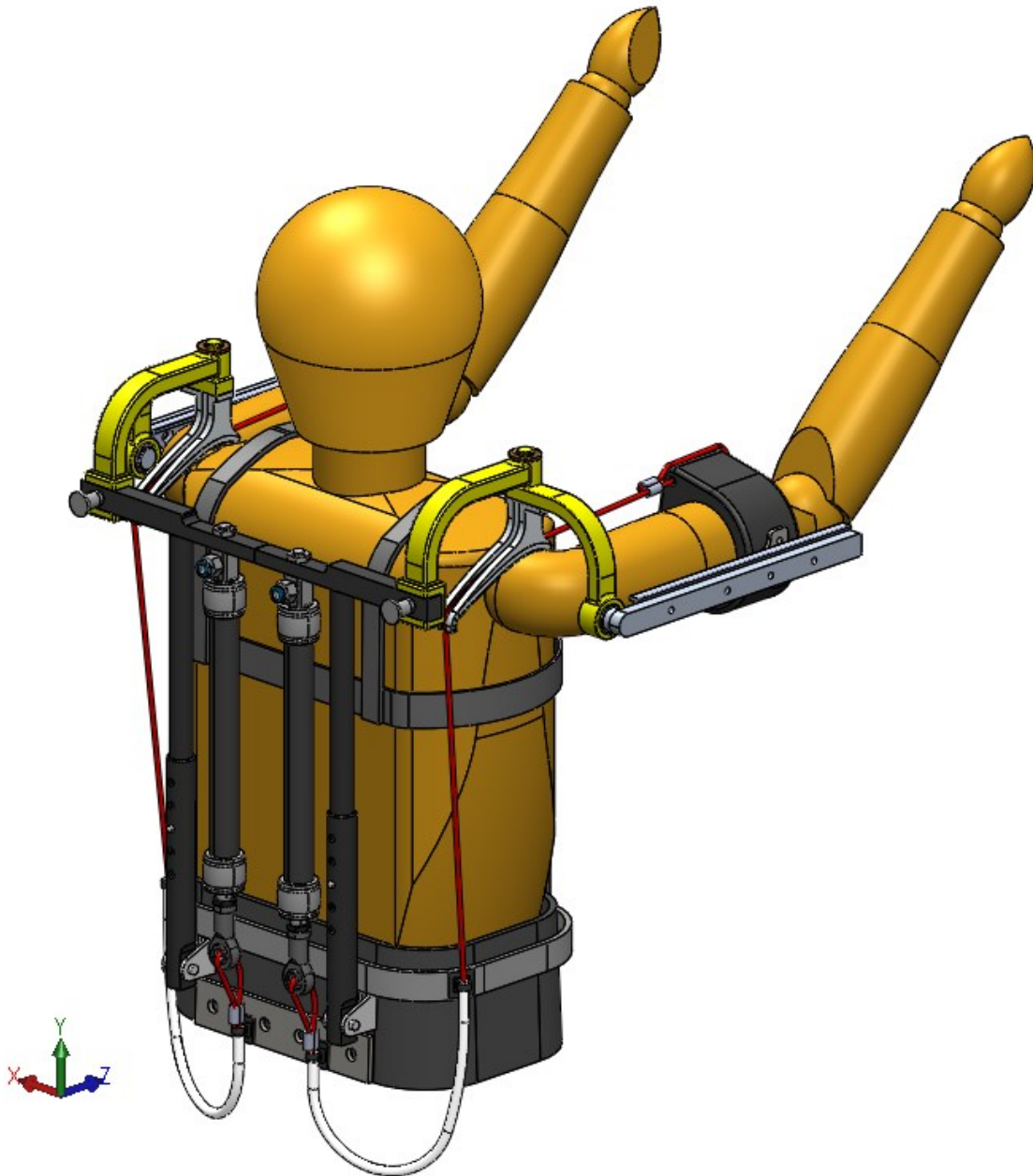


Figure 5.3 CAD model of the exoskeleton worn by the human body (with standard body parameters), including the safety harness, at elevation angle of the upper arm  $\vartheta_1 = 90^\circ$  and elevation angle of the forearm  $\vartheta_2 = 45^\circ$ .

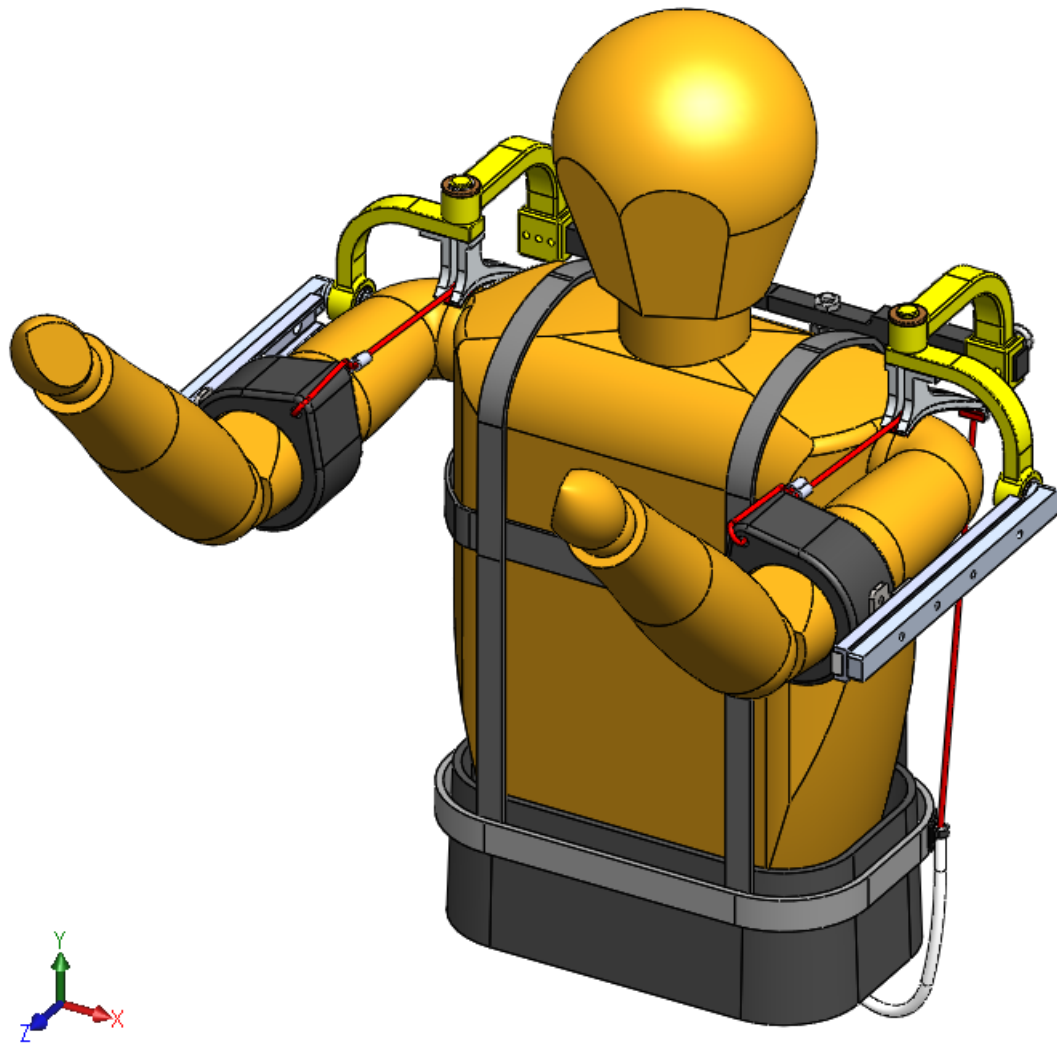


Figure 5.4 CAD model of the exoskeleton worn by the human body (with standard body parameters), including the safety harness, at elevation angle of the upper arm  $\vartheta_1 = 90^\circ$  and elevation angle of the forearm  $\vartheta_2 = 45^\circ$ .

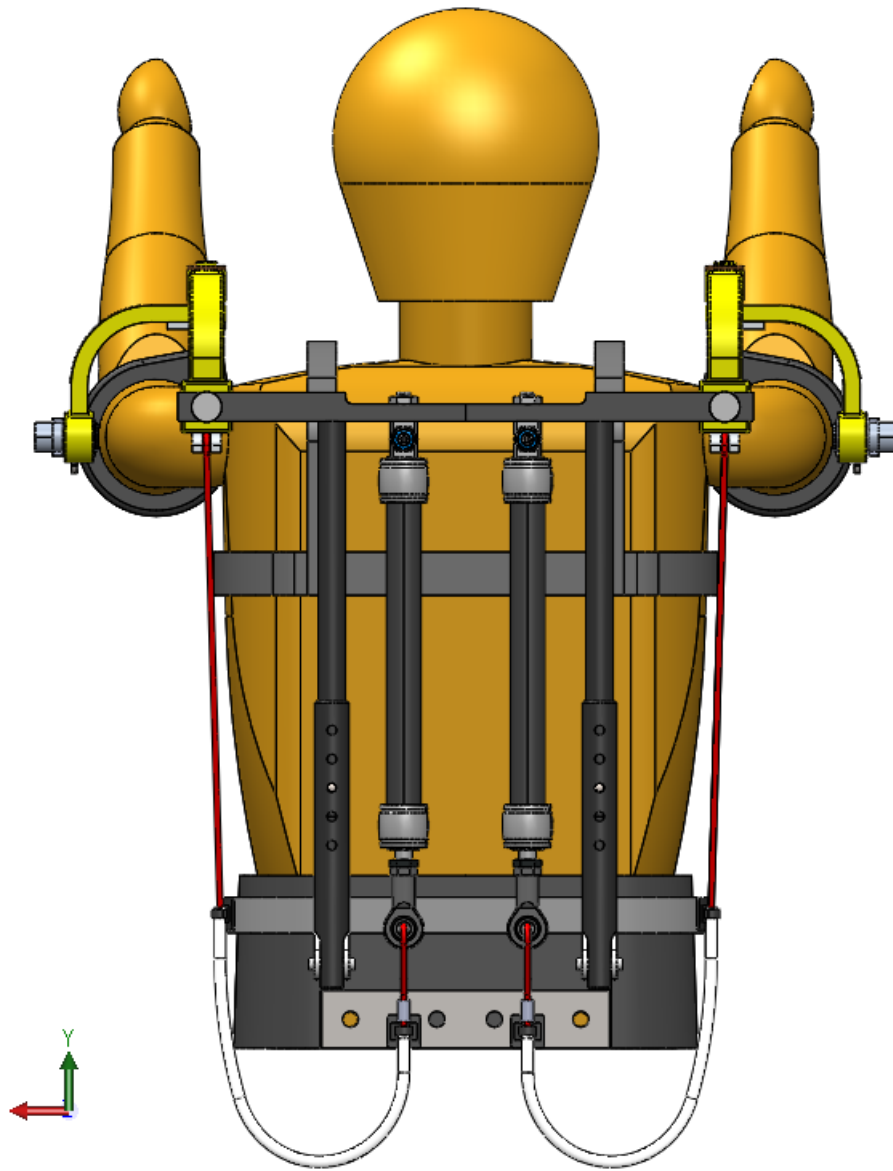


Figure 5.5 Rear part of the exoskeleton worn by the user.

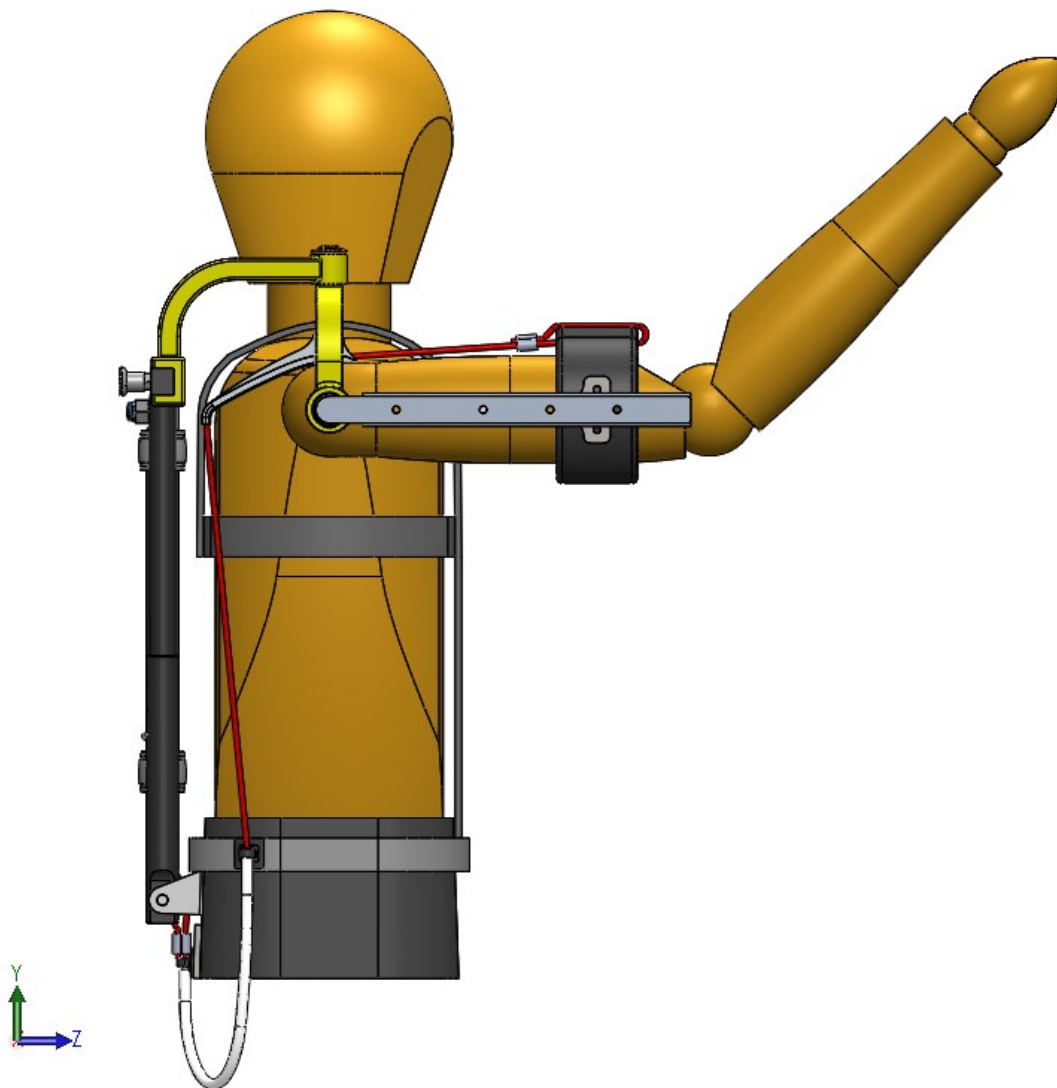


Figure 5.6 Lateral view of human body wearing the exoskeleton.

The model of the universal joint is shown in Figure 5.7, where the commercial bushings are mounted, by employing Seeger rings for axial locking of the bushings. The strut is meant to be realized as a linear telescopic guide, with a fixed element as rotating shaft of the bushing (SKF psm 202520), and a movable element that can slide along the fixed strut to allow the adjustment of the position of the bracelet. The movable element is welded to a plate which is screwed to the bracelet through two bolts and nuts. Then, the movable element of the strut is locked with another bolt and nut.

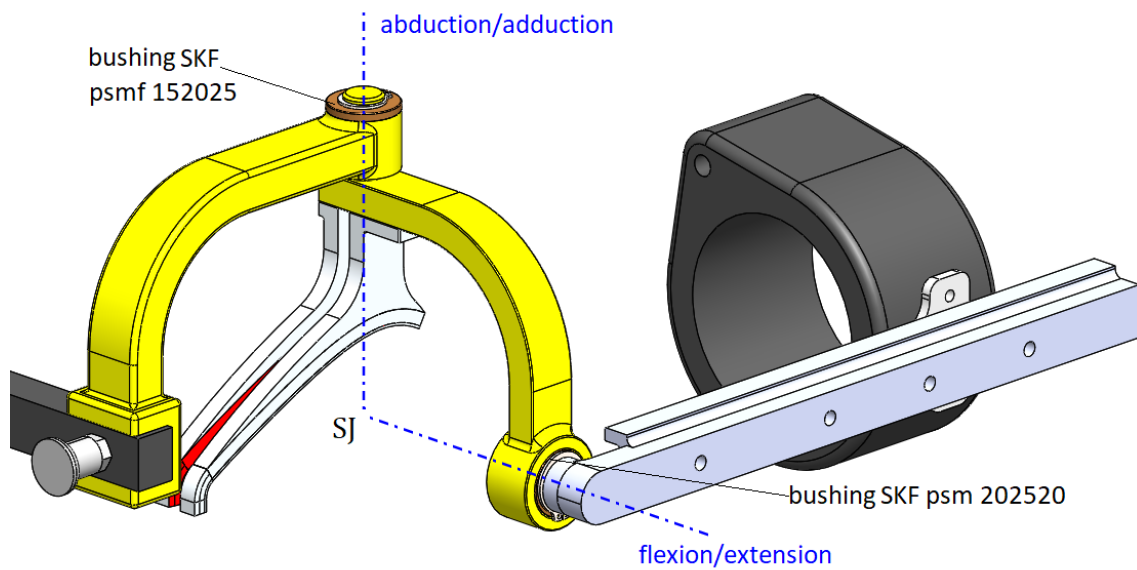


Figure 5.7 CAD model of the universal joint, with the commercial bushings and Seeger rings for axial locking. The axes of the bushings are to meet each other in the assumed centre of rotation of the shoulder joint (SJ).

To the hip belt, which is part of the harness, a commercial rear hinge is connected (rear hinge by ASCO), on which the telescopic rod is mounted, allowing the vertical adjustment through a pawl spring. The two sheath clips are those used for bicycle, for example the CLISPEED sheath clips are suggested. The second sheath clip (see Figure 5.8) is stuck on a plate connected to the hip belt, that improves the alignment of the second sheath clip to the rod eye at the free end of the PAM. For the purpose, a commercial flexible PVC sheath is employed, whose aim is to enable the reversal of the wire, for which a bicycle brake cable is suggested.

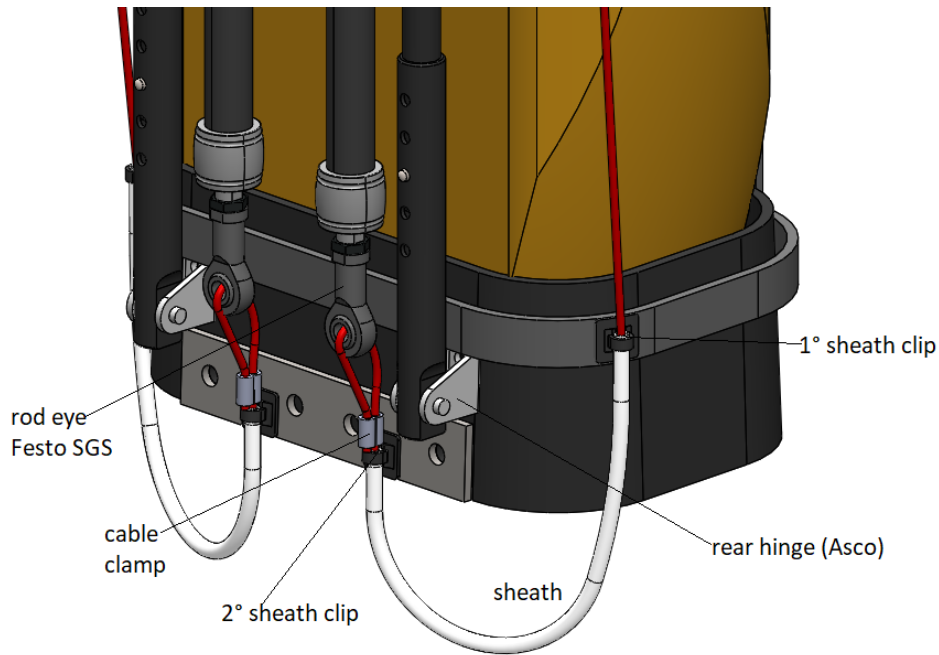


Figure 5.8 Sheath clips fixed to the hip belt of the harness, by carrying the sheath in which the wire passes for reversing its direction, then hooking the rod eye (by Festo) connected to the free end of the PAM.

Alternatively, a second solution was considered, which consists of fixing the PAM at the hip belt (bottom fixing solution). This solution is simpler because the wire, running out the profile of the shoulder pad, would be connected directly to the free end of the PAM below, through the rod eye and cable clamp, without the need of the sheath and sheath clips to reverse the direction of the wire. Yet, the bottom fixing solution requires the PAM to be vertically aligned with the profile of the shoulder pad, thus, by adjusting the position of the universal joint and shoulder pad from one user to another, the alignment fails. For this reason, the top fixing of the PAM is preferred, because this solution allows a freer adjustment of the position of the shoulder pad. Furthermore, this solution also improves the height adjustment of the device.

## 5.2 FEM analysis

For simulating the mechanism, the technique of Finite Element Analysis (FEM) has been used. This technique allows to run static structural analysis for the study of stresses in the CAD model, and therefore to check the static failure of the components. For this purpose, two software have been used to run the FEM analyses. First analysis were carried out through SolidWorks (Dassault Systèmes) which is mainly a 3D CAD drawing and design software, thus, then Altair HyperMesh was used, being a high-fidelity finite element modelling.

### 5.2.1 SolidWorks simulations

The model has been simulated, by assuming the upper limb extended horizontally, with  $\vartheta_1 = 90^\circ$  and  $\vartheta_2 = 0^\circ$ , to have the highest torque due to gravity, and the highest force exerted by the PAM at  $p = 2 \text{ bar}$ , with assumed initial contraction  $k_1 = 3.5\%$  of its nominal length. At first, the analysis has been run by considering the subassembly of bracelet, movable guide, strut and universal joint, whose fixtures, loads and connections must be defined for simulating the load condition. They are displayed in Figure 5.9.

- Fixtures: since the universal joint is supposed to be fixed to the horizontal beam through the spring plunger, the two interface surfaces of the fixed arch have been defined as fixed geometry constraint.
- External loads: by neglecting the weight force of the components, the subassembly model is subjected to four loads:
  1. The gravitational force of the upper limb,  $F_g = 35.38 \text{ N}$ , as  $\vartheta_1 = 90^\circ$  and  $\vartheta_2 = 0^\circ$ , which is applied in the centre of gravity of the arm, assumed to be rigidly connected to the bracelet.
  2. The tension of the wire pulling the bracelet,  $F_{mu} = 291.8 \text{ N}$  at supply pressure  $p = 2 \text{ bar}$  and initial contraction  $k_1 = 3.5\%$ , that is supposed to be exerted on the surface of the bracelet, directed towards the shoulder pad profile.
  3. The wire is supposed to slide without crawling along the shoulder pad profile, so the shoulder pad is subject to the tension of the wire too ( $F_{sh,A} = 291.8 \text{ N}$ ), in the same and opposite direction to the previous load, applied in the first contact point with the profile,  $A$ .
  4. The tension of the wire leaving the profile of the shoulder pad, in vertical direction, applied in the last contact point  $Z$  ( $F_{sh,Z} = 291.8$ ). For both tensions on the shoulder pad, friction is supposed to be null.
- Connections: between the bracelet and the movable guide two bolt connectors are defined, as well as the one between the movable guide and the strut, to lock the bracelet in position on the upper arm. For each bolt (supposed to be in steel) a preload of  $5 \text{ N}$  is defined. Thus, between the interface surfaces of the components connected by bolts, contact groups have been defined. Instead, everywhere else the bonded global contact is defined, so that the components are connected as were assembled, without penetration, and by assuming zero friction. Finally, the shoulder pad is supposed to be welded to the movable arch of universal joint, since they must be rigidly connected to each other.

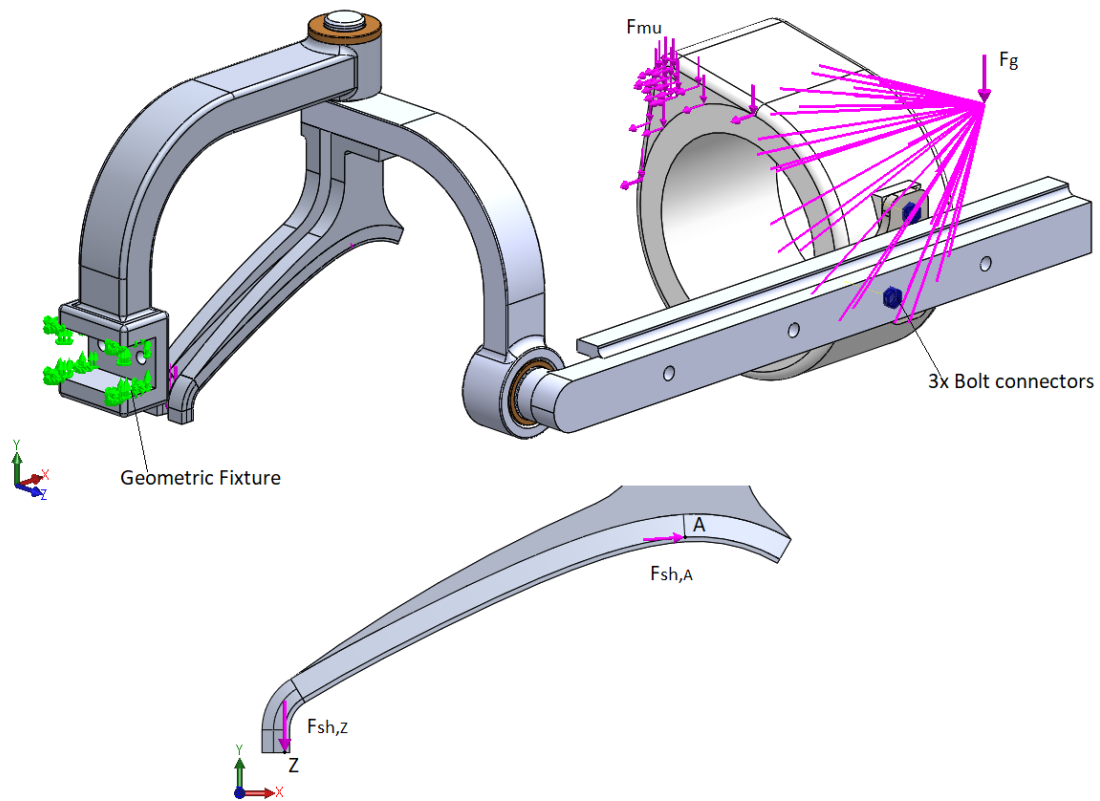


Figure 5.9 CAD model of the subassembly from universal joint to bracelet, with defined fixtures, external loads, and bolt connectors (top), detail of the tensions of the wire on the shoulder pad, applied in first and last contact points A and Z (down).

After defining fixtures, external loads and connections, the materials have been assigned. Several static analyses have been run, changing the materials, until finding the optimal combination to verify the static failure of all the CAD components, relying on simulation results produced by SolidWorks.

The final combination of materials is reported in Table 5.1 with their yield strength ( $R_{p0,2}$ ) or maximum tensile strength before breakdown for plastics ( $R_m$ ):

Table 5.1 Materials assigned to components of the subassembly from universal joint to bracelet.

	Material	$R_{p0,2} (R_m) [MPa]$
Bracelet	Polyester resin	190
Movable guide	39NiCrMo3 steel	785
Strut	Alufont-48 <sup>2</sup> T6	460
Movable arch	Silafont-70 <sup>3</sup> T6	390
Shoulder pad	Silafont-70 T6	390
Fixed arch	356.3 T6 aluminium alloy	240

After that, the tetrahedral curvature-based mesh of the model has been created, with minimum dimension of the element 3.4 mm and maximum 17.1 mm, by applying a control mesh, with element dimension 1.2 mm, in critical areas for instance on interface surfaces of the bolt connectors, near the holes, the seat of the bushing, while on the profile surface of the shoulder pad, the element dimension is 2 mm. This mesh produces 754865 nodes, with 96.4 % of finite elements in the model with aspect ratio lower than 3, checking an excellent quality of meshing. Running the static analysis simulation, the results displayed in next figures are found.

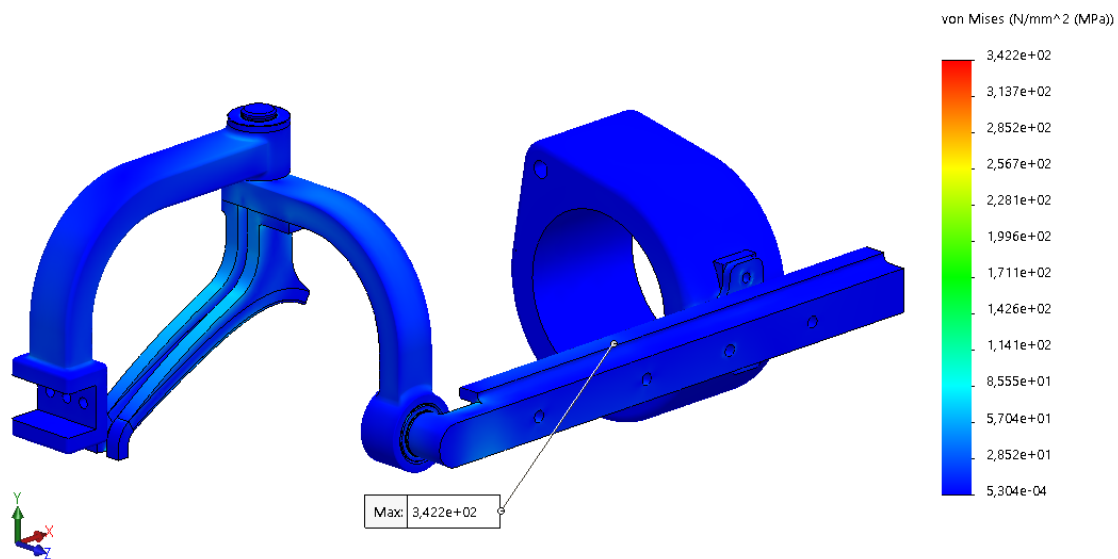


Figure 5.10 Von Mises stresses in the whole subassembly from SolidWorks static analysis.

<sup>2</sup> AlCu4TiMgAg aluminium alloy

<sup>3</sup> AlSi12CuNiMg aluminium alloy

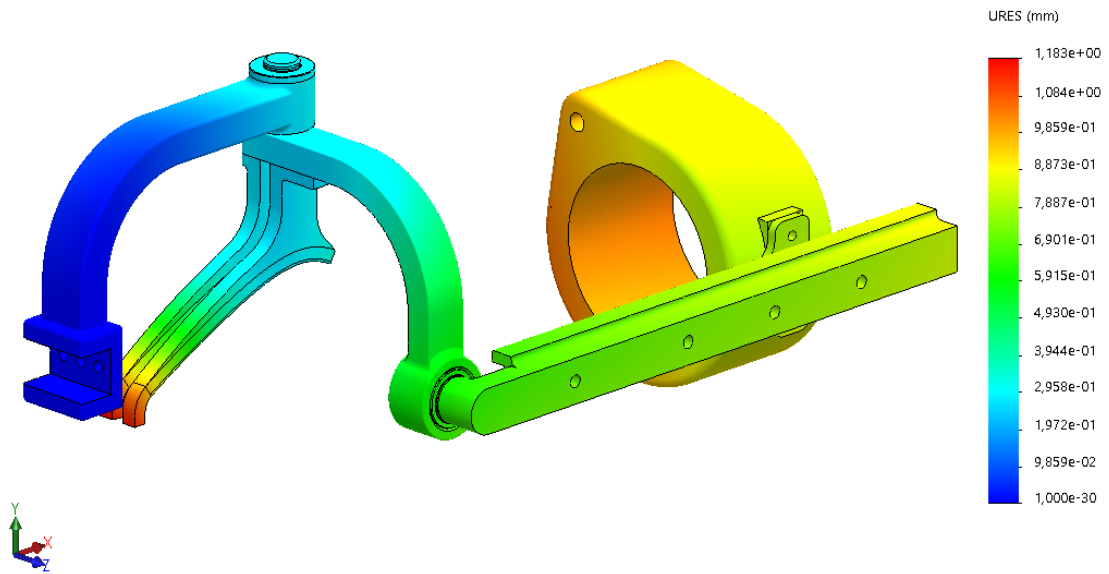


Figure 5.11 Magnitude of displacement of the whole subassembly from SolidWorks static analysis.

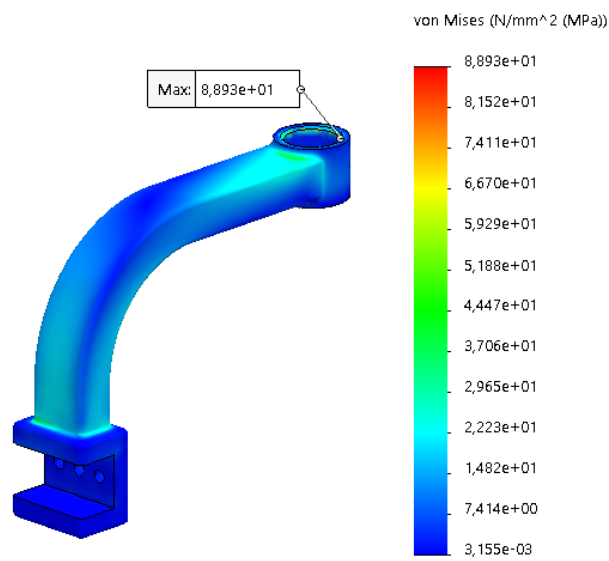


Figure 5.12 Von Mises stresses in the fixed arch of universal joint from SolidWorks static analysis.

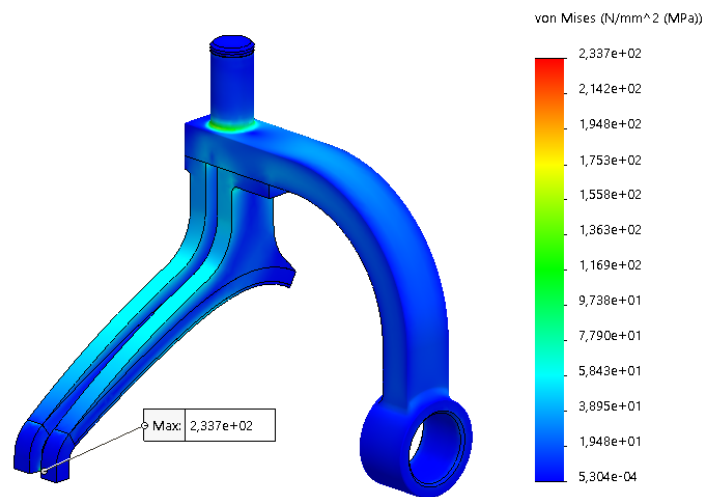


Figure 5.13 Von Mises stresses in the movable arch and shoulder pad from SolidWorks static analysis.

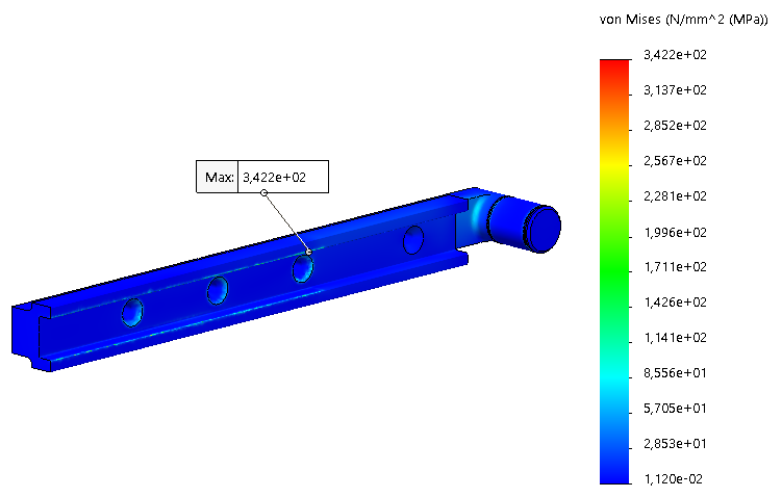


Figure 5.14 Von Mises stresses in strut from SolidWorks static analysis.

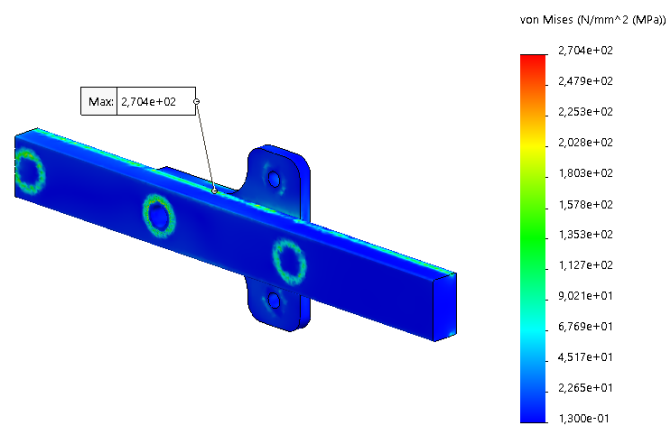


Figure 5.15 Von Mises stresses in the movable guide from SolidWorks static analysis.

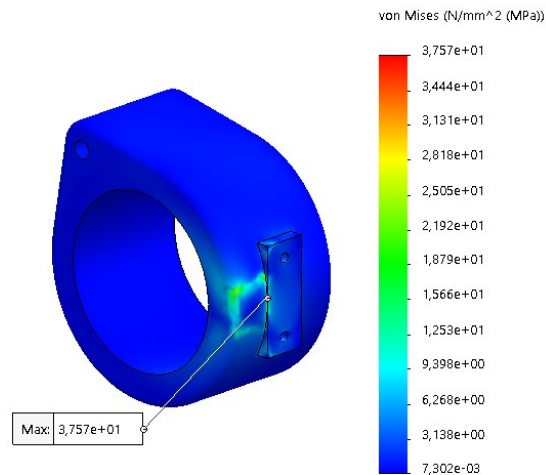


Figure 5.16 Von Mises stresses in the bracelet from SolidWorks static analysis.

Then, the static analysis has been run, by including the horizontal beam, to which the fixed arch of universal joint is attached, and the fixed end of the pneumatic artificial muscle too. As material, the 201.0 T6 aluminium alloy ( $R_{p0,2} = 349 \text{ MPa}$ ) is assigned. Since the PAM exerts a force by pulling the wire, by contraction, an additional load is defined in the model, in the centre of the hole into which the threaded end of the PAM is inserted, directed upwards ( $F_{mu}$ ). The geometric fixture of the beam is simulated by the interface surface with the telescopic rod, to which the beam is welded, as shown in Figure 5.17.

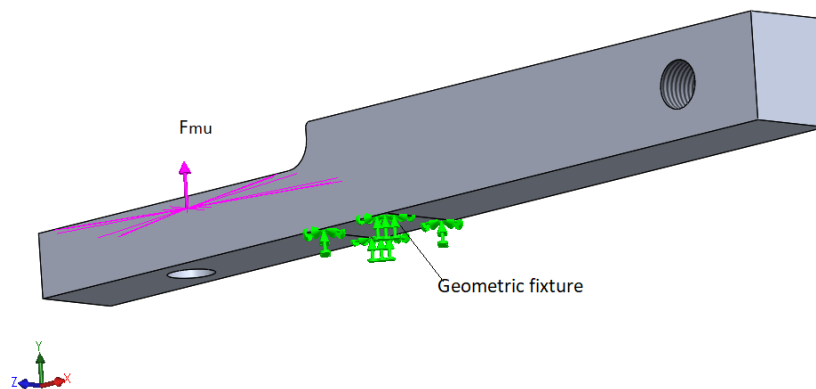


Figure 5.17 CAD model of the horizontal beam with additional load  $F_{mu}$  and geometric fixture.

The model has been meshed with minimum element size  $3.5 \text{ mm}$ , and maximum size  $17.5 \text{ mm}$ , while in critical areas the size is reduced to  $1.5 \text{ mm}$ . By running the static analysis, Figure 5.18 shows the calculated Von Mises stresses in the beam, and Figure 5.19 the magnitude displacement.

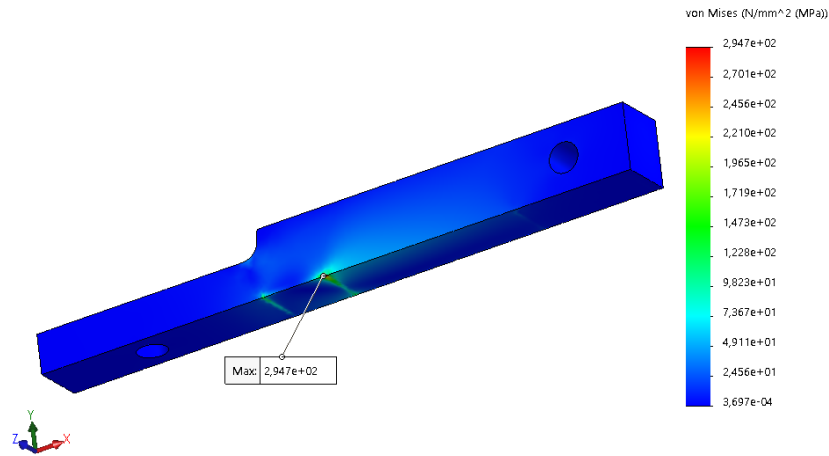


Figure 5.18 Von Mises stresses in the horizontal beam from SolidWorks static analysis.

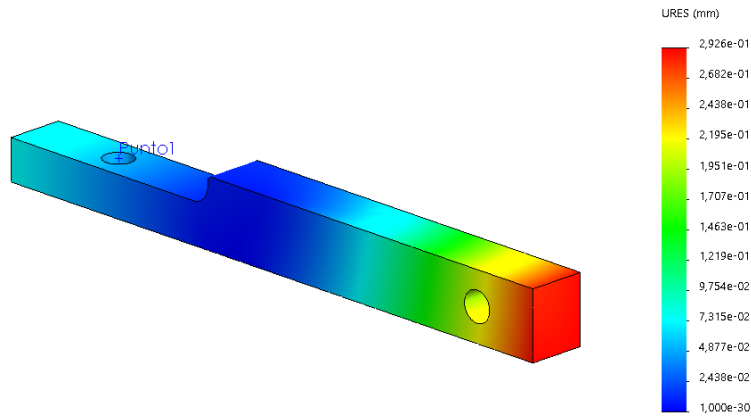


Figure 5.19 Magnitude of displacement of the horizontal from SolidWorks static analysis.

From the constraint reactions calculated by the program in the FEM analysis, the loads exerted by the horizontal beam on the telescopic rod are calculated, as forces and torques. These external loads are applied on the interface surface of the telescopic rod with the horizontal beam (see Table 5.2).

Table 5.2 External loads on the telescopic rod

$F_x$	48.33 N
$F_y$	-12.33 N
$F_z$	-14.19 N
$M_x$	297.64 Nmm
$M_y$	419.40 Nmm
$M_z$	332.27 Nmm

The geometric constraint is simulated by the cylindrical surface that fits into the pin of the rear hinge; besides a connector via pin is defined between the movable and fixed part of the telescopic rod, by simulating the steel pawl spring (see Figure 5.20). By assigning the *AlSi10Mg T6* aluminium alloy ( $R_{p0,2} = 260 \text{ MPa}$ ) to the parts, the static analysis calculates the stresses and magnitude displacement shown.

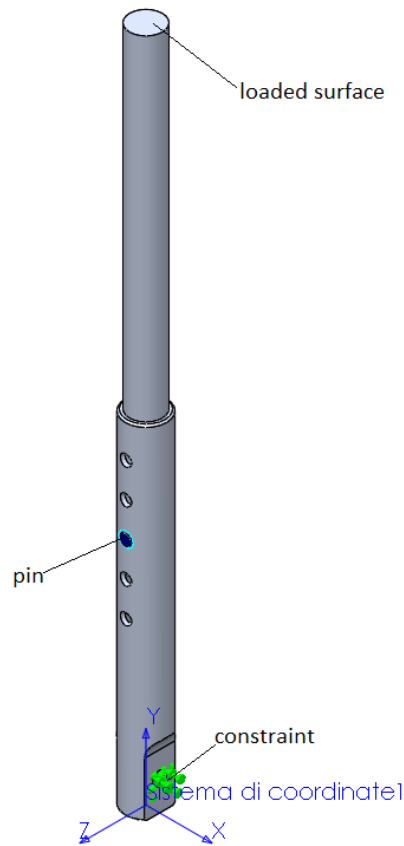


Figure 5.20 CAD model of the telescopic rod (movable and fixed part), with pin connector and surface constraint.

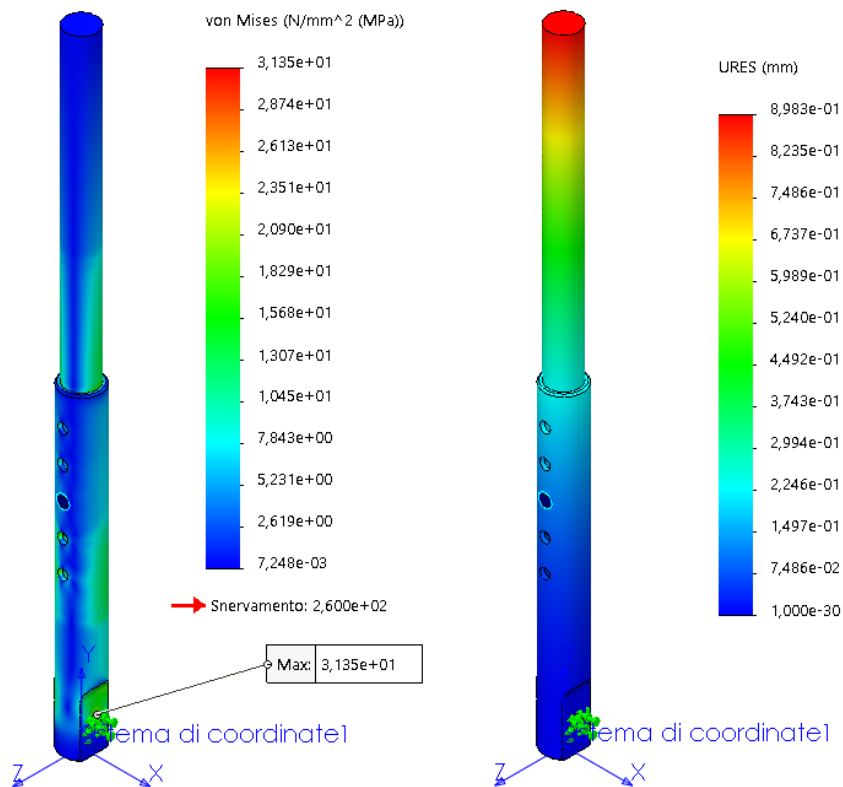


Figure 5.21 Von Mises stresses in the telescopic rod (left), magnitude displacement (right) from SolidWorks static analysis.

### 5.2.2 Altair HyperMesh simulations

Since SolidWorks is mainly a modelling and design software, Altair HyperMesh has also been used for running FEM static analyses, in order to obtain more accurate results. In fact, HyperMesh is the market-leading software for 3D finite element modelling, which allows to import the CAD geometry, for generating a high-quality mesh and then running the static simulation.

Thus, at first the subassembly from the universal joint to the bracelet has been tested, by assigning to the different components the same materials as for SolidWorks simulations (see Table 5.1). Besides, the same external loads have been applied, as the constraints. In particular for the geometric fixture on the fixed arch, the constraint has been specified to lock 6 DOF. Then, the model has been meshed with tetrahedral elements of size 2 mm, by thickening their density near the holes.

Yet, for defining the bolt connectors, beam elements were created between the extreme nodes, and then defining a rigid connection of these nodes with the CAD components. Thus, the mechanical properties of the bolts have been assigned, as the moments of inertia, the section area, the torsion modulus, and the mass per length. The drawback is that HyperMesh

do not allow to define a preload on the bolt connectors, and to do so, a thermal load has been simulated in the extreme nodes of the bolts, to generate the compression. The thermal load has been calculated by this equation:

$$\Delta T = \frac{P}{\alpha \cdot E \cdot A} = 0.226 \text{ } ^\circ\text{C} \quad (5.1)$$

$P$  is the preload, equal to 5 N,  $E$  the modulus of elasticity of the bolt material (Steel 210 GPa),  $\alpha$  is the coefficient of thermal expansion of steel ( $12 \cdot 10^{-6} \text{ } ^\circ\text{C}^{-1}$ ), and  $A$  the resistant section of the screw, calculated as:

$$A = \frac{\pi}{4} \cdot \left( \frac{d_2 + d_3}{2} \right)^2 \quad (5.2)$$

In the equation,  $d_2$  is the core diameter of the screw, and  $d_3$  is the average diameter (available by technical legislation). Since the default room temperature is set to 0 °C, a negative temperature is defined in the extreme nodes which identify the bolt connectors, simulating a compression load. Finally, the contact groups have been defined between the coupled components, assuming friction null.

By running the linear static analysis, the Von Mises stresses of the model are calculated. These values depend on the program solver, and so on the evaluation method of the stresses. For instance, the average stresses on the nodes can be considered, or the maximum calculated value in the nodes. To consider the most conservative condition, the Maximum averaging method has been chosen, because it shows the maximum stress in each node. These values are displayed in next figures.

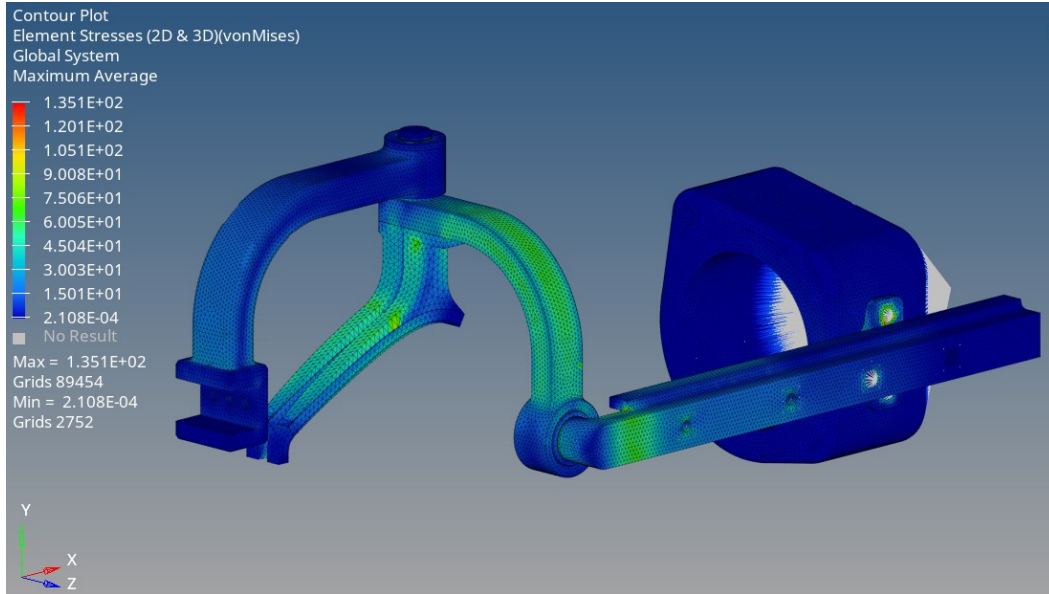


Figure 5.22 Von Mises stresses (*MPa*) in the whole subassembly, calculated by Maximum averaging method from HyperMesh linear static analysis.

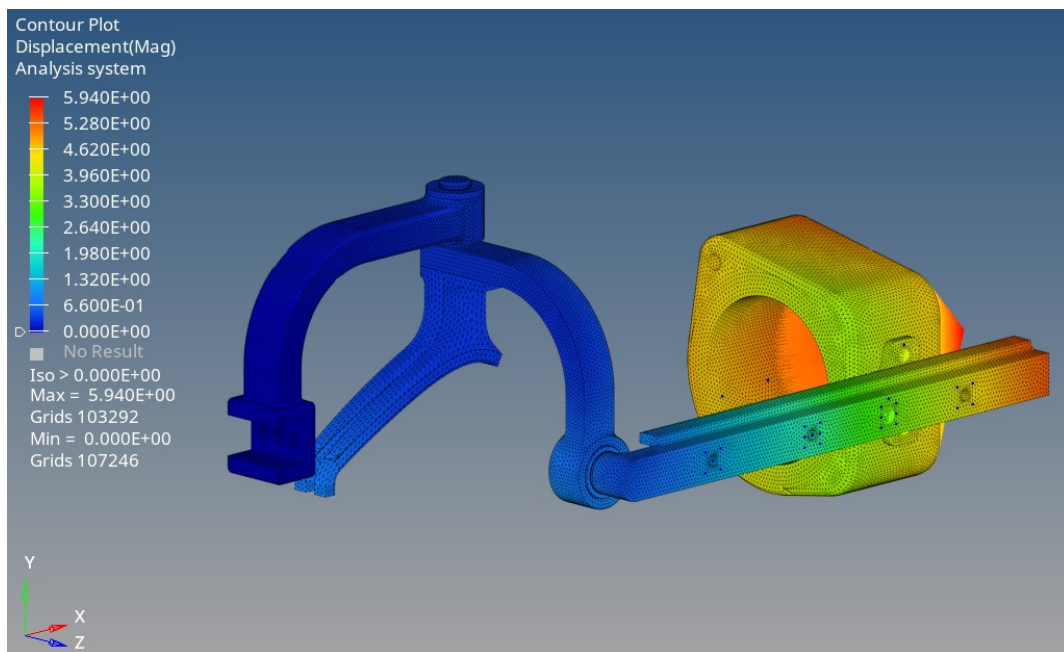


Figure 5.23 Magnitude displacement (*mm*) in the whole subassembly, calculated by Maximum averaging method from HyperMesh linear static analysis.

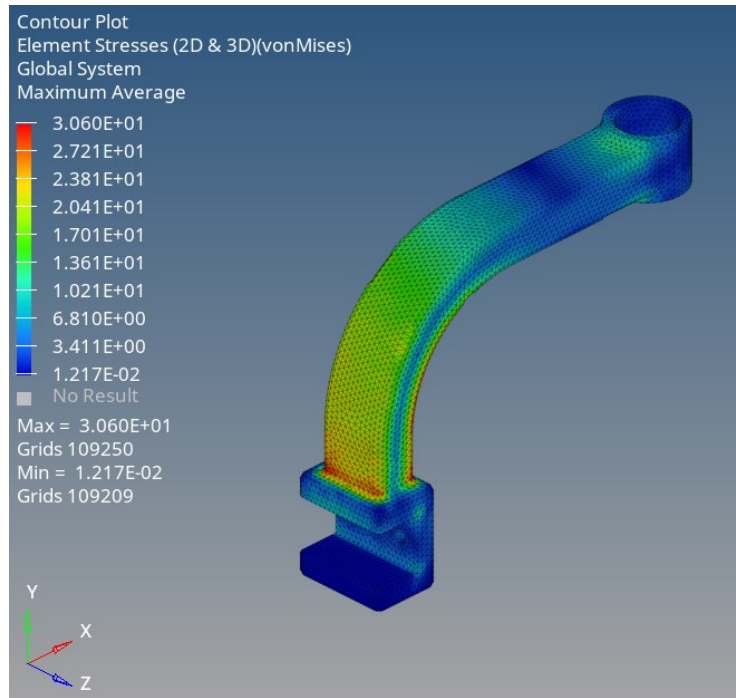


Figure 5.24 Von Mises stresses ( $MPa$ ) in the fixed arch, calculated by Maximum averaging method from HyperMesh linear static analysis.

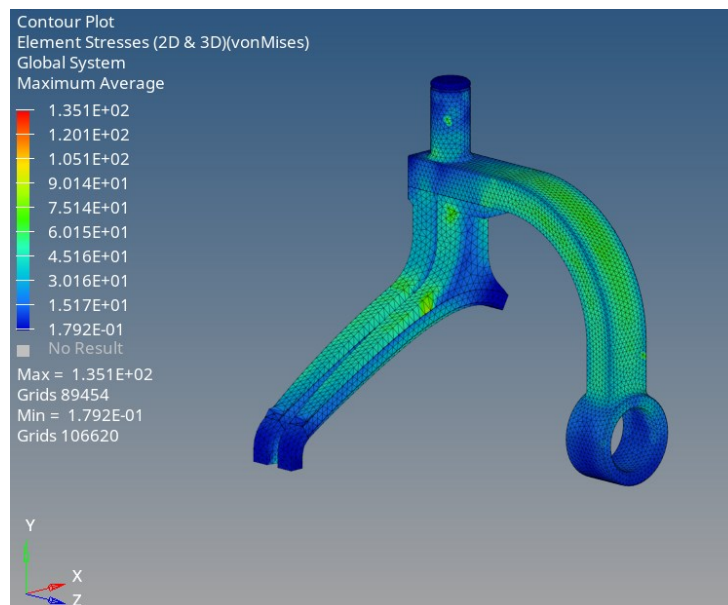


Figure 5.25 Von Mises stresses ( $MPa$ ) in the movable arch and shoulder pad, calculated by Maximum averaging method from HyperMesh linear static analysis.

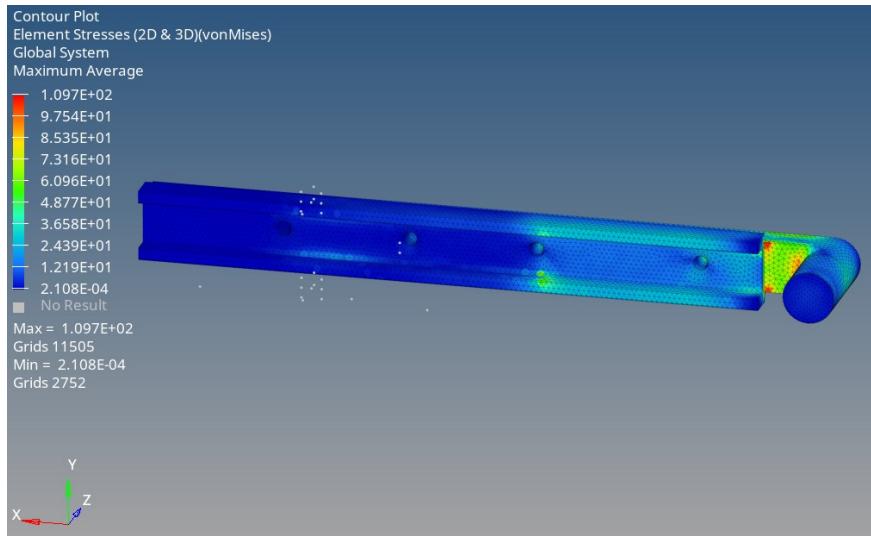


Figure 5.26 Von Mises stresses ( $MPa$ ) in the strut, calculated by Maximum averaging method from HyperMesh linear static analysis.

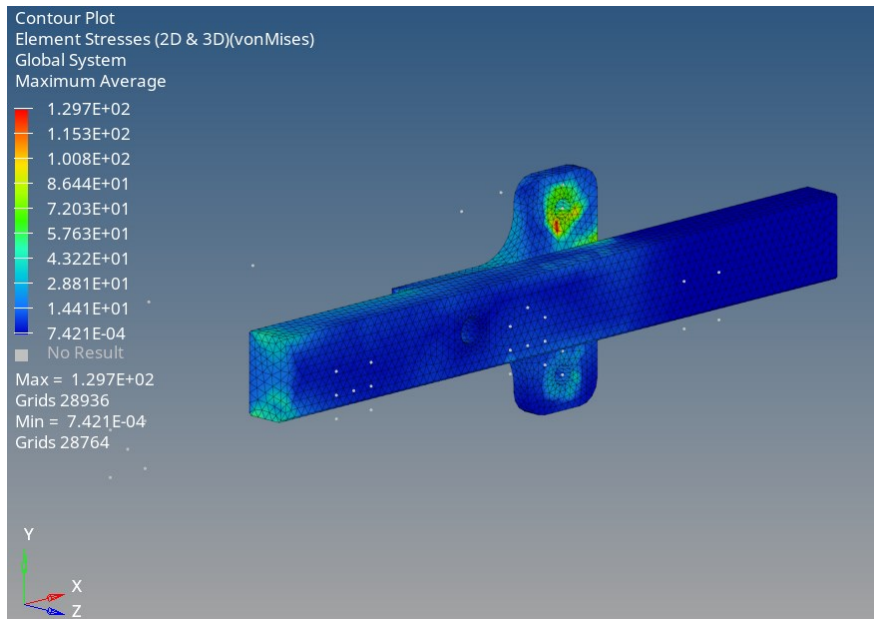


Figure 5.27 Von Mises stresses ( $MPa$ ) in the movable guide, calculated by Maximum averaging method from HyperMesh linear static analysis.

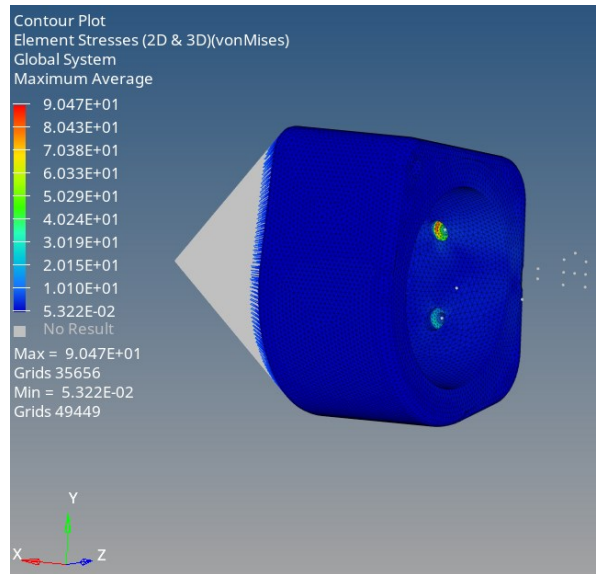


Figure 5.28 Von Mises stresses ( $MPa$ ) in the bracelet, calculated by Maximum averaging method from HyperMesh linear static analysis.

Then, from the constraint reactions in the fixed arch, the external forces and torques applied on the horizontal beam have been calculated, also adding the force due to the pneumatic muscle contraction, hanging from the horizontal beam, as for SolidWorks simulations. These external loads are applied on the model that includes the horizontal beam and the telescopic rod. By defining the contact groups between the components, with also a pin connection (in steel) between the movable and fixed part of the telescopic rod, the following Von Mises stresses have been calculated (from Maximum averaging method).

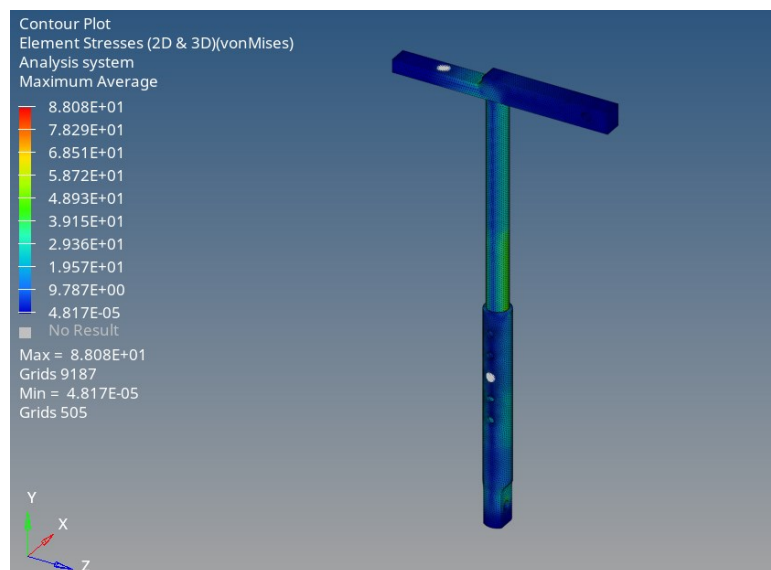


Figure 5.29 Von Mises stresses ( $MPa$ ) in the subassembly, calculated by Maximum averaging method from HyperMesh linear static analysis.

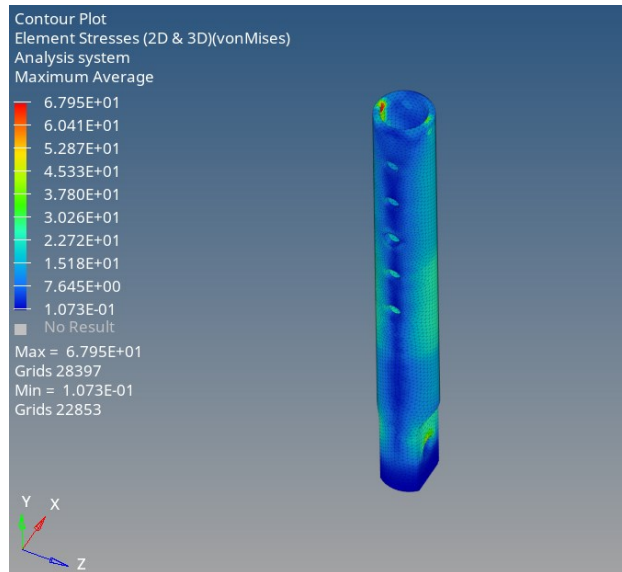


Figure 5.30 Von Mises stresses ( $MPa$ ) in the fixed part of telescopic rod, calculated by Maximum averaging method from HyperMesh linear static analysis.

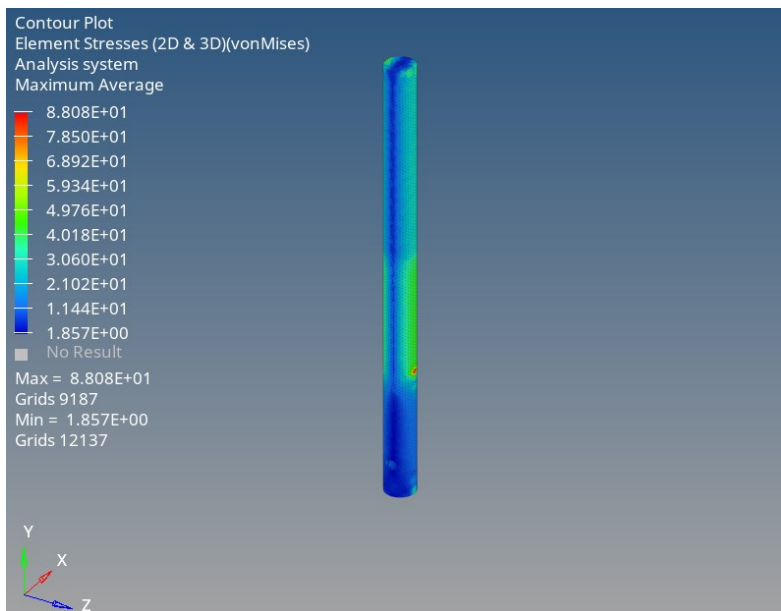


Figure 5.31 Von Mises stresses ( $MPa$ ) in the movable part of telescopic rod, calculated by Maximum averaging method from HyperMesh linear static analysis.

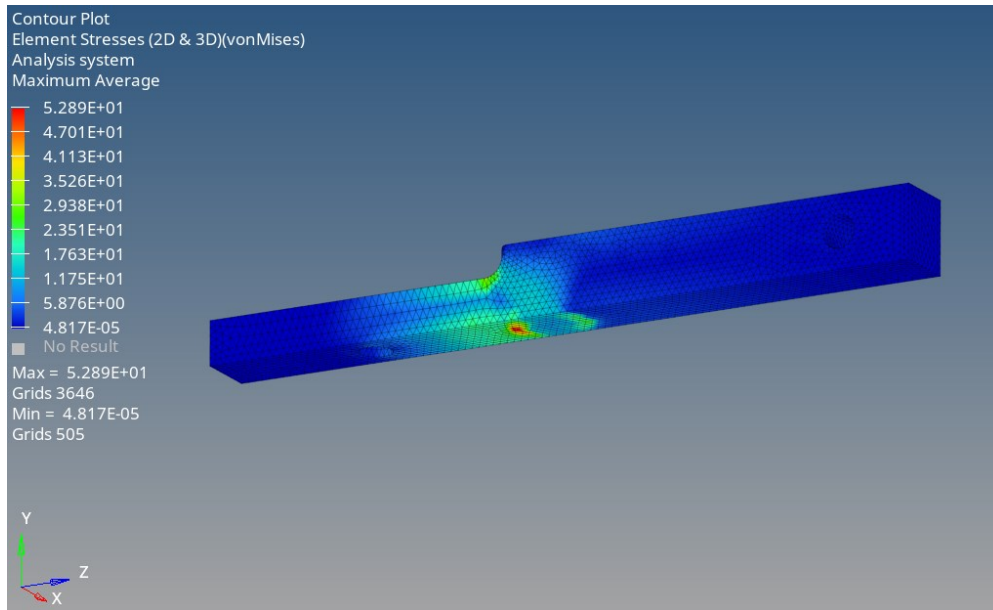


Figure 5.32 Von Mises stresses ( $MPa$ ) in the horizontal beam, calculated by Maximum averaging method from HyperMesh linear static analysis.

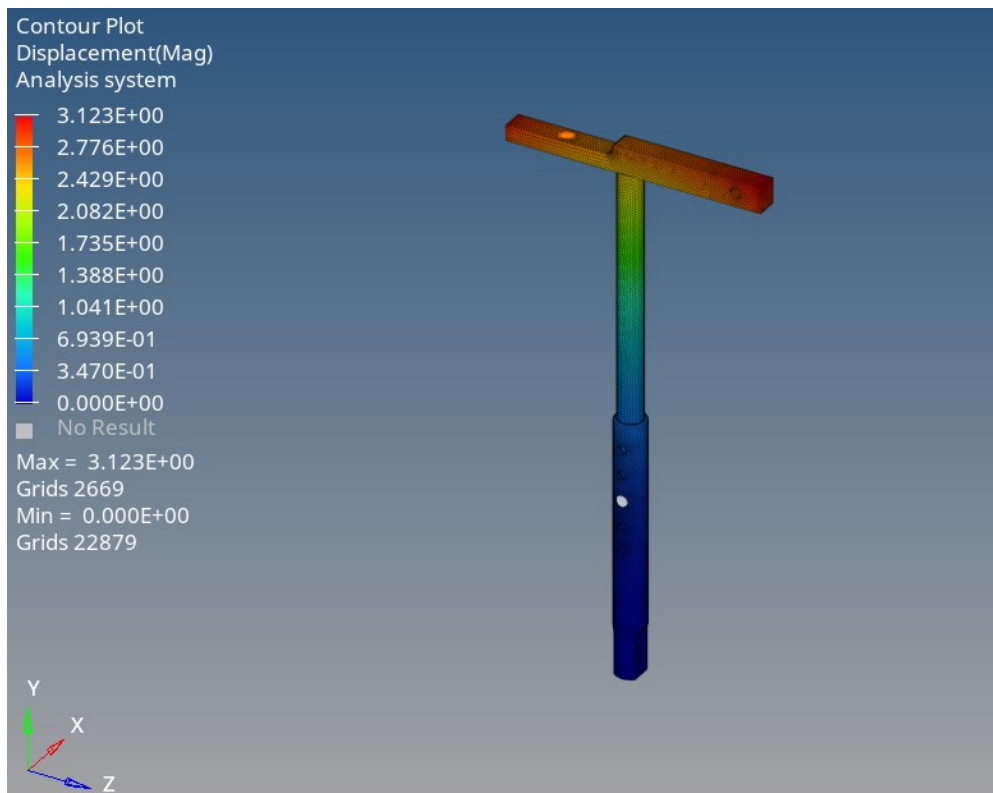


Figure 5.33 Magnitude displacement ( $mm$ ) of the subassembly, calculated by Maximum averaging method from HyperMesh linear static analysis.

As shown, there is a certain disparity between the values calculated with the two software. This is also due to the different processing method, the mesh quality and goodness of the program solver. Therefore, in order to treat the worst condition of stresses, the most critical results have been considered for choosing the materials to assign, and so to prevent the elastic static failure in both the simulation.

### 5.3 Exoskeleton weight

By assuming the materials suggested in FEM analysis, and employing the following commercial components shown in Table 5.3, the overall weight of the exoskeleton has been estimated, considering the mechanism for both the upper limbs, including bolts, and the commercial TITAN safety harness, by Honeywell.

Table 5.3 Overall weight of the exoskeleton.

	Q°	Material	Weight (g)
TITAN Harness (by Honeywell)	1	-	1000
Telescopic rod	2	<i>AlSi10Mg T6</i>	283.21
Horizontal beam	2	201.0 T6	153.78
Fixed arch	2	356.3 T6	219.33
Movable arch	2	Silafont-70 T6	135.84
Bushing psmf 152025 (SKF)	2	Sintered bronze	34.86
Bushing psm 202520 (SKF)	2	Sintered bronze	29.21
Festo DMSP-20-200N RMCM PAM	2	-	206.38
Push-in fitting QS-G1/4-8 (Festo)	2	-	15
Sheath clip (CLISPEED)	4	Aluminium alloy	6
Rear hinge P493AL420200A00 (ASCO)	2	Steel	80
Spring plunger PXA10 (Misumi)	2	-	20
Pawl spring	2	Steel	2.93
Seeger ring d15	2	-	0.714
Shoulder pad	2	Silafont-70 T6	85.39
Strut	2	Alufont-48 T6	333.37
Movable guide	2	<i>39NiCrMo3</i>	246.50
Bracelet	2	Polyester resin	421.20
Seeger ring d20	4	-	1.303
Rod eye SGS-M10-1.25 (Festo)	2	-	88
Belt plate	1	AISI 304	304.79
Sheath	2	PVC	9,73
Cable clamp (Double hole aluminium ferrule)	4	-	4.69
Slotted pan head screw ISO 1580 M4x20	4	-	2.76

Hex thin nut ISO 4035 M4	4	-	0.571
Slotted pan head screw ISO 1580 M5x35	2	-	6.797
Hex thin nut ISO 4035 M5	6	-	0.859
Slotted pan head screw ISO 1580 M5x12	4	-	3.252
Slotted pan head screw ISO 1580 M10x16	2	-	22.369
Hex thin nut ISO 4035 M10	2	-	6.313
		<i>Total weight (kg)</i>	6.18

## Chapter 6

# Results and discussion

### 6.1 Verification of PAM results

At the level of final verification, the torques are compared, by varying both the elevation angle of the upper arm ( $\vartheta_1$ ) and the forearm ( $\vartheta_2$ ). At first, in Figure 6.1, the torque due to gravity is shown as a 3D surface, function of the two elevation angles within the assumed biomechanical limits.

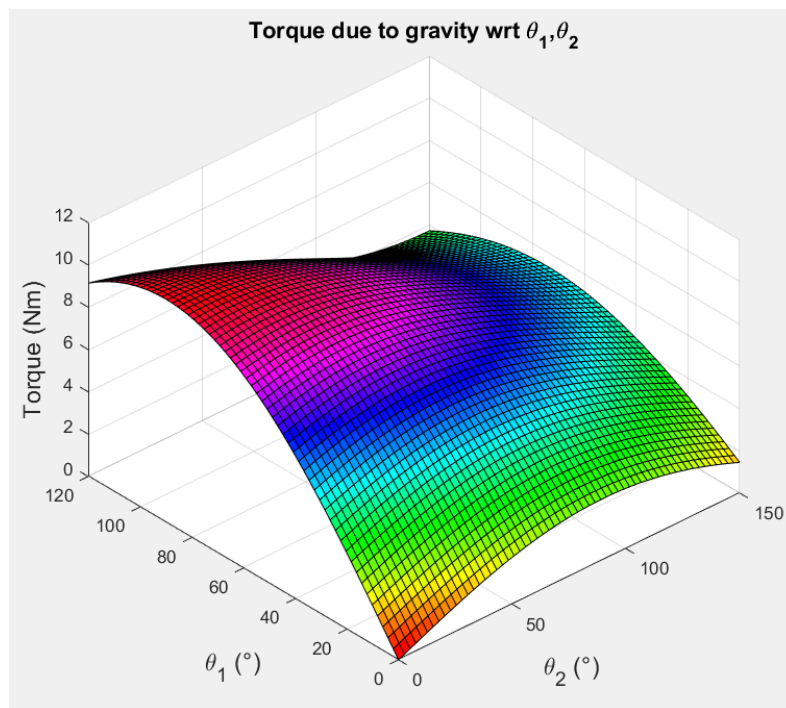


Figure 6.1 Torque due to gravity of the upper limb with respect to the elevation angle of the upper arm  $\vartheta_1$  and the elevation angle of the forearm  $\vartheta_2$ .

Then, this surface is compared with the one of the torque exerted by the pneumatic muscle, by employing the shoulder pad, at constant pressure, for example  $p = 2.5 \text{ bar}$ , in Figure 6.2.

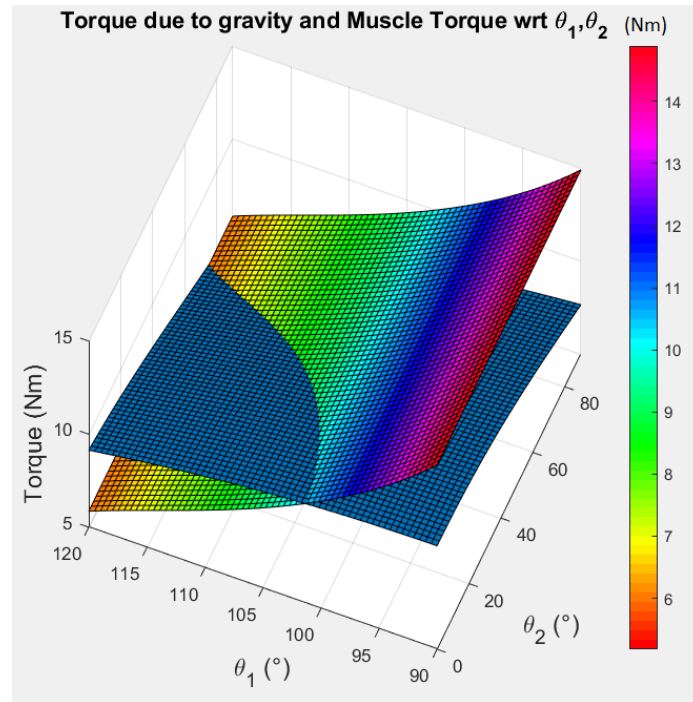


Figure 6.2 Comparison of the torque due to gravity (blue monochrome surface) with the torque generated by the PAM at  $p = 2.5 \text{ bar}$  (multicolour surface), with respect to  $\vartheta_1$  ( $90^\circ: 120^\circ$ ) and  $\vartheta_2$  ( $0: 90^\circ$ ).

Therefore, the difference of the two torques is calculated for each position (Figure 6.3), which is the torque that the shoulder complex muscles must provide to lift or to lower the upper limb from the equilibrium position.

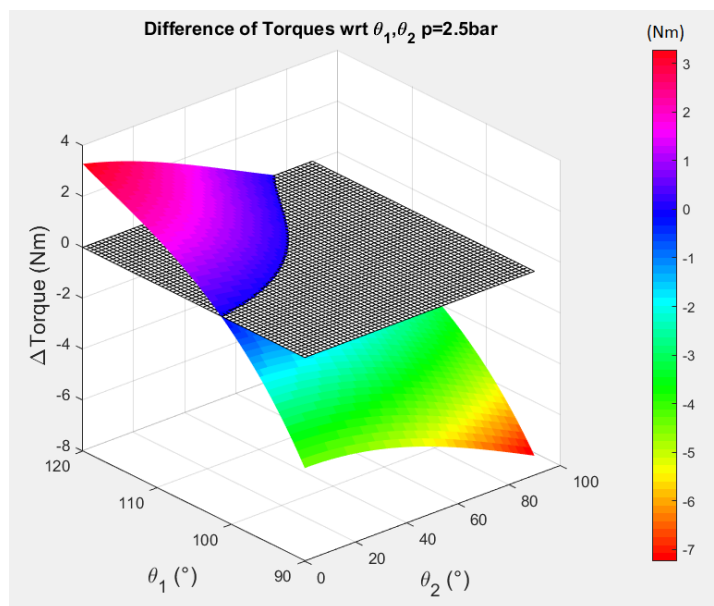


Figure 6.3 Surface of the difference between the torque due to gravity and the torque exerted by the PAM (multicolour surface), intersected by the plane  $\pi: \Delta Torque = 0$ .

In Figure 6.3 the plane  $\pi$ :  $\Delta Torque = 0$ , is shown because, by intersecting the surface of difference of the torques, the equilibrium curve is picked out, along which the torque generated by the PAM matches the torque due gravity, so the upper extremity muscles are unloaded. This equilibrium curve is displayed in Figure 6.4 (black curve), which is meant to sum up the performance of the exoskeleton in assisting the upper limb. In this figure, the absolute difference of the two torques is reported, and, by departing from the black equilibrium line, the curves at different  $\Delta Torque \neq 0$  are represented by the different colour, corresponding to increasing torques required on shoulder muscles.

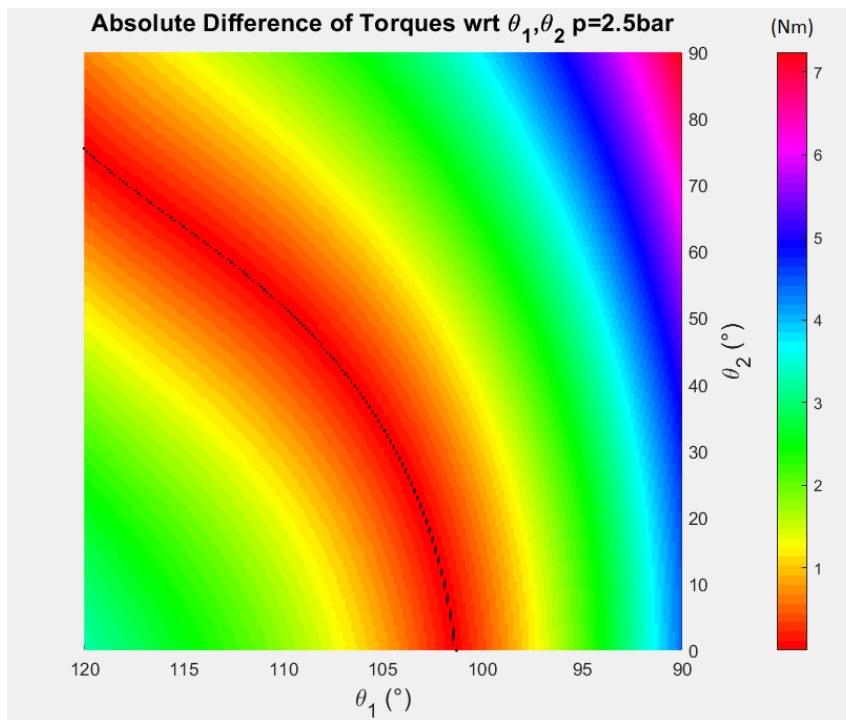


Figure 6.4 Surface of the absolute difference between the torque due to gravity and generated by the PAM, at  $p = 2.5 \text{ bar}$  projected on plane  $\pi$ :  $\Delta Torque = 0$ , with the equilibrium curve (black), from which the curves at  $\Delta Torque \neq 0$  depart distinguished by colour.

## 6.2 Verification of shoulder pad contribution

To appreciate the contribution of the shoulder pad in compensating the moment due to gravity of the upper limb, Figure 6.5 is produced. The figure compares the ratio of absolute difference between the torques to the maximum value of torque due to gravity, occurring within the assumed range of elevation angle  $\vartheta_1$ , and  $\vartheta_2$ , by employing the rod with passing joint (left), and by employing the shoulder pad designed in Chapter 4 (right). In Figure 6.6, a similar comparison is made at supply pressure  $p = 2 \text{ bar}$ .

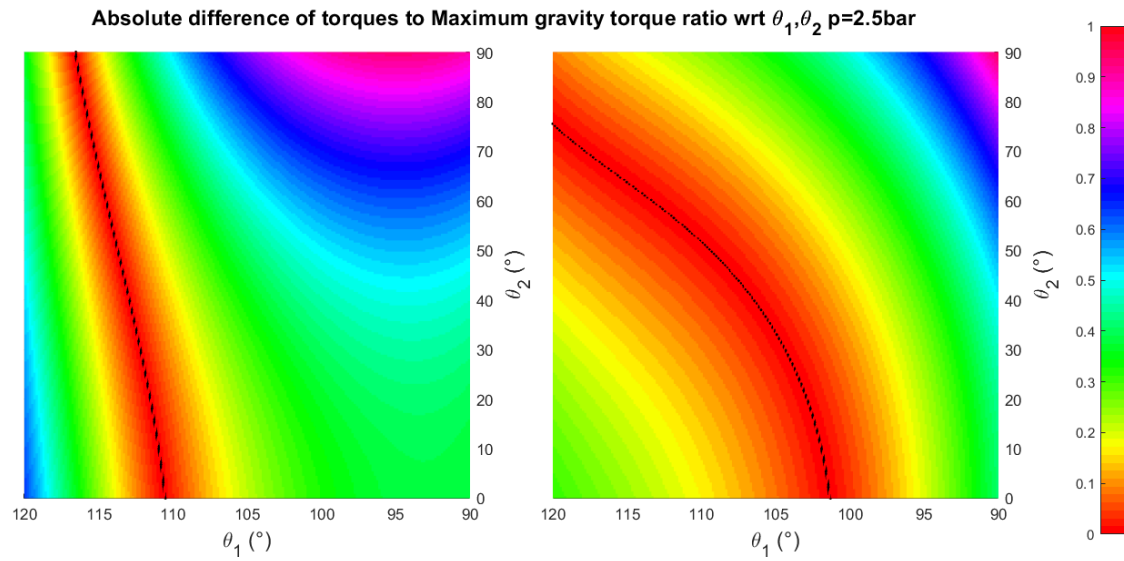


Figure 6.5 Surface of the ratio of absolute difference, between the torques due to gravity and generated by the PAM, at  $p = 2.5 \text{ bar}$ , to the maximum value of torque due gravity, projected on plane  $\pi$ :  $\Delta Torque = 0$ , with passing joint design (left), and by employing the shoulder pad (right).

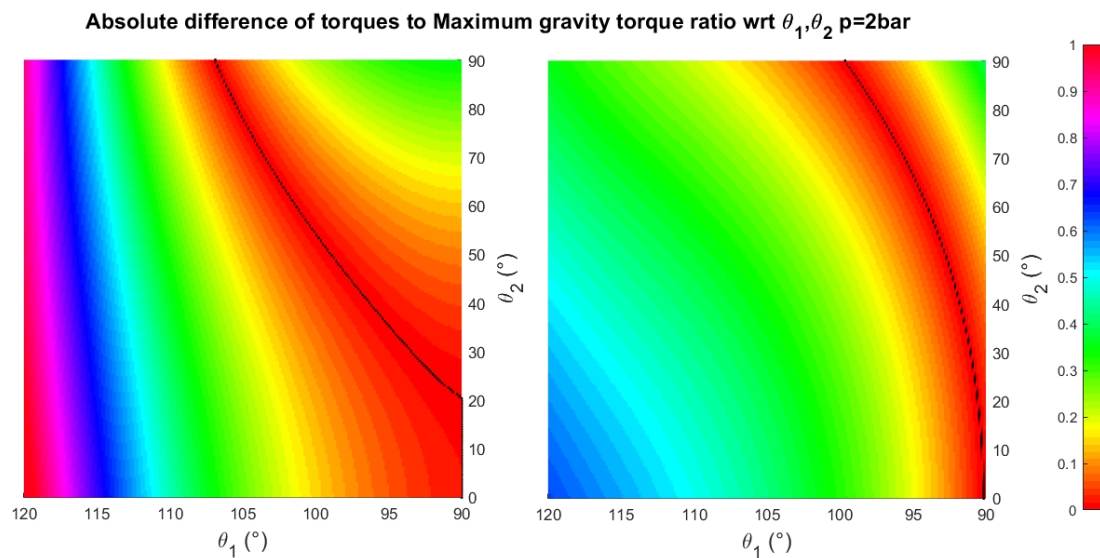


Figure 6.6 Surface of the ratio of absolute difference, between the torques due to gravity and generated by the PAM, at  $p = 2 \text{ bar}$ , to the maximum value of torque due gravity, projected on plane  $\pi$ :  $\Delta Torque = 0$ , with passing joint design (left), and by employing the shoulder pad (right).

The comparison shows a different distribution of values, around the equilibrium curves, that is asymmetrical in case of the passing joint. Besides, by employing the shoulder pad, the area in which the ratio keeps equal or close to 0.1 is larger than the results produced with the original design, and at relatively high elevation angle  $\theta_1$  the ratio keeps rather lower. Furthermore, despite even with the shoulder pad the highest ratio 0.9 can be reached, it occurs in fewer positions, at the very end of the assumed ranges. Besides, in Figure 6.6 the surfaces display a

significant reduction of the ratio values, in fact, at  $\vartheta_2 = 90^\circ$  the ratio comes up to 1 if the passing joint is used, while by employing the shoulder pad it comes up to a about 0.6.

These graphics demonstrate a real advantage of joining the shoulder pad in reducing the effort required to the upper extremity muscles both for lifting the arm to the desired position, and for move the upper limb from the equilibrium position, as shown also in Figure 6.7, that sums up the shoulder torques produced by the pneumatic muscle without and with the shoulder pad (designed to be mounted on the shoulder), at different supply pressures and working conditions, by assuming  $\vartheta_2 = 0^\circ$ , displaying a significant effect in lowering the effort required to the wearer's muscles especially at higher pressure values. If the upper limb is to be kept at  $\vartheta_1 = 115^\circ$  for instance, and the PAM is pressurized at 3 bar, by employing the shoulder pad the effort required to shoulder muscles is lowered from 2.3 to 0.9 Nm. Instead, if a load or a tool of 1kg is put in hand, the PAM is better to be pressurized at 4 bar, and with the shoulder pad the torque provided by the shoulder muscles is reduced, at  $\vartheta_1 = 115^\circ$ , from 6.5 to 2.2 Nm.

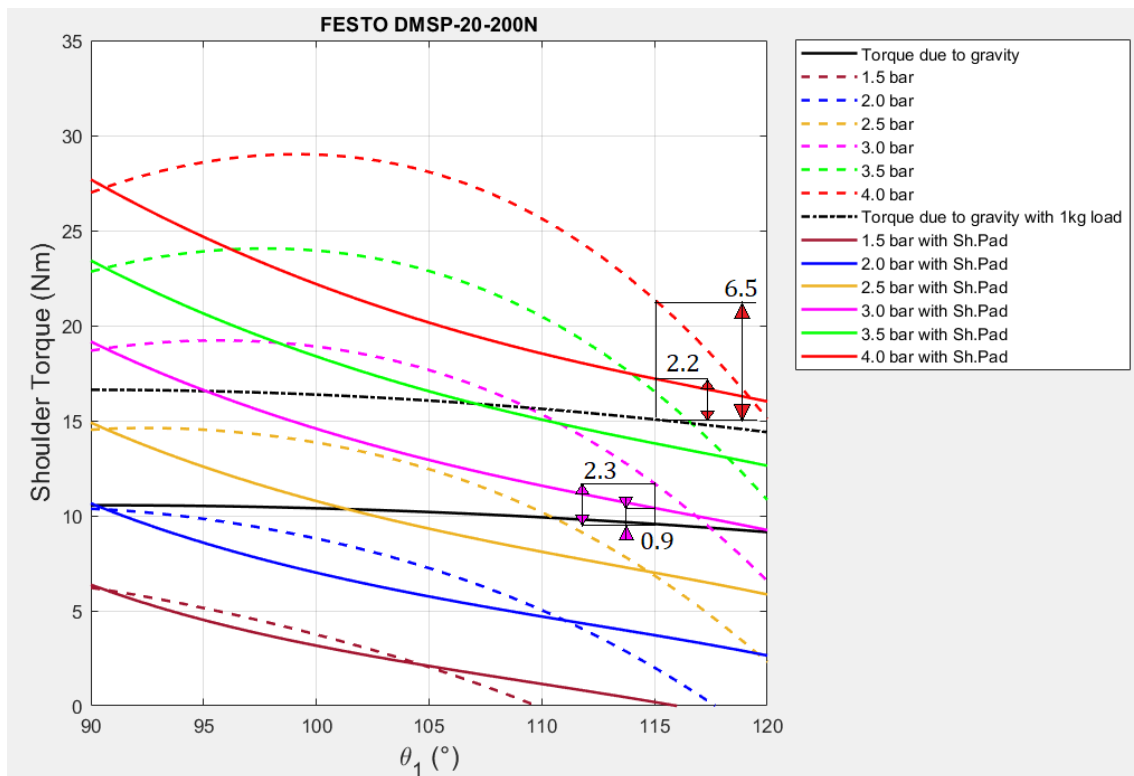


Figure 6.7 Shoulder torques due to gravity, without and with 1kg load (dash-dotted line), with torques generated by the pneumatic muscle without (dotted line) and by employing the shoulder pad designed (continuous line), at different supply pressures and working conditions, with elevation angle of forearm  $\vartheta_2 = 0^\circ$ .



## Chapter 7

# Conclusions and future developments

Industrial applications require solutions to perform hard, long, and repetitive tasks, while preserving quality and precision. Yet, even though programmed robotic systems represent a valuable answer, many tasks still need the experience, cognitive skills, sense, and flexibility of human beings. For this reason, several wearable exoskeleton systems have also been developed for assisting human jobs in industrial environment. They are meant to support and relieve human muscles from heavy loads, or just to assist human limbs and reduce muscular activity during movement, while preserving the quality of the job. This is the example of the passive upper limb exoskeleton design proposed in this paper, which is meant to provide a torque at the shoulder joint to (at least partially) balance the torque due to gravity of the upper limb, reducing the effort required to the shoulder complex muscles, while performing overhead tasks. The output torque is produced by a McKibben pneumatic artificial muscle that, by pressurizing it, exerts a tensile force by contraction according to the position of the arm, acting like a passive device.

For this reason, from Zatsiorsky-de Leva data, the standard human body inertia parameters have been defined, to estimate the torque due to gravity of the arm to balance, with respect to the elevation angles of the upper arm and forearm. Then, the static characteristics of the suggested commercial pneumatic artificial muscle has been achieved through Matlab Curve Fitting toolbox, by using a Hill model-based approach for the modelling of McKibben artificial muscles, producing a very good approximation of the pneumatic muscle behaviour.

Then, the concept of the shoulder pad has been introduced, by calculating its profile through graphic method, proving itself to be a significant expedient to approach the output torque to the torque due to gravity as much as possible, in order to reduce the effort required to shoulder muscles to move the upper limb. Yet, as the device should be mounted over the wearer's shoulder, the calculated profile has been revised, by increasing the base radius of the profile. This compromise shows itself to be less effective than the former profile, however testifying an improvement with respect to the condition in which the shoulder pad is not employed at all.

Therefore, a mounting solution of the PAM has been proposed, producing a CAD model, which consists of hanging it upwards from its fixed end, and using a sheath to reverse the direction of the wire from the shoulder pad to the free end of the PAM, because this mounting makes the position of the PAM to be independent from the position of the 2-DOF shoulder joint. By running the FEM static analysis on the CAD model, through two modelling and simulation software, the Von Mises stresses, occurring in the model when the torque due to gravity of the arm is the highest, are estimated to get the best combination of materials, in order to prevent static failure, as well as to get the structure as light as possible.

Thus, the overall weight of the exoskeleton has been estimated as 6.18 *kg*, of which 1 kg is the weight of the commercial safety harness.

Yet, some improvements of the exoskeleton design can be made, that can be subject of future developments:

- Build a prototype of the exoskeleton design
- Study of objective and subjective effects, evaluating the muscular activity with different benchmarks, while employing the exoskeleton and not, during long-term overhead tasks
- Estimate the real exerted force by the PAM and the losses
- Design an overhead air supply system, estimating the real pressure value inside the PAM
- Design a reducer, meant to enhance the short stroke of the PAM, while reducing the tension force of the PAM, and so revising the design of the shoulder pad profile
- Couple the PAM to a parallel passive device, such as another PAM or a spring and damper system, representing an antagonistic pair which can provide the compensation torque as in shoulder flexion as in extension, since Festo DMSP-20200N pneumatic artificial muscle exhibit a reduced pretensioning of 4% of its nominal length, in order to increase the useful range of motion of the shoulder joint.

# Bibliography

1. Agarwal, PARC, Deshpande, A K, "Exoskeletons: State-of-the art, Design Challenges, and Future Directions", In book: Human Performance Optimization. Researchgate, pp.234-259 (2019).
2. Gopura, RARC, Kiguchi, K, "Mechanical designs of active upper-limb exoskeleton robots: State-of-the art and design difficulties", in Rehabilitation Robotics, 2009.ICORR 2009. IEEE International Conference, pp. 178-187 .
3. Lo, H.S. and Xie, S.Q.: , "Exoskeleton robots for upper-limb rehabilitation: State of the art and future prospects". in Medical Engineering & Physics 34 (2012) pp. 261-268 (2012)
4. Spada, S., Ghibaudo, L., Gilotta, S., Gastaldi, L., Cavatorta, M.: Investigation into the applicability of a passive upper-limb exoskeleton in automotive industry. Procedia Manufacturing 11. 27<sup>th</sup> International Conference on Flexible Automation and Intelligent Manufacturing, FAIM2017, pp. 1255-1262 (2017).
5. de Looze, M.p., Bosch, T., Krause, F., Stadler, K.S., O'Sullivan, L.W.: Exoskeletons for industrial application and their potential effects on physical work load. Ergonomics 59, pp. 671-681 (2016).
6. Gopura, R., Kiguchi, K., Bandara, D.: A Brief Review on Upper Extremity Robotic Exoskeleton Systems. ResearchGate. 2011 6<sup>th</sup> International Conference on Industrial and Information Systems, ICIS (2011).
7. Engin, A.E.: On the Biomechanics of the Shoulder Complex. J. Biomechanics, vol.13, pp. 575-590 (1980).
8. Martini, F.H., Timmons, M.J., Tallitsch, R.B.: Human Anatomy. Prentice Hall, Pearson Education, Inc, ch.8 (2003).
9. Culham, E., Peat, M.: Functional anatomy of the shoulder complex. J. Orthopaedic Sports Phys. Ther. 18, pp.342-350 (1993).
10. Gupta S., Singla E, Agrawal A.: Wearable Exoskeletons: Generations, Design Challenges and Task Oriented Synthesis: Advances in Theory and Practice. ResearchGate (2016).
11. Ergin, M.A., Patoglu, V.: A self-aligning shoulder-elbow exoskeleton. 2012 IEEE International Conference on Robotics and Automation. IEEE, pp. 2479-2485 (2012).
12. Cloud, W.: Man amplifiers: Machines that let you carry a ton. Popular Science, vol. 187, no. 5, pp. 70-73&204 (1965).
13. Gosselin, C.: Gravity Compensation, Static Balancing and Dynamic Balancing of Parallel Mechanisms. Smart Devices and Machines for Advanced Manufacturing. Springer London, pp. 27-48 (2008).
14. Manna, S.K., Dubey, V.N.: Comparative study of actuation systems for portable upper limb exoskeletons. Medical Engineering and Physics 60, pp. 1-13 (2018).
15. Sanjuan, J.D., Castillo, A.D., Padilla, M.A., Quintero, M.C., Gutierrez, E.E., Sampayo, I.P., Hernandez, J.R., Rahman M.H.: Cable driven exoskeleton for upper-limb rehabilitation: A design review. Robotics and Autonomous Systems 126 103445 (2020).

16. Nef, T., Mihelj, M., Kiefer, G., Perndl, C., Riener, R.: Armin exoskeleton for arm therapy in stroke patients. 2007 IEEE 10<sup>th</sup> International Conference on Rehabilitation Robotics. IEEE, pp. 68–74 (2007).
17. Just, F., Baur, K., Riener, R., Klamroth-Marganska V., Rauter, G.: Online adaptive compensation of the armin rehabilitation robot. 6th IEEE International Conference on Biomedical Robotics and Biomechatronics (BioRob). IEEE, pp. 747–752 (2016).
18. Garrec, P., Friconeau, J., Measson, Y., Perrot, Y.: Able, an innovative transparent exoskeleton for the upper-limb. 2008 IEEE/RSJ International Conference on Intelligent Robots and Systems. IEEE, pp. 1483-1488 (2008).
19. Perry, J.C., Rosen, J., Burns, S.: Upper-limb powered exoskeleton design. IEEE/ASME Trans. Mechatronics 12 (4), pp. 408-417 (2007).
20. Xiao, F., Gao, Y., Wang, Y., Zhu, Y., Zhao, J.: Design and evaluation of a 7-dof cable-driven upper limb exoskeleton. J. Mech. Sci. Technol. 32 (2), pp.855-864 (2018).
21. Cui, X., Chen, W., Jin, X., Agrawal, S.K.: Design of a 7-dof cable-driven arm exoskeleton (carex-7) and a controller for dexterous motion training or assistance. IEEE/ASME Trans. Mechatronics 22 (1), pp. 161-172 (2017).
22. Cappello, L., Binh, D.K., Yen, S.C., Masia, L.: Design and preliminary characterization of a soft wearable exoskeleton for upper limb. 2016 6th IEEE International Conference on Biomedical Robotics and Biomechatronics (BioRob), IEEE, pp. 623–630 (2016).
23. Park, H.S., Ren, Y., Zhang, L.Q.: Intelliarm: An exoskeleton for diagnosis and treatment of patients with neurological impairments, 2008 2<sup>nd</sup> IEEE RAS & EMBS International Conference on Biomedical Robotics and Biomechatronics, IEEE, pp. 109–114 (2008).
24. Dehez, B., Sapin, J.: ShouldeRO, an alignment-free two-DOF rehabilitation robot for the shoulder complex. 2011 IEEE International Conference on Rehabilitation Robotics (2011).
25. Gopura, R., Kiguchi, K., Li, Y.: Sueful-7: A 7dof upper-limb exoskeleton robot with muscle-model-oriented emg-based control. 2009 IEEE/RSJ International Conference on Intelligent Robots and Systems, IEEE, pp. 1126–1131 (2009).
26. Ball, S.J., Brown, I.E., Scott, S.H.: Medarm: a rehabilitation robot with 5dof at the shoulder complex. 2007 IEEE/ASME International Conference on Advanced Intelligent Mechatronics, IEEE, pp. 1–6 (2007).
27. Hu, F.Q., Watson, J.M., Payne, P.A., Page, M.: A Fast Opto-Pneumatic Converter for Pneumatic Actuation. IEE Colloquium on Robot Actuators, Digest 1991/146, pp. 10.1-2 (1991).
28. Schulte, R.A.: The Characteristics of the Mckbben Artificial Muscle. Application of External Power in Prosthetics and Orthotics, Publ. 874, Nas-RC, pp. 94-1 15 (1962).
29. Winters, J.M.: Braided Artificial Muscles: Mechanical Properties and Future Uses in Prosthetics/Orthotics. RESNA 13th Conf. Washington, USA, pp. 173-174 (1990).
30. Tavakoli, M., Marques, L., de Almeida A.T.: A comparison study of pneumatic muscles and electrical motors. ResearchGate (2009).
31. Andrikopoulos, G., Nikolakopoulos, G., Manesis, S.: A survey on Applications of Pneumatic Artificial Muscles. 19<sup>th</sup> Mediterranean Conference on Control and Automation (2011).

32. Balasubramanian, S., Wei, H.R., Perez, M., Shepard, B., Koeneman, E., Koeneman, J., et al.: Rupert: an exoskeleton robot for assisting rehabilitation of arm functions. 2008 virtual rehabilitation. IWVR, pp. 163–7 (2008).
33. Sasaki, D., Noritsugu, T., Takaiwa, M.: Development of Active Support Splint Driven by Pneumatic Soft Actuator (ASSIST). *Journal of Robotics and Mechatronics*, vol.16, pp. 497-502 (2004).
34. Klein, J., Spencer, S., Allington, J., Minakata, K., Wolbrecht, E., Smith, R., Bobrow, J., Reinkensmeyer, D.: Biomimetic orthosis for the neurorehabilitation of the elbow and shoulder (bones). 2008 2nd IEEE RAS & EMBS International Conference on Biomedical Robotics and Biomechatronics. IEEE, pp. 535–541 (2008).
35. Tsagarakis, N.G., Caldwell, D.G.: Development and Control of a ‘Soft-Actuated’ Exoskeleton for Use in Physiotherapy and Training. *Autonomous Robots* 15, 21-33. 2003 Kluwer Academic Publishers. (2003).
36. Vitiello, N., Cattin, E., Roccella, S., Giovacchini, F., Vecchi, F., Carrozza, M.C., Dario, P.: The neurarm: towards a platform for joint neuroscience experiments on human motion control theories. 2007 IEEE/RSJ International Conference on Intelligent Robots and Systems, IEEE, pp. 1852-1857 (2007).
37. Rahman, T., et al.: A Simple Technique to Passively Gravity Balance Articulated Mechanisms. *Journal of Mechanical Design* 117(4), pp. 655-658 (1995).
38. Kahn, L., Averbuch, M., Rymer, W., Reinkensmeyer, D.: Comparison of Robot-Assisted Reaching to Free Reaching in Promoting Recovery From Chronic Stroke. *Proceedings of the Seventh ICORR '01*, pp. 39–44 (2001).
39. Rahman, T., Sample, W., Jayakumar, S., King, M.M., Wee, J.Y., Seliktar, R., Alexander, M., Scavina, M., Clark, A.: Passive exoskeletons for assisting limb movement. *Journal of Rehabilitation Research and Development, JRRD*, Volume 43, number 5, pp. 583-590 (2006).
40. Stienen, A.H.A., Hekman, E.E.G., Prange, G.B., et al.: Dampace: Design of an Exoskeleton for Force-Coordination Training in Upper-Extremity Rehabilitation. *Journal of Medical Devices* (2009).
41. Schneider, E., Irastorza, X., Bakhuys Roozeboom, M., Houtman, I.: OSH in figures: occupational safety and health in the transport sector-An overview. Eur. Agency for Saf. and Health at Work (2010).
42. MATE, 2019. EXOSKELETON MATE, Wearable Ergonomic Support. <https://www.comau.com/en/our-competences/robotics/exoskeleton>.
43. Maurice, P., Camernik, J., Gorjan, D., Schirrmeister, B., Bornmann, J., et al.: Objective and Subjective Effects of a Passive Exoskeleton on Overhead Work. *IEEE Transactions on Neural Systems and Rehabilitation Engineering*, Institute of Electrical and Electronics Engineers (2019).
44. SUITX, 2018. SUITX LAUNCHES V3 SHOULDERX. <https://www.suitx.com/>.
45. Kim, S., Nussbaum, M.A., Esfahani, M.I.M., Alemi, M.M., Alabdulkarim, S., Rashedi, E.: Assessing the influence of a passive, upper extremity exoskeletal vest for tasks requiring arm elevation: Part I “Expected” effects on discomfort, shoulder muscle activity, and work task performance. *Appl. Ergon.* 70, pp. 315–322 (2018).

46. HIEIBER, 2019. Hyetone Industrial EXO Intelligent Boost Exoskeleton Robot (HIEIBER). Guangzhou Hyetone Mechanical and Electrical Equipment Co., Ltd, The China, [www.hyetone.com](http://www.hyetone.com).
47. Yin, P., Yang, L., Qu, S., Wang, C.: Effects of a passive upper extremity exoskeleton for overhead tasks. *Journal of Electromyography and Kinesiology* 55 102478 (2020).
48. Moyon, A., Poirson, E., Petiot, J.F.: Experimental study of the physical impact of a passive exoskeleton on manual sanding operations. *Procedia CIRP*, vol. 70, pp. 284–289 (2018).
49. Theurel, J., Desbrosses, k., Roux, T., Savescu, A.: Physiological consequences of using an upper limb exoskeleton during manual handling tasks. *Applied Ergonomics* 67, pp. 211-217 (2018).
50. Ayoub, M.A.: Control of manual lifting hazards: I. training in safe handling. *J. Occup. Med. Official Publ. Industrial Med. Assoc.* 24, pp. 573–577 (1982).
51. Hyun, D.J., Bae, K., Kim, K., Nam, S., Lee, D.: A light-weight passive upper arm assistive exoskeleton based on multi-linkage spring- energy dissipation mechanism for overhead tasks. *Robotics and Autonomous Systems* 122 103309 (2019).
52. Stadler, K.S., Altenburger, R., Schmidhauser, E., Scherly, D., Ortiz, J., Toxiri, S., Mateos, L., Masood, J.: Robo-mate an exoskeleton for industrial use-Concept and mechanical design. *Advances in Cooperative Robotics*; World Scientific, pp. 806–813 (2017).
53. Ebrahimi, A., Gröninger, D., Singer, R., Schneider, U.: Control parameter optimization of the actively powered upper body exoskeleton using subjective feedbacks. *Proceedings of the 3rd International Conference on Control, Automation and Robotics (ICCAR)*, pp. 432–437 (2017).
54. Vermeulen, M., Wisse, M.: Intrinsically Safe Robot Arm: Adjustable static balancing and low power actuation. *Int J Soc Robot* 2, pp. 275-288 (2010).
55. Zhu, Y., Zhang, G., Li, H., Zhao, J.: Automatic load-adapting passive upper limb exoskeleton. *Advances in Mechanical Engineering*, vol.9, pp. 1-8 (2017).
56. Tondu, B.: Modelling of the McKibben artificial muscle: a review. *J. Intell. Mater. Syst. Struct.* 23, pp. 225-253 (2012).
57. Chou, C.P., Hannaford, B.: Measurement and Modeling of McKibben Pneumatic Artificial Muscles. *IEEE Transactions on Robotics and Automation*, vol. 12, no. 1, pp. 90-102 (1996).
58. Tondu, B., Lopez, P.: Modeling and Control of McKibben Artificial Muscle Robot Actuators. *IEEE Control Systems Magazine*, vol. 20, no. 2, pp. 15-38 (2000).
59. Yee, N., Coghill, G.: Modelling of a Novel Rotary Pneumatic Muscle. *Australasian Conference on Robotics and Automation*, pp. 186-190, 27-29 (2002).
60. Ramasamy, R., Juhari, M.R., Mamat, M.R., Yaacob, S., Mohd Nasir, N.F., Sugisaka, M.: An Application of Finite Element Modeling to Pneumatic Artificial Muscle. *American Journal of Applied Sciences*, vol. 2, no. 11, pp. 1504-1508 (2005).
61. Hošovský, A., Havran, M.: Hill's muscle model based modeling of pneumatic artificial muscle. *Annals of DAAAM for 2011 & Proceedings of the 22nd International DAAAM Symposium*, pp. 1005-1006 (2011).

62. Tòthová, M., Pitel, J., Hošovský, A., Sàrosi, J.: Numerical Approximation of Static Characteristics of McKibben Pneumatic Artificial Muscle. *International journal of mathematics and computers in simulation*, vol.9 (2015).
63. <https://www.informedhealth.org/how-does-the-shoulder-work.html>.
64. de Oliveira Sato, T., Coury, Hansson, G., H.G.: Goniometer Crosstalk Compensation for knee Joint Applications. *Sensors* 10(11): 9994-100005 (2010).
65. Kapsalyamov, A., Hussain, S., Jamwal, P.K.: State-of-the-Art Assistive Powered Upper Limb Exoskeletons for Elderly. *IEEE Access* (2020).
66. <https://www.crossfit.com/essentials/movement-about-joints-part-1-shoulder>.
67. Hill, A.V.: The heat of shortening and the dynamic constants of muscle. *Proceedings of the Royal Society of London Series B-Biological Sciences*, vol.126 (1938).
68. <https://bleex.me.berkeley.edu/research/exoskeleton/bleex/>.
69. <https://www.army-technology.com/projects/raytheon-xos-2-exoskeleton-us/>.
70. Nef, T., Guidali, M., Riener, R.: Armin iii—arm therapy exoskeleton with an ergonomic shoulder actuation, *Appl. Bionics Biomech.* 6 (2), pp. 127–142 (2007).
71. Soleymani, R., Khajehsaeid, H.: A mechanical model for McKibben pneumatic artificial pneumatic muscle based on limiting chain extensibility and 3D application of network alteration theories. *International journal of solids and structures* 202, pp. 620-630 (2020).
72. Sarosi, J., Biro, I., Nemeth, J., Cveticanin, L.: Dynamic modeling of a pneumatic muscle actuator with two-direction motion. *Mechanism and Machine Theory* 85, pp. 25-34 (2015).
73. de Leva, P.: Adjustments to Zatsiorsky-Seluyanov's segment inertia parameters. *J.Biomechanics*, vol.29, no.9, pp. 1223-1230 (1996).
74. <https://www.verywellhealth.com/what-is-normal-range-of-motion-in-a-joint-3120361>.
75. <https://www.healthline.com/health/shoulder-range-of-motion>.
76. Lo Piccolo, M.V.: Passive exoskeleton for assistance in heavy operation. Master's thesis. Politecnico di Torino. 2019.
77. [https://www.festo.com/cat/en-us\\_us/data/doc\\_enus/PDF/US/DMSP-MAS\\_ENUS.PDF](https://www.festo.com/cat/en-us_us/data/doc_enus/PDF/US/DMSP-MAS_ENUS.PDF).
78. Lenzi, T., Vitiello, N., De Rossi, S.M.M., Roccella, S., Vecchi, F., Carrozza, M.C.: Neuroexos: A variable impedance powered elbow exoskeleton. 2011 IEEE International Conference on Robotics and Automation, IEEE, pp. 1419–1426 (2011).
79. Lessard, S., Pansodtee, P., Robbins, A., Baltaxe-Admony, L.B., Trombadore, J.M., Teodorescu, M., Agogino, A., Kurniawan, S. Crux: A compliant robotic upper-extremity exosuit for lightweight, portable, multi-joint muscular augmentation. *Proceedings of the 2017 International Conference on Rehabilitation Robotics (ICORR)*, London, pp. 1633–1638 (2017).
80. McDonald, C.G.; Dennis, T.A., O'Malley, M.K: Characterization of surface electromyography patterns of healthy and incomplete spinal cord injury subjects interacting with an upper-extremity exoskeleton. *Proceedings of the International Conference on Rehabilitation Robotics (ICORR)*, pp. 164–169 (2017).
81. MyoPro Orthosis Available online: <https://myomo.com>.

82. Kim, S., Nussbaum, M.A., Esfahani, M.I.M., Alemi, M.M., Jia, B., Rashedi, E: Assessing the influence of a passive, upper extremity exoskeletal vest for tasks requiring arm elevation: Part II- "Unexpected" effects on shoulder motion, balance, and spine loading. *Appl. Ergon.* 70, pp. 323-330 (2017).
83. Manti, M., Cacucciolo, V., Chianchetti, M.: Stiffening in Soft Robotics: A Review of the State of the Art. *IEEE Robot. Autom. Mag.*, vol.23, no. 3, pp. 93-106 (2016).
84. Copaci, D., Flores, A., Rueda, F., Alguacil, I., Blanco, D., Moreno, L.: Wearable elbow exoskeleton actuated with shape memory alloy. *Converging Clinical and Engineering Research on Neurorehabilitation II*, Springer, pp. 477-481 (2017).
85. Villoslada, A., Flores, A., Copaci, D., Blanco, D., Moreno, L.: High-displacement flexible shape memory alloy actuator for soft wearable robots. *Rob. Auton. Syst*, vol. 73, pp. 91-101 (2015).
86. Karpelson, M., Wei, G., Wood, R.J.: Driving high voltage piezoelectric actuators in microrobotic applications. *Sensors and Actuators A: Physical*, vol. 176, pp. 78-89 (2012).
87. Waters, A.: *The Magneto-elastic Effect*. Williams Press, York (1990).
88. De Rossi, D., Carpi, F., Lorussi, F., Scilingo, E.P., Tognetti, A.: Wearable kinesthetic systems and emerging technologies in actuation for upperlimb neurorehabilitation. *Annual international conference of the IEEE engineering in medicine and biology society*, pp. 6830-6833 (2009).

## Appendix

One of the critical issues of pneumatic artificial muscles is their restricted stroke, so they can exert a very high force but for a limited range. In fact, even though employing the shoulder pad improve their trend, the output torques exerted keep themselves positive for a limited range of elevation angle  $\vartheta_1$ . To try to resolve this limit, a reducer is proposed to join the mechanism. In this way, as the pneumatic muscle contracts a little, the reducer is meant to amplify the shortening of the wire, in order to extend the useful range of elevation angle in which the output torque keeps positive, yet the tension force transmitted on the shoulder pad is reduced.

The proposed reducer consists of three pulleys on which the wire is wound (see Figure A. 1). Two of them are concentric and rigidly connected with each other, but with different radius. The pulleys are positioned in the rear part of the exoskeleton to arrange a transmission system from the PAM to the shoulder pad.

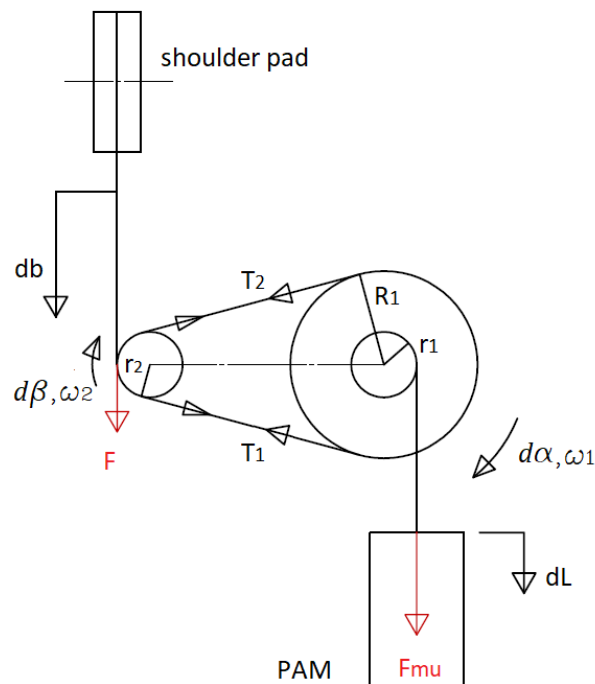


Figure A. 1 Scheme of the reducer, consisting of three pulleys positioned in the rear of the exoskeleton, for transmitting force from the PAM to the shoulder pad.

- $F_{mu}$  is the force exerted by the PAM by contraction
- $dL$  is the shortening of the PAM
- $d\alpha, \omega_1$  are the rotation angle and the angular speed of the first two concentric pulleys, as a result of  $dL$

- $T_2$  is the tension force on the upper branch of the transmission between the larger pulley of radius  $R_1$  and the last pulley of  $r_2$
- $T_1$  is the tension force on the lower branch of the transmission between the larger pulley of radius  $R_1$  and the last pulley of  $r_2$
- $F$  is the force transmitted by the last pulley on the shoulder pad, through the wire
- $d\beta, \omega_2$  are the rotation angle and the angular speed of the last pulley
- $db$  is the shortening of the wire

By neglecting the inertia of the pulleys and the weight of the PAM, the following system of equations is imposed, with  $T_2 > T_1$  since the concentric pulleys rotate clockwise, by assuming an efficiency of the transmission equal to 1, and without considering the sliding of the wire:

$$\begin{cases} (T_2 - T_1) \cdot R_1 - F_{mu} \cdot r_1 = 0 \\ (T_2 - T_1) \cdot r_2 - F \cdot r_2 = 0 \\ \omega_1 \cdot R_1 = \frac{d\alpha}{dt} \cdot R_1 = \omega_2 \cdot r_2 = \frac{d\beta}{dt} \cdot r_2 \end{cases} \quad (\text{A. 1})$$

$$\begin{cases} F = F_{mu} \cdot \frac{r_1}{R_1} \\ F = (T_2 - T_1) \\ d\beta = d\alpha \cdot \frac{R_1}{r_2} \end{cases} \quad (\text{A. 2})$$

Since the shortening of the wire is  $db = d\beta \cdot r_2$  and the shortening of the PAM is  $dL = d\alpha \cdot r_1$ , these relations are valid:

$$\begin{cases} F = F_{mu} \cdot \frac{r_1}{R_1} \\ - \\ db = dL \cdot \frac{R_1}{r_1} \end{cases} \quad (\text{A. 3})$$

Therefore, while the shortening of the wire is amplified by the ratio  $\tau = R_1/r_1$ , the transmitted force along the wire  $F$  is equal to the pneumatic muscle force  $F_{mu}$  reduced by the same value. Thus, the profile of the shoulder pad has been recalculated with the same graphic approach, by assuming the same initial contraction of the PAM  $k_i = 3.5\%$  and the same initial radius  $r_i = 37 \text{ mm}$ , by joining the reducer. The same equations as in Chapter 4 have been applied, yet, this time, the shortening of the PAM is equal to the shortening of the wire, reduced by the  $\tau$  factor, as the output transmitted force  $F$  is amplified by  $\tau$  with respect to the PAM force. For choosing the optimal reduction ratio,  $\tau$  value has been varied until the highest output torque at  $\vartheta_1 = 120^\circ$  was reached. The optimal value found is:

$$\tau = R_1/r_1 = 1.6 \tag{A. 4}$$

The new profile obtained is shown in Figure A. 2, which is almost the same as the one in Chapter 4 (Figure 4.8).

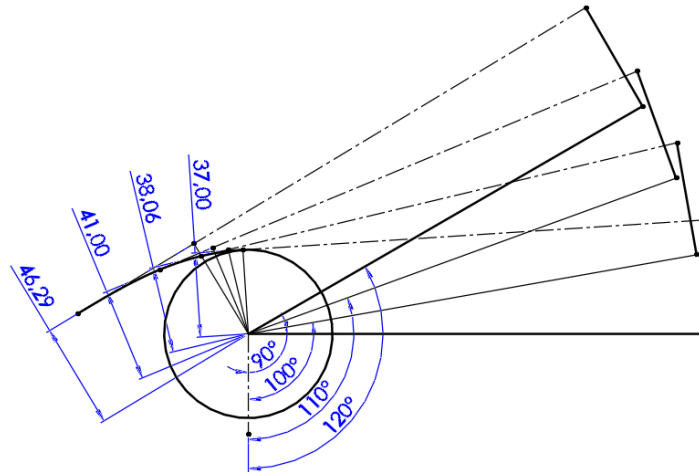


Figure A. 2 Profile of the shoulder pad for Festo DMSP-20-200N by joining also the reducer, from graphical approach from intermediate configurations with  $r_i = 37.00 \text{ mm}$  and  $\kappa_1 = 3.5\%$  at  $\vartheta_1 = 90^\circ$  and  $r_f = 46.29 \text{ mm}$  at  $\vartheta_1 = 120^\circ$ . The lever arms are in blue, as the corresponding elevation angles, the point-dotted line represents the wire in different positions.

Figure A. 3 displays the output torques, generated at different supply pressure, by employing the reducer with  $\tau = 1.6$ .

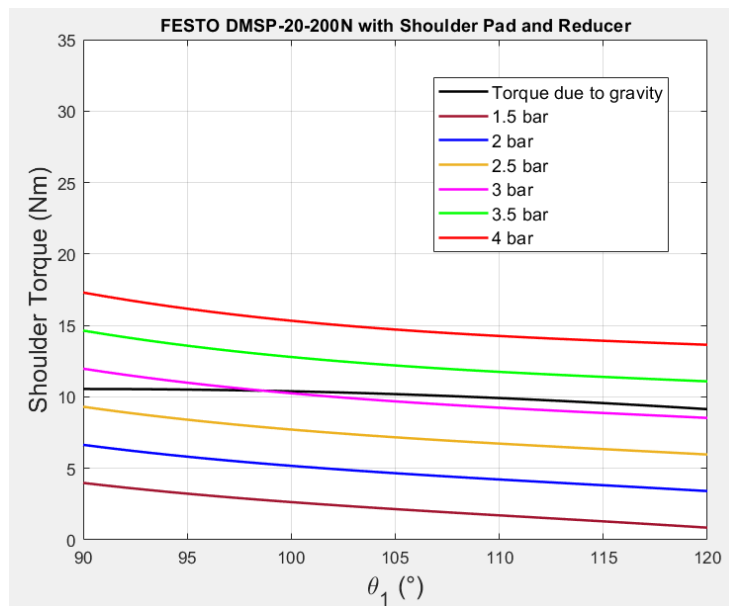


Figure A. 3 Torque due to gravity of the arm, and output torques exerted by the exoskeleton at different supply pressures, by employing the shoulder pad, whose profile is obtained in Figure A. 2 and the reducer with  $\tau = 1.6$ .

Then, next figure compares the effect of the designed reducer on the output torques of the exoskeleton, already equipped with the shoulder pad. Figure A. 4 displays a discreet effect of the reducer in extending the range of elevation angle in which the output torque keeps positive. Yet, the main effect is that the reducer brings the trend of the output torque curves closer to the one of the torque due to gravity, so that the effort required to the shoulder muscles to move the arm from one elevation angle to another is reduced. Nonetheless, at constant supply pressure, the maximum values of torques are lowered by employing the reducer, therefore, to accomplish a good compensation an increase of the supply pressure is needed.

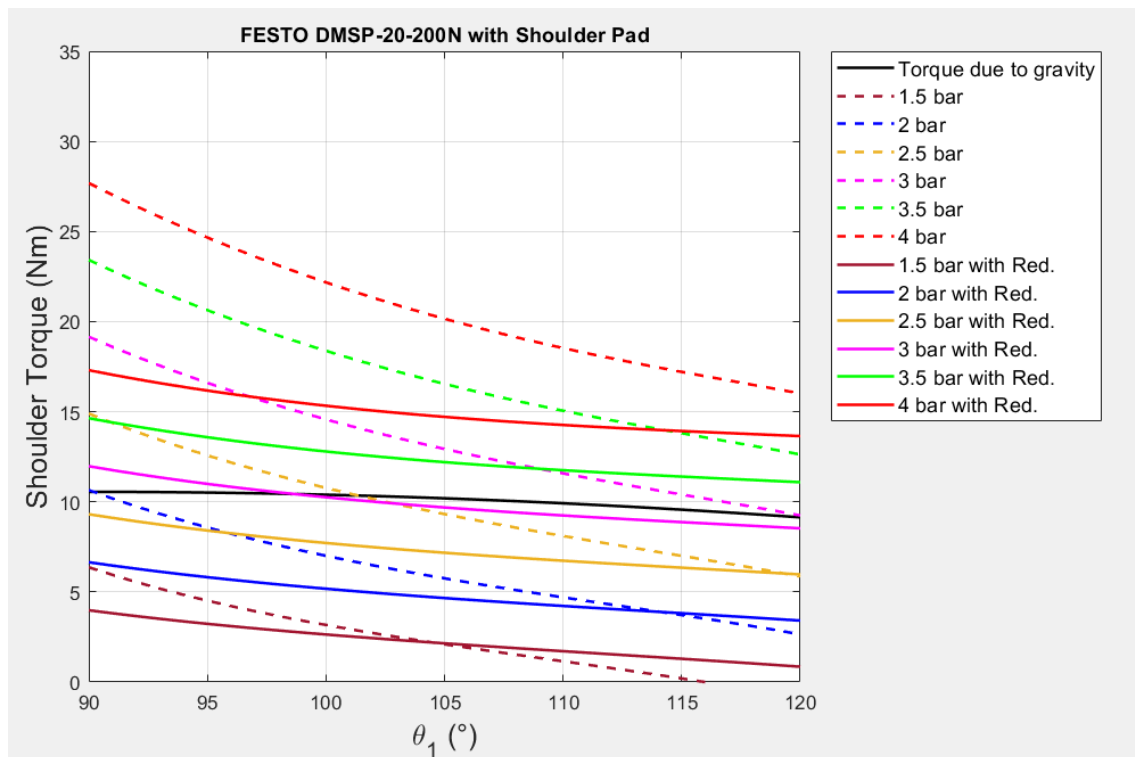


Figure A. 4 Shoulder torques due to gravity, with output torques generated by the exoskeleton by employing only the shoulder pad (dotted lines), at different supply pressures, and employing both the shoulder pad and the reducer with  $\tau = 1.6$  at the same supply pressures (continuous lines).